Sensor Innovations Based on Modified Carbon Electrodes

Ibrahim, Norahim

Award date:
2012

Awarding institution:
University of Bath

Sensor Innovations Based on Modified Carbon Electrodes

PhD Thesis

Norahim Bin Ibrahim

Contents

Acknowledgements

First of all, I would like to express my deepest gratitude to my supervisor for his tremendous and never ending support throughout all this years during my stay in the UK for my PhD study at the University of Bath. Thank you so much for your encouragement and for all kinds of support you have given me and for the inspirational dedication towards excellence in academic and research you have shown. Next, to all the Marken group members for the great teamwork and co-operation, especially to John Watkins for preparing the carbon nanoparticle used for experiments in chapter 5, to Kate for preparing another type of carbon nanoparticle for experiments in chapter 6.

Thank you also to Luke Keenan, from Andrew Burrow's group for lending his hands preparing cobalt phenanthroline for the experiments in chapter 5 and chapter 7.

And the most importantly, my beloved wife and my wonderful children for their patience and for their eternal love and support you have given me.

Finally, I thank you the Government of Malaysia for granting me a lifetime opportunity to undertake my PhD study in the UK.

Summary

This thesis describes experimental work on electrochemical sensing mechanisms. Chapter 1 and Chapter 2 provide an introduction to electrochemical and surface science techniques as well as nano-carbon materials which are of interest in electroanalysis and sensing.

Chapter 3 and Chapter 4 focus on electrochemical processes at liquid | liquid | electrode triple phase boundary systems. In Chapter 3 the electrochemical behaviour of CoPc (cobalt phthalocyanine) dissolved into an organic water –insoluble liquid and deposited as microdroplets on a graphite electrode is studied. Both cation and anion transfer are observed at the liquid | liquid phase boundary. Chapter 4 describes redox processes of a highly hydrophobic anthraquinone derivative where preferential transfer of protons and pH sensitivity are observed. Both systems, CoPc and anthraquinone derivative, are investigated towards CO_2 sensitivity.

In Chapter 3 and 4 graphite electrodes are employed, but in Chapter 5 graphitic carbon nanoaprticles are employed with a surface functionalisation to provide binding capability to DNA fragments. Layer-by-layer deposition of DNA-carbon nanoparticle composite film electrodes is demonstrated and the electrochemical properties of the films are investigated. A novel type of DNA hybridisation sensing mechanism based on a nano-gap generator – collector electrode system is proposed.

Chapters 6 and 7 are dedicated to gas sensing with a novel electrochemical system based on ionomer spheres in contact to the working electrode. In Chapter 6 Dowex ionomer particles are impregnated with carbon nanoparticles which are functionalised with DOPA to provide redox activity and Faradaic current responses. The effect of ionomer type and gas composition is studied. In Chapter 7 Prussian blue nanoparticles are immobilised onto the ionomer particle surface to provide a sensing system with peroxide sensitivity.

Overall, this thesis contributes to sensing of bio-molecules and of gases. By introducing new types of interfaces (triple phase boundary, ionomer contacts, carbon nanoparticle redox systems) it is shown that sensitivity and selectivity can be tailored. In future these types of sensor prototypes could be further developed for specific applications.

List of Abbreviations

AA	ascorbic acid
AC	alternating current
AFM	Atomic Force Microscopy
bppg	basal plane pyrolitic graphite
CMWNT	carbon multiwalled nanotube
CNF	carbon nanofiber
CNP	carbon nanoparticle
CNT	carbon nanotube
CR-GO	chemical reduced graphene oxide
CRG	chemically reduced graphene
CV	cyclic voltammetry
CVD	chemical vapor deposition
DC	direct current
DNA	Di nucleic acid
DPV	Differential Pulse Voltammetry
EDS	Energy Dispersed X-Ray Spectrometer
EMF	Electromotive Force
FEGSEM	Field Emission Gun Scanning Electron Microscopy
GC	glassy carbon
GO	graphene oxide
GOD	glucose oxidase
HOMO	Highest Occupied Molecular Orbital
IHP	Inner Helmholtz Layer
ITO	Indium induced Titanium Oxide
IC	integrated circuit
LUMO	Lowest Unoocupied Molecular Orbital
MG	methylene green
MGNFs	multilayer graphene nanoflake films
MOD	Metal Organic Deposition
NP	nanoparticle
OHP	Outer Helmholtz Layer
PECVD	plasma enhanced chemical vapor deposition
RF	radio frequency
SLG	single layer graphene
SHE	Standard Hydrogen Electrode
SCE	Saturated Calomel Electrode
SEM	Scanning Electron Microscopy
SPM	Scanning Probe Microscope
SWNT	single wall nanotube
TCVD	thermal chemical vapor deposition

List of Symbols

Symbol	Quantity	Units
A	electrode surface area	cm^2
A	frequency factor	-
C	capacitance	$F\ m^{-2}$
c	concentration	$mol\ cm^{-3}$
D	Diffusion coefficient	$cm^2\ s^{-1}$
E	potential	V
E_{eqm}	equilibrium potential	V
E_{pz}	potential of zero charge	V
F	Faraday constant	$C\ mol^{-1}$
ΔG	Gibbs free energy	$kJ\ mol^{-1}$
ΔG^*_{red}	Gibbs free energy of reduction	$kJ\ mol^{-1}$
h	Planck's constant	J s
i_p	peak current	A
j	flux of reactant	$mol\ cm^{-2}\ s^{-1}$
j_{cap}	capacitive current density	$A\ m^{-2}$
k	wavenumber	-
k^0	standard electrochemical rate constant	$cm\ s^{-1}$
R	gas constant	$Jmol\ K^{-1}$
T	temperature	K
ρ	charge	C
Φ	potential	V
η	potential difference / overpotential	V
α	charge transfer coefficient	-
λ	wavelength	m
ν	frequency	-
ν	scan rate	$mV\ s^{-1}$

Chapter 1

Introduction to Electrochemical Methods

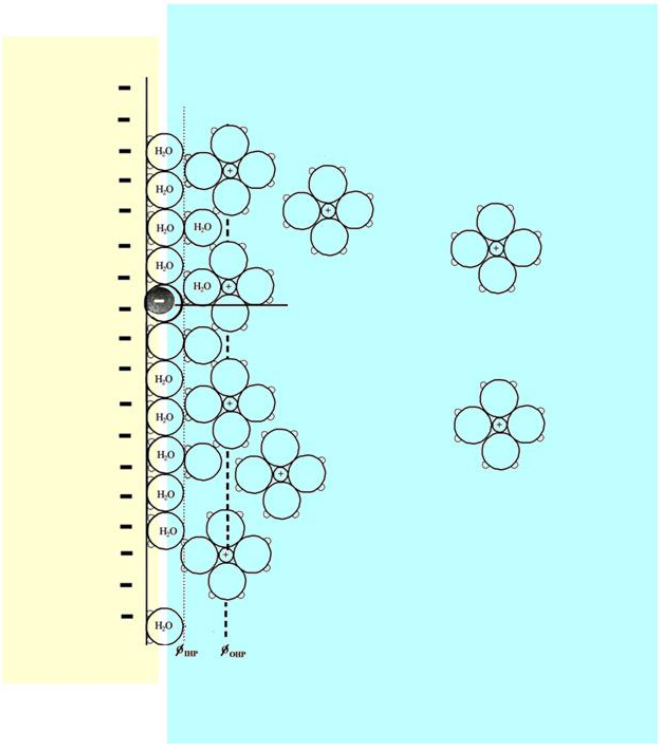

This chapter provides an introduction into experimental methods and theory for electrochemical methods and surface analysis techniques.

Contents

1.1 Polarization of Interfaces

1.1.1 Interfacial Region

Electron transfer is an event in a molecular scale where a negatively charged entity passes through between an electrode and a species in solution. The reason for electron transfer to occur is the potential gradient present at the electrode surface which results from the difference in potential values when two different materials or phases come in contact with each other; between a solid electrode and the electrolyte solution. For example, the potential difference between a local electrode and the adjacent solution may be 1 V, measured over a gap between 1 nm, then the potential gradient shall be of the order of 10^9 V m^{-1} [1]. When studying the rate of electron transfer, a considerable thought on the potential gradient at the interfacial region is of vital importance.

Whenever a potential is applied to the electrode surface, a charging characteristics involving the electrostatic effect is observed. Ions and dipoles with opposite charges are most likely attracted to the electrode surface. This eventually results in the formation of "electrical double layer" [2]. The movement of ions to the adjacent of electrode surface causes changes in the potential field and this factor is indispensable when considering the kinetics of electron transfer.

1.1.2 The Electrical Double Layer

Supposed that there shall be no electron transfer occurring at the interface of the elecrode and the solution. In other words, no chemical changes take place and so no faradaic current passes. Such an electrode is called ideally polarized electrode as there is no electrode reactions can occur within a certain range of potential values [3]. Ideally polarized electrode behaves like a capacitor and only capacitive current flows upon a change of potential. A lot of electrodes posses this kind of characteristic but only within an electrode potential range called the double-layer range.

As mentioned previously, if a potential is applied to an electrode immersed in a solution, the electrode surface will become charged. The amount of charge on the electrode surface is proportional to the electrode material, the electrolyte and potential applied. If the potential applied is negative, then the electron will flow into the surface eventually turning the surface to be negatively charged. In an opposite way, if the applied potential is positive, electron will move out of the surface, gradually results in it being positively charged. Accompanying this phenomenon is the rational that for every electrode/electrolyte combination, there must be a potential whereby the surface shall be neutrally charged. This potential is called zero charge, E_{pzc}. The surface charge on the electrode is in fact balanced by the movement of counter ions from the bulk solution.

Extending the argument above, whenever the electrode potential is negative to E_{pzc}, its surface will become negative. Balancing this, the cations and dipoles such as water molecules begin to be attracted to the electrode surface. Similarly, if the potential applied is positive relative to the E_{pzc}, the electrode surface becomes positively

charged thus inviting anions and dipoles to its adjacent. It shall be noted that in this case, the orientation of the dipoles will be reversed. Either way, there shall be an organized layer consists of cations or anions formed very close to the electrode surface resulting from the potential changes. It shall also be stated that the higher value the applied potential is, the stronger the electrostatic forces produced. As a matter of fact, competition for sites on the electrode surface does exist between the ions and water dipoles in order to form a well organized double layer. An example of the formation of double layer is depicted in Figure 1 [1].

Thus when the potential of an electrode in an aqueous electrolyte is negative to E_{pzc}, its surface will be negatively charged and both cations and dipoles, particularly water molecules, will be attracted to the surface. Moreover, the more negative the applied potential, the stronger are the electrostatic forces leading to the formation of an organized layer of cations adjacent to the electrode surface. Conversely, positive to E_{pzc}, the electrode surface will be positively charged and it is anions and dipoles which are attracted (note, the orientation of the dipole will be reversed). In practice, there will be competition between the ions and water dipoles for sites on the surface and the electrostatic forces leading to a totally organized structure are opposed by the thermal motion of the ions. Figure 1.1 shows the generally accepted model for the interfacial region when $E<E_{pzc}$ and which includes the following features.

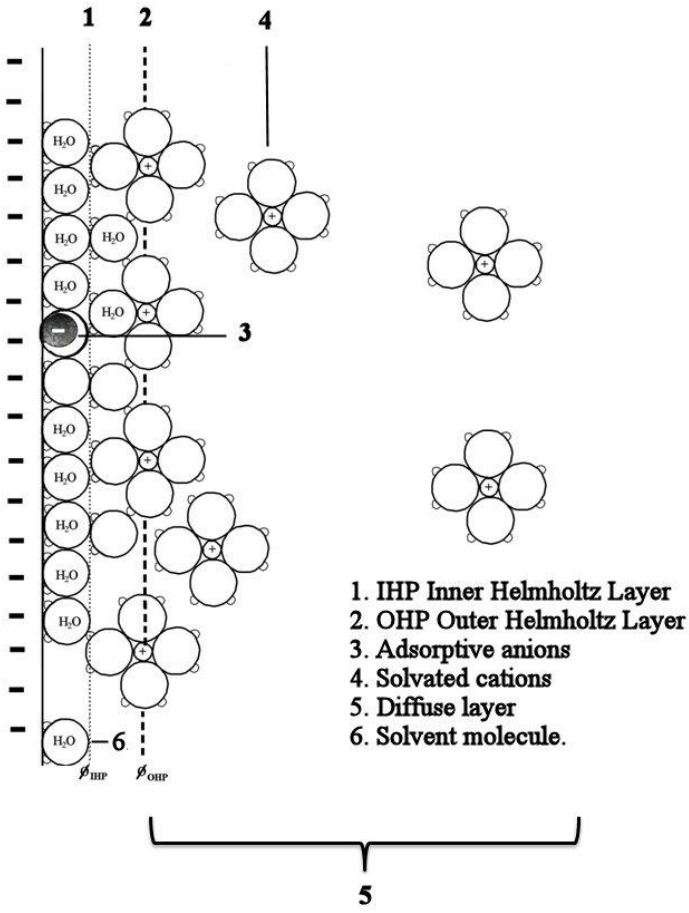

Figure 1.1 Model of electrical double layer at the interfacial region at the electrode surface for potentials negative to the potential of zero charge [1**].**

1.1.3 Charging Currents

It was stated that any change in the potential of an electrode is the driving force of change in the charge on the metal side of the electrode surface. Coupled to this, ions and dipoles reorganization will also occur in the double layer on the solution side. Changing the potential of the electrode means that there will be electron flowing into or out of the electrode. In practice, these electrons will eventually pass out through the external circuit and virtually seen as current and called "charging current".

Charging current is additional to the Faradaic current, which comes from the reactive species in the cell. Its presence is always regarded as "noise" as it complicates the signals produced by the reaction desired in the particular experiment setup. It shall be emphasized that the effect of charging current is only a minor problem for short timescale experiments as reorganization of double layer according to the potential change occurs very fast and, once the new structure has been formed the charging current effect can be totally neglected [1].

For example, in linear potential sweep or cyclic voltammetric experiment, the charging current may be estimated from equation 1. A typical value of capacitance is 0.2 F m^{-2} so that at scan rates of 0.1 and 100 V s^{-1} the observed capacitive current density j_{cap} = 0.02 and 20 A m^{-2}, respectively.

$$j_{cap} = C \times \nu \tag{1.1}$$

The current density is given by equation 1.1. Here C is the capacitance and ν is the potential scan rate. The capacitive current at high scan rate commonly is of the same order of magnitude or higher compared to the Faradaic current for a diffusion controlled reaction.

1.2. Electrode Kinetics

An example of a reduction for a cation can be taken from Figure 1.1. In order for the electron transfer to occur at a potential negative to E_{pzc}, the cation must be as close as possible to the electrode. Let's say it has to sit on the plane of closest approach. It is important to note that whether or not the electron transfer occurs at the interface, the structure and properties of the double layer remains the same. Also, it shall be emphasized that the resulting structure as well as the behaviour of the double layer originates from the electrostatic effect, not chemical. For these reasons, in a system where the electroactive species exist in a large excess of inert electrolyte, it will solely the ions which will determine the characteristics of the double layer. In practice, the effect of double layer is always minimized by using inert electrolyte.

To understand the the electrode kinetics, consider a reduction process for hexacyanoferrate(III) to hexacyanoferrate(II) in a solution using an electrode surface area of A cm^2, with a suitable negative potential applied [4].

$$Fe(III)(CN)_6^{3-}(aq) + e^- \leftrightarrow Fe(II)(CN)_6^{4-}(aq) \tag{1.2}$$

In order for electron transfer to occur between two phases (metal/solution), the electroative species, $Fe(CN)_6^{3-}$ has to be as close as 10-20 Å from the electrode surface. Reduction of the $Fe(CN)_6^{3-}$ anion is only possible if it diffuses within this vicinity, from bulk solution to electrode surface.

The movement of electron in return creates the current which flows through the electrode and external circuit. The relationship between the current generated from the electron transfer can be shown as below.

$$i = FAj \tag{1.3}$$

F = Faraday constant

A = electrode surface area

j = flux of reactant undergoing electrolysis

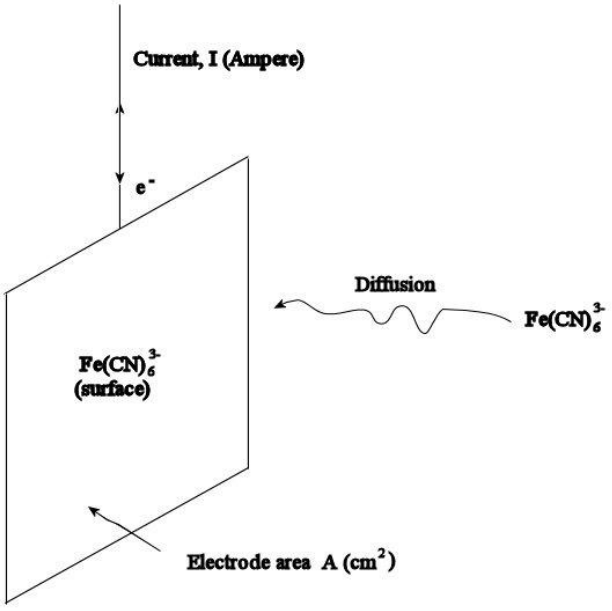

Figure 1.2 Diffusion process of $Fe(CN)_6^{3-}$ to the electrode from bulk to solution [5].

Here, the flux can be best described as the rate of the heterogeneous reaction at the electrode interface. The unit is mol cm^{-2} s^{-1}, and is measured the same way for homogeneous chemical reaction which can be shown as below.

$$j = d[reac\tan t]/dt \qquad (1.4)$$

The flux for a heterogenous reaction at the electrode-solution interface can be written as:

$$j = k(n)[reac\tan t]_n^0 \qquad (1.5)$$

Where n is the rate order of the reactant, k(n) is a nth order rate constant and the subscript represents the concentration of reactant at the electrode surface, which implies the minimum electron tunnelling distance. As far as the equation 1.5 is concerned, there are three main considerations that shall be emphasized.

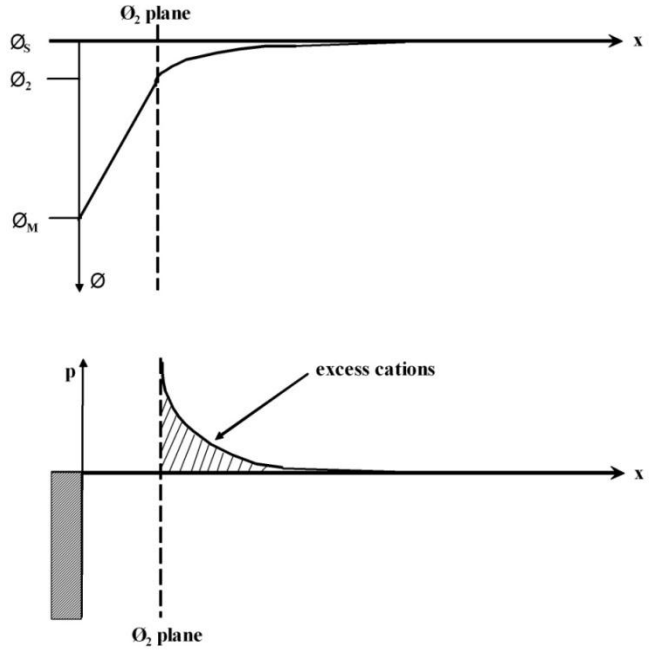

Figure 1.3 Qualitative representation of the charge, ρ, and potential, Ø, as a function of distance from the surface resulting from the model of Figure 1.1 [1].

Firstly, it is very significant to point here that for a first order heterogeneous reaction, n is always equal to 1, and this makes the unit for k(1) are in cm s^{-1}. In contrast to the first order homogeneous reaction, which differs only in s^{-1} in dimensions. Secondly, the concentration of the electroactive species where the electron transfer occurs, the ψ –plane, is not the same as in bulk solution. The concentration of at the ψ-plane may be lower, the same, or higher than that of the bulk solution depending whether the electroactive species are cations or anions, or whether the applied potential is positive or negative to the E_{pzc}. Thirdly, it goes without telling that temperature and pressure are two important parameters in determining the heterogeneous rate constant as well as in homogeneous reactions, but the most critical point of all for interfacial reactions is the applied potential. The driving force for electron transfer relies on the potential difference between the electrode and the ψ_2-plane, ψ_m-ψ_2, rather than the full potential difference across the interface, ψ_m-ψ_s [1] (see Figure 1.3). The phenomenon of loss of the driving force from the applied potential is called iR drop and it is a dynamic process dependent on the flow of current which is causing further imbalance in the charge distribution across the electrode – solution interface.

1.3. Adsorption at Electrode Surfaces

Adsorption is the binding of species from the solution phase to the electrode surface. The adsorbates may be atoms, ions, molecules, reactant, intermediate, or product of the electrode reaction regardless of whether they are organic or inorganic in their nature. Whatever they are, adsorbates do affect the reaction rate as well as the mechanism involved at the electrode of interest. Adsorption of both organic and inorganic species involving either ions or even neutral molecules can occur at the

electrode surface and in variety of environments. For instance, consider a covalent bond formed at the electrode surface for the next following reactions, e.g.

$$H^+ + e^- + Pt \leftrightarrow Pt\text{-}H \quad (1.6)$$

$$CH_3OH + 2Pt \leftrightarrow Pt\text{-}CH_2H^+ + Pt\text{-}H \quad (1.7)$$

In addition to covalent bonding-based technique, adsorption can also occur by means of electrostatic forces. This can be achieved if the electrode surface is electrostatically charged with either positive or negative which eventually attracts ions or dipoles with opposite charge to it. The accumulation species with counter charge enable adsorption via electrostatic method to be achieved. An example of a reversible adsorption process is shown in equation (1.6), meanwhile an irreversible one can be represented as shown in equation (1.7) [1]. Feasibility to adsorb electroactive species of interest from solution onto the electrode surface at open circuit is a great plus, but one can always vary the surface charge simply by varying the electrical potential applied to the electrode surface. Generating a positively or negatively charged electrode surface is also a very simple process as it only requires the application of required potential to the electrode of interest.

1.4. Mass Transport

The supply of reactant and removal of product to / from the electrode surface are essential to a continuing chemical change. In order electron transfer to occur, the reactants have to transport themselves towards the electrode surface, and once the reaction is complete the product will automatically diffuses away from the electrode

surface. Generally, there are three different modes of transportations, diffusion, convection, and migration.

Diffusion. In nature the difference of concentration between two points in a solution normally ends up with a movement of a more concentrated species to the area of the less. This will last until the concentration between them reaches equality. This phenomenon which originates from the concentration gradient is called diffusion [1]. Diffusion plays an important role when considering a reaction an electrode. Very often, the electron transfer process occurs at the vicinity of an electrode. For example, when a species O undergo a reduction process at a considerable rate to become R at the electrode, in theory it shall be considered that the concentration of the former at the electrode surface is lower than at the bulk solution. In other words, the concentration of the reduced species R at the electrode surface will be higher than in the bulk solution. Fick's first law defines diffusion as diffusional flux which represents the number of moles diffusing per unit area (see Eq 1.8). Fick then derived his second law which applies to cases whereas the change of concentration within a specific area is thought (see Eq 1.9) [6]. In these equations, j_{ox} is the flux, D is the diffusion coefficient, [Ox] is the concentration of the species, and x is the distance of the species from the electrode surface.

$$j_{ox} = -D_{ox}\frac{\partial[Ox]}{\partial x} \tag{1.8}$$

$$\frac{\partial[Ox]}{\partial t} = -D_{ox}\frac{\partial^2[Ox]}{\partial x^2} \tag{1.9}$$

In most of the electrochemical measurements where the oxidation and reduction of active species due to the applied electrical potential are concerned, the Fick's second law is more preferable as both former processes always result in changes of concentration at the electrode surface with the elapse of time.

Convection. The presence of thermal gradient or difference in density within a solution can lead to another form of mass transport namely convection. Convection may occur in nature or deliberately induced by means of applying external forces such as shaking or sparging the solution in the electrochemical cell where the electrode reaction is considered. In general, in an unstirred solution, convection is always caused by the chemical reaction at the adjacent of electrode surface which probably generates slight changes in density or even temperature. Meanwhile, unnatural convection is always considered as unfavourable as these changes eventually induce the movement within the cell solution. Very often, in electrochemical experiments, convection can be controlled by flowing the electrolyte solution over the electrode surface at a known rate or by the usage of rotating disc electrode [4].

Migration. Migration by definition is a form of mass transport which originates from the potential gradient induced by the movement of charged species such as ions in the electrochemical cells. As in all electrochemical experiments, the application of electrical voltages between electrodes which generates the passing of current between the former involves the creation of potential drop at the electrode | electrolyte solution surface. Migration, which occurs due to the electrostatic forces is an integral part of the electrode reaction consideration since it balances any changes in charge capacity. However, it is not compulsorily desired in all circumstances of electrochemical

reactions. To overcome this problem, very often the addition or usage of supporting electrolyte solution to the electroactive solution is a common practice as it helps minimizing the effect of migration. It shall be noted that although the reactant or product in the electrode cell may be charged species, with the presence of excess electrolyte solution, they will be enclosed by the ions of the supporting electrolyte solution, therefore these ions are the charged species which moves, not the electroactive themselves [1].

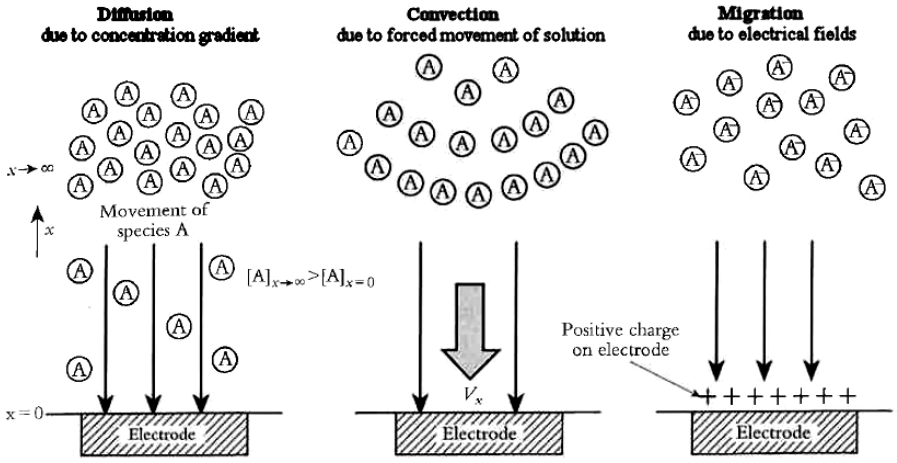

Figure 1.4 Three different forms of mass transport for electroative species in solution to the electrode surface [4].

1.5. Voltammetric Techniques

1.5.1 Electrochemical Experimental Considerations

Electrochemistry is the study of electron transfer reactions between electrodes and reactant molecules, usually, and as this report is concerned, in the solution phase. In this work particularly, techniques used for the study of these reactions include linear sweep voltammetry, cyclic voltammetry and potential step voltammetry. There are many experimental set ups that can be used to carry out these measurements but the most common used is the three electrode cell. This involves placing the working electrode, reference electrode counter electrode into a cell containing a solution of the redox system under investigation and an inert background electrolyte. The solution is purged of oxygen with nitrogen or argon gas and the experiment is controlled using a potentiostat and personal computer.

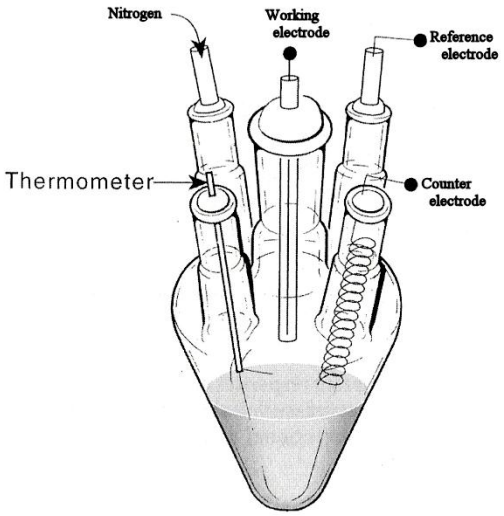

Figure 1.5 Standard electrochemical cell consisting of three electrodes, reference electrode, working electrode, and counter electrode.

The most important part when conducting voltammetric measurements is the apparatus, called potentiostat. It acts as a potential provider to the electrochemical cell and gives out the resulting flowing current. The output of a voltammetric scan is called voltammogram, which shows the relationship between the applied potential and the current produced. Modern potentiostats in general employ a three-electrode setup as shown in Figure 1.5.

Typically, the potential difference is applied between a reference electrode and a working electrode. Since that electron transfer occurs at the working electrode, it is of vital importance so as to ensure that consistent measurements between the former electrode is possible, thus the counter electrode is then introduced into the cell. However, two-electrode experimental system is possible only when the conducting current is low. In this case, counter electrode is not needed and experiments can be performed using only the reference electrode and working electrode.

There are varieties of working electrodes available depending on the experimental purposes. As far as this investigation is concerned, the working electrodes include bare glassy carbon electrode, modified basal plane pyrolitic (bppg) electrodes (with metallophtalocyanine groups and TODAQ), and modified ITO electrodes (with nanoparticles and DNA strands).

The simplest counter electrode (used in this investigation) is normally composed of a piece of platinum wire with a large surface area, and often immersed directly into the cell solution during measurements. The reason for having a reasonable large area relative to the working electrode is not to limit the flowing of current in the total

circuit. Supposed that current resulting from a reduction process takes place at the working electrode, to balance out, an oxidation process then will occur at the counter electrode and vice versa. In large scale experimental setups where measurements are taken over a long timescale, accumulation of products at the counter electrode may happen. To circumvent this problem, salt bridges are sometimes used.

A reference electrode is essential as it provides a stable potential base relative to the working electrode of interest. Some of the mostly used reference electrodes may include the followings:

(a) Standard hydrogen electrode (SHE)

$Pt \mid H_2(g) , H^+(aq)$

(b) Saturated calomel electrode (SCE) (used in this investigation)

$Hg \mid Hg_2Cl_2$ (s), KCl (aq)

(c) Silver-silver chloride electrode

Ag |AgCl (s), KCl(aq)

With the potential of 0 V at all temperatures, it may sound very convenient to use SHE electrode in experiments. However, SHE is prone to physical poisoning and cannot be used in solutions which contain redox species, making it unsuitable for repeated usage. Reference electrode consists of a metal in contact with its sparingly soluble salts, immersed in a saturated salt solution that contains common anions such

as saturated calomel electrode (SCE) and silver-silver chloride electrode are more stable for long timescale experiments.

Very often that solutions, which can be defined as a mixture of conducting electrolyte and the electroactive species, are used as solvent in electrochemical experiments. Vase majority of electrochemical setups use water as a solvent, while other options include organic based solvents are also common. The bottom line when selecting a solvent for a particular experiment is to ensure that it does not allow high concentration of electrolyte solution to be formed to obtain a solution with a reasonable conductivity. Another important aspect to consider would be its compatibility with chemistry that occurs at the electrode surface and that the reactants for the electrode process has an acceptable level of solubility required for the reaction of interest.

Addition of supporting electrolytes with high degree of ionization is essential so as to provide sufficient conductivity of the solution. Increasing amount of electrolytes makes the solution less resistive, in other words, facilitates the flowing of current occurring from the interfacial electrode process. It is also vital to keep the electrode-solution distance so that the potential drop shall be maintained in the range of 10-20 Å to allow smooth electron tunnelling as well as to avoid from the migration effect in the solution. Presence of additional supporting electrolytes also helps in keeping the ionic strength constant throughout the electrolysis. This is because of the relatively high concentration of supporting electrolytes to reactants and products. It also contributes in holding the activity coefficients for both reactants and product equal so that they will cancel out in the Nernst equation.

Most fundamental setups in electrochemical cell are designed with an inert gas inlet/outlet. This is required so as to minimize the interference of signals from oxygen molecules during experiments. Nitrogen gas and argon gas are two most well-known examples of inert gas. Nitrogen is always preferred for its low cost, while argon sometimes is another option as it is heavier than air.

1.5.2. Equilibrium Conditions

The simplest electrochemical measurement can be made when equilibrium is reached between a metallic electrode (m) and a redox active species in an aqueous solution phase (aq). For a general one electron transfer process the following equation can be written:

$$O(aq) + e^{-}(m) \leftrightarrow R(aq) \qquad (1.10)$$

Where the oxidized species O can be reduced at the electrode surface to the species R (or vice versa). As the reaction involves the transfer of an electron between two distinct phases and as the reaction moves towards equilibrium, a net charge separation occurs between the electrode and the solution. This charge separation creates a potential difference at the electrode-solution interface.

The potential difference is fixed for a particular system providing no current is passed through the system. This can be measured simply by placing a reference electrode into the solution and attaching it to the working electrode via a voltmeter. The potential difference is then measured relative to the standard reference electrode, which by

convention has a potential difference of zero. Since no current is drawn through the cell, the equilibrium potential reached is dependent on the relative concentrations of the species O and R. Nernst[1] showed that for a particular system the equilibrium potential, E_{eqm}, could be calculated from equation 1.11.

$$E_{eqm} = E^0 + \frac{RT}{F} \ln \frac{[O]}{[R]} \qquad (1.11)$$

Here E^0 is the standard electrode potential, R is the gas constant, T is the absolute temperature, n the number of electrons transferred per molecule, F is the Faraday constant, and [O]/[R] the concentration ratio of the species at the electrode surface, which under equilibrium conditions is the same as the bulk. From equilibrium measurements thermodynamics parameters such as free energies, entropies, enthalpies and equilibrium constants can be calculated for the system.

1.5.3. Nernst Equation

Most of reactions in electrochemistry will involve heterogeneous electron transfer between the working electrode and the redox active species in the solution. Normally the redox active species will have to diffuse towards the electrode surface, and once it is in the electrode surface region, the redox form will be subject to either homogeneous or heterogeneous chemical reactions that may be accompanied by the electron transfer. If the electron transfer rate is extremely fast relative to the mass transfer of the redox active species, then the electrode reaction is said to be reversible.

Under this condition, the ratio concentrations of oxidized and reduced forms of the redox couple can be described by so-called Nernst equation.

In electrochemical measurements, energy is being supplied in the form of electrical voltage. This energy source is the driving force of all possible chemical reactions. In redox reactions, the movement of charged particles (may be electrons or ions) always give rise to potential difference between the electrode and the solution. The maximum potential difference is called the electromotive force (EMF), E, and the maximum electric work W is the product of charge, q, in Coulomb (C), and the potential ΔE in Volt (J/C).

$$W(J) = q\Delta E \qquad (1.12)$$

Since that the Gibbs free energy, Δ*G*, takes the opposite sign of the maximum electric work, it can be written as

$$\Delta G = -W = -q\Delta E \qquad (1.13$$

In a redox reaction, definite amounts of reactants and products are clearly stated. The number of electrons taking place in the reaction is also proportional to the amount of charge transferred in order to complete the reaction. The Faraday constant, F, defines that one mole electron contains a charge of 96485 C. Thus,

$$q = nF \qquad (1.14)$$

and,

$$\Delta G = -nF\Delta E \tag{1.15}$$

At standard conditions, the Gibbs free energy can be written as

$$\Delta G^0 = -nF\Delta E^0 \tag{1.166}$$

The Nernst equation represents the correlation between the Gibb's Free Energy and EMF in a chemical reaction or also known as the galvanic cell. Consider a reaction scheme below

$$aA + bB \leftrightarrow cC + dD \tag{1.17}$$

As changes in Gibb's Free Energy, ΔG, can be shown as

$$\Delta G = \Delta G^0 + RT\ln Q \tag{1.18}$$

and

$$Q = \frac{[C]^c[D]^d}{[A]^a[B]^b} \tag{1.19}$$

Combining equation 1.16 and equation 1.18 will give

$$\Delta G = -nF\Delta E = \Delta G^0 + RT \ln Q \quad (1.19$$

Therefore

$$-nF\Delta E = -nF\Delta E^0 + RT \ln Q \quad (1.20)$$

Thus, the above equation can be re-written as

$$\Delta E = \Delta E^o - \frac{RT}{nF} \ln \frac{[C]^c [D]^d}{[A]^a [B]^b} \quad (1.21$$

In a simple reaction as shown in equation 8, the above Nernst equation can be simplified as

$$\Delta E = \Delta E^o - \frac{RT}{nF} \ln \frac{[R]}{[O]} \quad (1.22$$

or

$$\Delta E = \Delta E^o + \frac{RT}{nF} \ln \frac{[O]}{[R]} \quad (1.23$$

At equilibrium, $\Delta E = 0$, to result in

$$0 = \Delta E^o - \frac{RT}{nF} \ln \frac{[R]}{[O]} \quad (1.24$$

Thus,

$$E_{eqm} = \Delta E^{o} = \frac{RT}{nF} \ln \frac{[R]}{[O]} \qquad (1.25$$

It shall be emphasized that when the electron transfer rate is too small relative to the mass transfer rate, the observed current will not be a function of the mass transport. In such case, the Nernst equation is no longer applicable.

1.5.4. Electrolysis

Electrochemical cells can be operated under conditions where a current flows and this is achieved by applying a potential that is different to E_{qm}. The current induces the exchange of electrons between the electrode and molecule in solution. This can happen in either direction so that O is reduced to R:

$$\mathrm{O(aq)} + \mathrm{e^-(m)} \rightarrow \mathrm{R(aq)} \qquad (1.27)$$

or so that R can be oxidized to O:

$$\mathrm{R(aq)} \leftrightarrow \mathrm{O(aq)} + \mathrm{e^-(m)} \qquad (1.28)$$

The magnitude of the current is given by equation 1.29.

$$I = AFj \qquad (1.26$$

Here A is the area electrode, F is the Faraday constant and j is the flux of electroactive species reaching the electrode surface. The flux, j, in turn is related to the concentration of the reactant at the electrode surface, $[O]^0$, and also the heterogeneous rate constant, k^0, for the electrochemical reaction (see equation 1.30).

$$j = k^0[O]^0 \qquad (1.30)$$

The heterogeneous rate for the transfer of an electron may depend on several steps of the reaction. This includes the concentration of the reactant species O at the electrode surface, which is different from that in the bulk and depends on the method of mass transport taking place in the cell. These typically are diffusion, convection and migration and need to be taken into account in an experiment or eliminated as much as possible by stirring or by using the rotating disc electrode. The electron transfer step is a quantum-mechanical tunnelling process. Similarly to chemical reactions the transition state model can be used to describe the electron transfer, where there action path involves the reactants overcoming an energy becoming product.

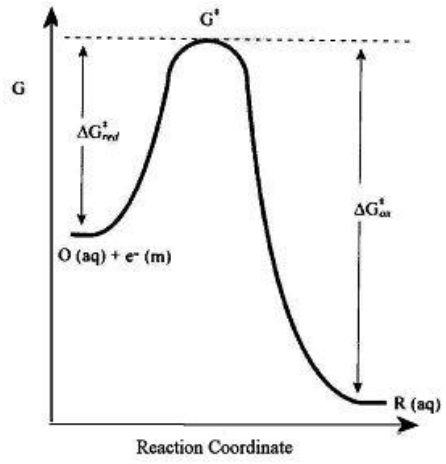

Figure 1.6 Free energy plot for a one-electron reduction of O(aq).

In Figure 1.6 electron transfer is possible when the transition state is reached and the rate determining step is linked to the vibrational reorganisation of the system including redox active molecule and solvent shell [7]. The heterogeneous standard rate constant for electron transfer, k_{red}, is predicted as shown in equation 1.31.

$$k_{red} = A\exp\left(\frac{-\Delta G^{*}_{red}}{RT}\right) \qquad (1.27$$

ΔG^{*}_{red} is the free energy of activation and A is a frequency factor to account for the number of collisions of the molecules with the electrode. Importantly the rate constant for both cases can, in turn, be controlled but the electrical potential applied to the system and more accurately the over potential are required for the reaction to take place.

1.5.5. Overpotential and Energy Levels

A pure crystal contains a lattice of closely packed atoms whose atomic orbitals will all be of a similar energy and so overlap. Instead of considering them as discrete energy levels, the orbitals can be thought of as bands; the valence band which is analogous to the HOMO and the conductance band which can be thought of as the LUMO. In a metal there is no gap between the valence and conductance and so the bands overlap and electrons can move freely through the metal. The level of the band up to which electrons occupy is called the Fermi level and an electrical potential applied to a metal acts to increase or decrease the energy of the Fermi level.

For an electron transfer to occur between the electrode and species O, the Fermi level must be higher than LUMO of the species O. In the figure below, the Fermi level is below the LUMO and so the process is unfavourable and reduction does not occur. However, if the Fermi level in the metal is raised by the application of a negative electrical potential to above the LUMO of O, the electron transfer becomes favourable. The electrical potential that must be applied to a system, above E_{eqm}, in order to make the electron transfer process favourable is called the overpotential, η.

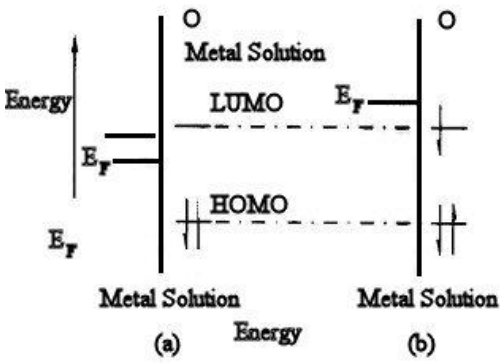

Figure 1.7 Representation of electronic energy levels when (a) the Fermi level is too low for electron transfer to occur and (b) at a level where the electron transfer process becomes favourable.

1.5.6. Cyclic Voltammetry

Linear sweep voltammetry works simply by changing the potential of the working electrode from a set value of E_2 to E_1 usually from a situation where electron transfer does not occur to one where it is driven rapidly. As the change in potential is set over a specific time, then it is a measurement of the change in current over both a potential and time range.

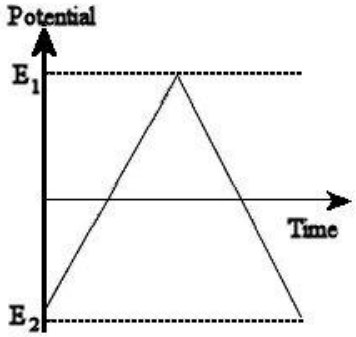

Figure 1.8 Variation of potential with time during a cyclic voltammetry experiment.

Meanwhile, cyclic voltammetry (CV) is an extension of linear sweep voltammetry so that once E_2 is reached, the direction of the sweep is reversed and the electrode potential is scanned back to E_1. CV has become an important and widely used electroanalytical technique in many areas of chemistry. It is rarely used for quantitative determinations, but it is widely used for the study of redox processes, for understanding reaction intermediates, and for obtaining stability of reaction products. This technique is based on varying the applied potential at a working electrode in both forward and reverse directions (at some scan rate) while monitoring the current. For example, the initial scan could be in the negative direction to the switching potential. At that point the scan would be reversed and run in the positive direction. Depending on the analysis, one full cycle, a partial cycle, or a series of cycles can be performed. The response obtained from a CV can be very simple, as shown in Figure 1.9 for the reversible redox system:

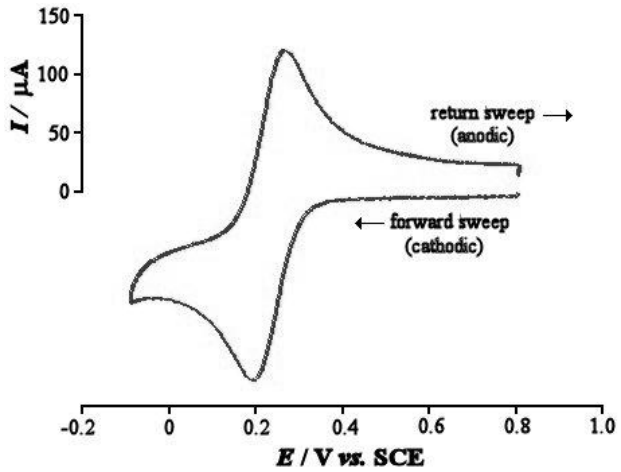

Figure 1.9 Simple reversible cyclic voltammogram.

.

A stationary working electrode, usually a platinum disc, in an unstirred solution is employed, and the potential is varied at a finite rate as a linear function of time. Typical sweep rates are in the range of 0.5 - 100 V s^{-1}, and the current potential curves no longer have the S-shape known from techniques with infinitesimally small sweep rates, but exhibit peaks. If a rapid triangular sweep is applied, and an oscilloscope or a fast x-y recorder is used a cyclic voltammogram is obtained. If, for example, the sweep towards lower potentials produces reduced molecules in the vicinity of the electrode, then they are re-oxidized during the reverse sweep to the same concentration which was initially present in the solution, provided that the rate at which the potential is taken back to its initial value is more rapid than the diffusion processes needed to establish equilibrium with the bulk of the solution. If the reduced species undergoes irreversible secondary reactions in a shorter period than that of triangular sweep, then new waves may be found in the reverse sweep and the height of the wave corresponding to the forward reaction is reduced.

The peak current i_p in this voltammogram is given by Randles-Sevcik equation (1.28).

$$i_p = \left(2.69 \times 10^5\right) n^{3/2} A D^{1/2} \upsilon^{1/2} C \qquad (1.28)$$

Here i_p is the peak current (in amperes), n is the number of electrons passed per molecule of analyte oxidized or reduced, A is the electrode area (in cm^2), D is the diffusion coefficient of analyte (in cm^2 s^{-1}), ν is the potential sweep rate (in V s^{-1}), and C is the concentration of analyte in bulk solution (in mol cm^{-3}).

The midpoint potential of the two peaks in the voltammogram is given by

$$E_{mid} = \frac{E_{red} + E_{ox}}{2} \qquad (1.28$$

The midpoint potential E_{mid} can written as shown in equation 1.33. Here, E_{red} is the reduction potential, E_{ox} is the oxidation potential, and n is the number of electrons transferred per molecule.

The maximum potential E_p in the current-potential curve in the linear scan voltammetric experiment for a reversible one-electron transfer is given by equation 1.34.

$$E_p = E_{1/2} - \frac{28.5}{n} \quad \text{mV at } 25°\text{C} \qquad (1.29$$

Finally, the separation between the two peaks of the voltammogram is given by

$$\Delta E_p = E_{ox} - E_{red} = 2.4RTnF = 59\ \text{mV/n} \ \ (\text{at } 25^{o}\text{C}) \qquad (1.30$$

Hence, depending on what is already known about a given system, one could determine the concentration, the diffusion coefficient, the number of electrons per molecule of analyte oxidized or reduced, and/or the redox potential for the analyte, all from a single experiment.

On the reverse scan, the position of the reoxidation peak is not identical with the potential of the forward scan. It depends on the switching potential, if the reverse

sweep starts at less than 100 mV/n cathodic of the reduction peak. If the switching potential however, is set further apart, the separation of the two peaks will be 57 mV/n and is independent of the scan rate of the potential scan. These two criterion, together with the equal height of the steps in the forward and reverse reactions, are commonly taken as diagnostic for reversible, purely diffusion controlled charge transfer, and cyclic voltammetry has been used simply to obtain potentials which could also have been measured by slow techniques, and at the same time to demonstrate reversibility of the electron transfers.

If the scan rate in cyclic voltammetry is increased to values greater than 0.1 V s^{-1}, then the redox couples do not behave like ideal reversible systems because electron transfer rates are not infinitely large and the current is controlled by a mixture of diffusion and charge transfer kinetics. This is called the *quasi-reversible* case and cyclic at varying scan rates can be used to measure electron transfer rates. Detailed discussion on the reversibility in electrochemical measurement will be presented in the later section.

1.5.7. Reversible and Irreversible Reactions

The term reversible is always misunderstood and sometimes can be confusing in chemistry as it has two different meanings depending on the context of the reaction. In general reversibility can be divided into two categories; chemical and electrochemical.

In order to explain the term ‘reversible’ clearly, the following simple reaction shall be considered.

$$O + ne^- \leftrightarrow R \quad (1.36)$$

The reaction scheme shows that the reactant, in the reduced form, is being transformed into a product by means of having an n number of electron on the time scale of the voltammetric experiment. From the chemical point of view, this Ox/Red couple can be reproduced chemically as represented by the double-sided arrow. Therefore the oxidation reaction can then be expressed as

$$R \leftrightarrow O + ne^- \quad (1.37)$$

Meanwhile, the heterogeneous process taking place between a metal working electrode and an electroactive species at the vicinity of the electrode surface results in electron transfer. In electrochemical experiments, electron transfer can be affected by the potential applied and the concentration of the electroctive species at the electrode. Therefore the rate constants play very important role in determining the electrochemical reversibility of a reaction.

Using the same chemically reversible reaction scheme above, electrochemical reversibility can be explained the following way. Supposed that the rate constants for reduction and oxidation as k_{red} and k_{ox} respectively.

$$O + ne^- \rightarrow R \quad (1.38)$$

When the applied potential is equal to E^0 of the redox couple at equilibrium, the standard electrochemical rate constant can be represented as k^o and will have the units,

cm s^{-1}, derived from the concentration of electroactive species shown in mol cm^{-3} and electron transfer to the electrode surface with surface area in cm^2. Here rate constant for electron transfer in both forward and backward direction of the above reaction scheme can be represented in the following manner

$$k_{red} = k^0 \exp\left(\frac{-\alpha_{red} nFE}{RT}\right) \quad (1.31$$

$$k_{ox} = k_{red} \exp\left(\frac{\alpha_{ox} nFE}{RT}\right) \quad (1.40)$$

Here the rate constants for both reduction and oxidation processes driven by the potential difference or overpotential, $\eta = E - E_{0,}$ from the applied electrical potential, E, can be shown by

$$k_{red} = k^0 \exp\left(\frac{-\alpha_{red} nF(E - E_0)}{RT}\right) \quad (1.41)$$

$$k_{ox} = k^0 \exp\left(\frac{-\alpha_{OX} nF(E - E_0)}{RT}\right) \quad (1.42)$$

k^o is the rate constant at the electrode surface at equilibrium, α_{red} is the cathodic transfer coefficient, α_{ox} is the anodic transfer coefficient, and R is the gas constant (8.314 (V C) / (mol K)). α is defined as the fraction of the interfacial potential at an electrode-solution interface that helps in lowering the activation energy barrier for electron transfer process.

Another way to derive the equation of standard electrochemical rate constant is by comparing the equation representing the diffusion layer, $\delta_{diffusion}$, with that of the reaction layer, $\delta_{reaction}$. The reaction layer, $\delta_{reaction}$, is best described as the diffusion layer at a particular scan rate of interest .

$$\delta_{diffusion} = \sqrt{\frac{D}{\upsilon}} \tag{1.43}$$

$$\delta_{reaction} = \frac{D}{k^0} \tag{1.44}$$

It shall be noted that at the transition point, from reversible to irreversible condition, the thickness of the diffusion layer and the reaction layer is equal. Therefore,

$$\frac{D}{k^0} = \sqrt{\frac{D}{\upsilon}} \tag{1.32}$$

If a constant RT/F is multiplied to both sides of the equations,

$$\frac{D}{k^0} = \sqrt{\frac{DRT}{\upsilon F}} \tag{1.33}$$

To give

$$k^0 = \sqrt{\frac{D\upsilon F}{RT}} \tag{1.34}$$

It shall be noted that under room temperature the diffusion coefficient shall take the value of $D = 10^{-9}$ m^2 s^{-1}. Based on the equation 1.47, by substituting various values of potential scan rates, the corresponding k^0 can be determined accordingly. The following table can be used in dictating the electrochemical reversibility.

$k^o > 0.020$ cm s^{-1}	reversible
5.0×10^{-5} cm $s^{-1} < k^o <$ 0.020 cm s^{-1}	quasi-reversible
$k^o < 5.0 \times 10^{-5}$ cm s^{-1}	irreversible

Table 1 Dictation of electrochemical reversibility of a reaction.

Although electrochemically reversibility of reaction can be determined from the above figures, it is also very useful to use a more practical approach when cyclic voltammetric experiments are conducted in the laboratory. This method has proven to be extremely helpful when voltammetric responses are being measured within a wide range of scan rates as it is a common practice to record voltammograms over a wide potential window so as to determine the reversibility of a reaction. In practice, there are three parameters which can be used.

(a)Peak to peak separation, ΔE_{pp}.

In a reversible voltammogram, the magnitude of the peak to peak separation, $\Delta E_{pp,}$ shall be approximately 57 mV at room temperature (298 K) regardless of scan rate values. On the contrary, in the case of quasi- and irreversible conditions, the ΔE_{pp} will depend on the potential sweep rate.

b) Peak current, I_p.

In both reversible and irreversible conditions, the peak current generated is always proportional to the square root of the scan rate values. However, as for quasi-reversible, scan rate does not hold any effects. At room temperature (at 298 K) a simple one electron reduction of O to R can be simplified by

Reversible

$$I_p = 0.446FA[O]_{bulk}\sqrt{\frac{FD\upsilon}{RT}} \quad (1.35$$

$$= 2.69\times10^5 AD^{1/2}[O]_{bulk}\sqrt{\upsilon} \quad (1.36$$

Irreversible

$$I_p = 0.49\sqrt{\alpha}FA[O]_{bulk}\sqrt{\frac{FD\upsilon}{RT}} \quad (1.50)$$

$$= 2.99\times10^5 \alpha D^{1/2}[O]_{bulk}A\sqrt{\upsilon} \quad (1.51)$$

It shall be noted that under room temperature as for the parameters involved, these following assumptions shall apply; electrode surface area, A = 1 cm^2, concentration of species O, [O] = 10^{-3} M, charge transfer coefficient, $\alpha = \beta = 0.5$ cm s^{-1}, diffusion coefficient for species O and R, $D_0 = D_R = 10^{-5}$ cm^2 s^{-1}.

c) Waveshape of the forward peak.

The difference between the peak current potential, E_p, and half peak current potential, $E_{1/2}$, can come in handy when distinguishing a reversible voltammetric signal from an irreversible one as shown below. All the values for the parameters used in the equations correspond to those of at room temperature (at 298 K).

Under reversible condition,

$$\left|E_p - E_{1/2}\right| = 2.218\frac{RT}{F} \tag{1.52}$$

whereas under irreversible reduction

$$\left|E_p - E_{1/2}\right| = 1.857\frac{RT}{F} \tag{1.53}$$

or

$$\left|E_p - E_{1/2}\right| = \frac{44.7}{\alpha} mV \tag{1.54}$$

and under irreversible oxidation

$$\left|E_p - E_{1/2}\right| = 1.857\frac{RT}{(1-\alpha)F} \tag{1.37}$$

1.5.8. Differential Pulse Voltammetry

The characteristics of the linear sweep and cyclic voltammetric methods hitherto discussed in the previous section has revealed that they are very useful analytical tools in electrochemical measurements as the maximum current flowing resulting from the electroactive species in the solution is proportional to its concentration, thus a very sensitive electroanalytical method. A close relationship between current and concentration gives quantitative information on the system studied and this can be clearly seen if diffusion controls the current magnitude. Although sensitivity-wise, they are undeniably a superior method, it lacks the ability to distinguish between faradaic and capacitive currents thus there is a need for complimentary method to complete the relevant information of interest.

Meanwhile, in differential pulse voltammetry, DPV, fixed voltage pulses are superimposed on a linear potential ramp and are applied to the working electrode at a period of selected time just before the potential pulse drops. The current will be measured twice, which first at a point just before the pulse is being imposed, and then again just before the pulse begins to drop. The interesting point in DPV is that when a potential pulse is applied to an electrode, the capacitive current flows proportionally to it, but decays exponentially with time. The magnitude of the faradaic current, on the other hand, decreases as an exponential function versus $(t)^{1/2}$.

Figure 1.10 shows a typical diagram on how potential pulses, approximately for 50 milli-seconds, are applied on a linear ramp. The first current measured, $i(t_1)$ will be subtracted from the second one, $i(t_2)$, and the difference $[\Delta t = i(t_2) - i(t_1)]$ will be plotted against the applied potential. The resulting voltammogram will show current

peaks which are in direct proportion with the concentration of the electroactive species of interest.

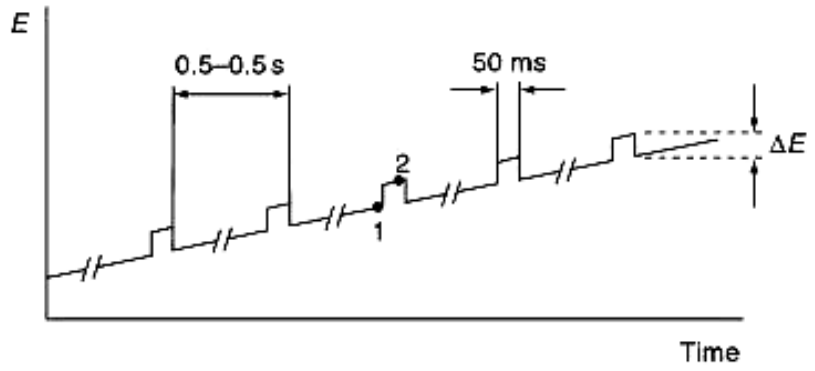

Figure 1.10 Excitation signal for differential–pulse voltammetry.

In DPV, the charging current contribution is so small, about more than an order of magnitude than that of normal-pulse voltammetry, that it is negligible. Conversely, the Faradaic current decays accordingly to the square root of time, producing an excellent signal to noise ratio. Due to these significantly enhanced characteristics, DPV enables the detection at a nano-molar level (1 μg L^{-1}) thus proving hugely useful in electrochemical sensing applications.

1.5.9. Ion Transfer at Triple Phase Boundary (TPB)

A phase boundary is created whenever two or more immiscible phases are brought to contact with each other. As a simple case, if a hydrophobic phase is brought close to a hydrophilic phase, a phase boundary represented as liquid | liquid is said to be formed. In a more advanced situation, when a solid phase electrode is placed into a liquid | liquid system made up of an organic phase and an aqueous phase, a triple phase boundary is created. Figure 1.11A explains the situation in where a conventional

liquid | liquid interface is created, while Figure 1.11B illustrates the formation of a TPB.

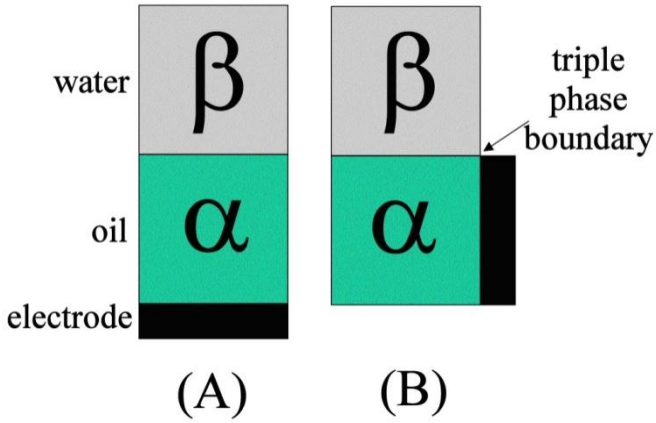

Figure 1.11 Schematic showing (A) a conventional liquid | liquid interface and (B) a liquid | liquid | solid interface, forming a triple phase boundary [8].

A study of the electrode processes occur at the TPB was studied by Marken et al. where a microdroplets of a very higly water insoluble N,N,N,N-tetrahexylphenylenediamine (THPD) is deposited onto a solid electrode and then completed immersed in a aqueous solution consists of totally supporting electrolyte. In this study, the electrode potential was first scanned in a selected potential window (0 to 0.6 V), followed by a visual inspection of the electrode by a microscope. It was observed that a formation coloured ring-like area was confirmed at the TPB. Further investigation by chemical microanalysis disclosed the fact that during the oxidation of THPD, the anions have to move across the liquid | liquid phase boundary and forcedly transported into the organic phase microdroplets (see Figure 1.12b). When the potential scanning was then performed in a negative range, expulsion of anions was then observed [9]. This proves that the insertion / expulsion of anions at the TPB is a reversible process (see Figure 1.12c). Following that, changing the types of anions

and pH in the aqueous phase helps to understand the tell-tale shift in the oxidation potential [10]. The potential shift due to the different types of anions is mainly caused by the Gibbs energy of ion transfer (required energy for anion to cross liquid | liquid phase boundary), while the effect of different pH values explains the applicability of Nernst equation when a transition from an anion exchange to proton exchange is considered [**Error! Bookmark not defined.**].

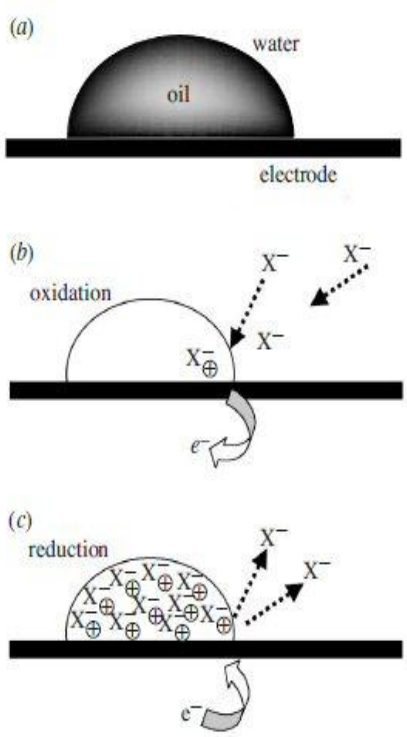

Figure 1.12 Schematic of (a) an oil droplet forming a three-phase junction with an aqueous phase and the electrode; (b) an oxidation process within the droplet, triggering anion transfer from the aqueous into the oil phase; (c) the reverse reduction process, triggering the expulsion of anions into the aqueous phase.

The oxidation of the microdroplets causes the organic phase to possess positive charge, and to balance this out, anions needs to move into the organic from the aqueous solution. This redox process can only happen at the vicinity of the TPB

(liquid | liquid and solid | liquid interfaces). Ball *et al.* proposed that convection partly contributes in maintaining an effective charge transfer at these interfaces [11].

The study of electrochemically driven ion transfer at the TPB has developed a lot in recent years and proven to be a very useful tool especially in elucidating the biological and physiological processes. A compilation of Gibbs free energies measured at the TPB for anions such as amino acids [12], oligo-peptides [13], anionic drugs [14], and cations [15] revealed voltammetric is a reliable method in providing these information.

A combination of having organic microdroplets and a TPB makes it feasible for the study of ion exchange processes to be carried out without the usage of electrolyte to provide for electrical conductivity as electron transfer can take place at the electrode | organic | aqueous electrolyte interface. In Chapter 3 and Chapter 4, the concept of TPB and formation of organic phase microdroplets is exploited.

In Chapter 3, this technique is used to study electrochemical processes for a novel system, microdroplets of 4-(3-phenylpropyl)pyridine (PPP) containing an electroactive MPc is immobilized at basal pyrolytic graphite (bppg) electrode. The organic solvent PPP is non-volatile, highly water immiscible, and a suitable medium for water insoluble transition metal complexes such as those of phthalocyanines. Altogether, a simple quantitative CO_2 detection will be shown. Meanwhile, in Chapter 4, using the same concept, a redox active material, namely TODAQ is incorporated into microdroplets of NOP deposited onto glassy carbon electrode, and pH sensing application will be discussed.

1.6. Surface Characterization Techniques

1.6.1. Scanning Electron Microscopy (SEM)

Scanning Electron Microscopy (SEM) was first commercially invented in the 1960's. It is an imaging technique used to determine topological structure particularly that of sample surfaces. SEM gained its popularity due to its ability to produce images with resolution in the 10 nm range, about 1000 times better than that of any other optical microscope. Figure 1.13 shows a schematic of a typical SEM.

The basic operating scheme of an SEM can be illustrated as shown in Figure 1.13. At the electron gun, high energy electron beam of typically 10 keV are generated. The electron gun is normally made of a tungsten filament of where a massive magnitude of current is flown through it. The filament is heated up to around 2700 K so that the thermionic emission temperature is reached. In a Field Emission Gun (FEGSEM), instead of tungsten filament, a sharply-pointed single crystal tungsten wire fabricated by means of electrolytic etching method is used. Through the tunnelling effect, the electrons are sent out from the FEG. This is achieved as the sharp tip contains a high electric field around it enabling it to extract electrons out of the cathode. These electrons then are passaged below the potential barrier. Unlike the tungsten, the FEG cathode is at room temperature and requires clean vacuum environment .

Using a series of scan coils, a minute beam is produced from the emitted electrons which then will be forwarded to the sample. The direction of the beam can be changed variably as required towards the sample by controlling the current flowing through the

scan coils which is held more positive relative to the electron gun so as to separate them from the filament.

There are a few most likely effects that may follow whenever electrons are directed to the sample surface. Electrons may hit the sample surface and rebound without energy loss, or they may be absorbed by the sample to generate emission of secondary electrons, whose energy is lower called secondary electron, together with X-rays. Other probable consequence is that the electrons may be absorbed by the sample, but this it will produce emission of visible light, which effect is known as cathodoluminiscence or cause the sample to be electrified to produce current within it. Any of these effects can be used to generate information on the sample, but it is very commonplace that the secondary electrons take the role to generate sample images.

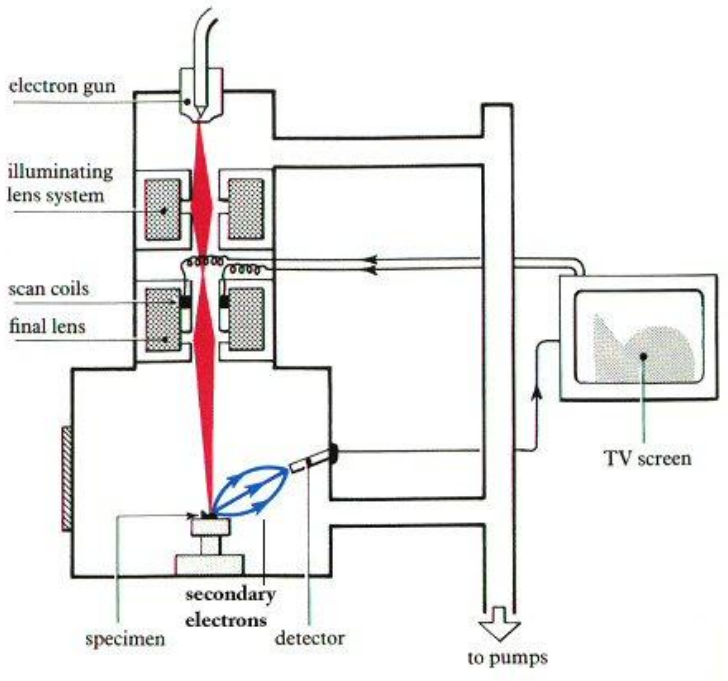

Figure 1.13 Schematic drawing of an SEM [16].

Selection of secondary electrons is performed by drawing them to a grid at a low positive potential approximately 50 V relative to the sample. At the rear side of the grid, a disc coated with a scintillator, (a material that absorb energy and re-release it in the form of light) normally aluminium, so that each time the electrons reach them emission of light would be seen. A photomultiplier tube then detects the light emitted and convert this into a voltage signal. The magnitude of the resulting voltage is proportional to the amount of electrons colliding with the disc. The voltage produced is then focused out to an electronic console which processes and amplifies this signal to create point of brightness on a cathode ray tube or a tv screen.

The images produced by the sample on the tv screen is built up by scanning the electron beam over it simultaneously with the scan of the electron beam in the cathode ray tube. In contrast to optical microscopes, the SEM is not able to magnify the resulting image through contact lenses. Alternatively, a close up look on the sample is gained by altering the ratio of the area scanned to the area of the TV screen. Often, to increase magnification of the SEM images, a smaller restricted area of the sample is first selected and then the electron beam is scanned across it. Occasionally, artefacts resulted from the charging effect are observed in the sample image but can be minimized by evaporating a thin conductive layer on the sample.

1.6.2. Energy Dispersive X-ray Spectroscopy (EDX)

The ability to view three dimensional images of samples of interest does not always solve a problem in an analysis. Occasionally, further complimentary techniques are required to for example when there is a necessity to identify the different elements co-exist within the same sample. For such cases, a typically built-in spectrometer called

Energy Dispersive X-ray Spectrometer (EDS) will be extremely helpful. This non-invasive method is sometimes referred as EDS or EDAX analysis, and used in conjunction with SEM but does not stand alone without the latter.

To further explain, an electron beam hits a sample surface which will be pre-coated to make it conducting. The energy supplied by the electron beam is normally in the region of 10-20 keV. This energy supplies sufficient force for some electrons from the atoms on the sample surface to be knocked off. The vacation of electron from the atom inner shell then filled by the transfer of electrons from the atom outer shell. As the energy levels of the outer shell electrons are higher than that of the inner, the energy difference is then emitted as x-ray.

During EDX Analysis, the specimen is bombarded with an electron beam inside the scanning electron microscope. The bombarding electrons collide with the specimen atoms' own electrons, knocking some of them off in the process. A position vacated by an ejected inner shell electron is eventually occupied by a higher-energy electron from an outer shell. To be able to do so, however, the transferring outer electron must give up some of its energy by emitting an X-ray. Since that the every atom dissipates unique energy level for each electron transfer, identification of the atom from which the x-ray was emitted can be established.

The results from the EDX analysis is called EDX spectrum. In principle it shows a plot of frequency of x-ray emission has occurred for each energy level. As each peak is unique for each atoms, quantitative or qualitative analysis of elemental

composition can be resolved. Higher peaks value simply means a higher concentration of the element is.

Not only that EDX is responsive towards the element according to each peak, it can also reveals the type of X-ray to which it corresponds as well. Each emission from one electron orbital to another carries difference values of energy level and can be represented as in Figure 1.14.

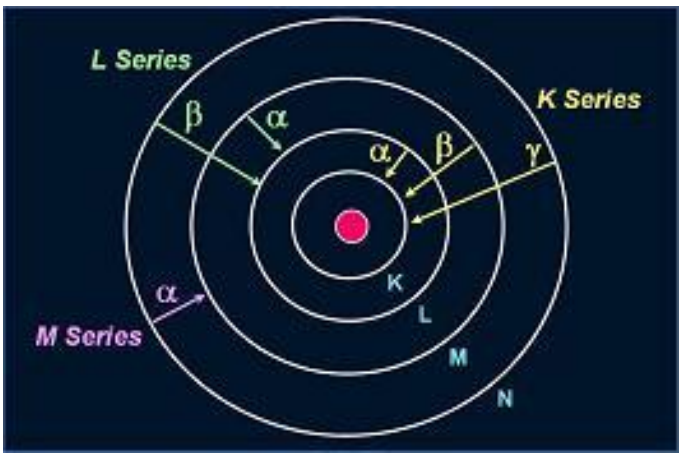

Figure 1.14 Elements in an EDS spectrum are identified based on the energy content of the X-rays emitted by their electrons as these electrons transfer from a higher-energy shell to a lower-energy one [17].

1.6.3. Atomic Force Microscopy (AFM)

Atomic force microscopy (AFM) belongs to the family of Scanning probe microscopes (SPM), used to study topology of a wide variety of samples. AFM is particularly used in surfaces imaging and in measurement of surface morphology. In principle, AFM operates based on the interaction between the tip and the sample surface. In an AFM a fixed force is kept between the tip and the sample while the probe being rastered across the sample surface, with a tip-probe separation less than

0.5nm. Compared to other conventional optical microscopes, for instance, Scanning Electron Microscopy (SEM), which offers imaging resolution in the order of a few nm, AFM allows a better resolution in atomic scales taken in a three dimensions. Unlike the previous which requires complicated measurement settings such the necessity of having an electrically conductive samples or sample pre-treatments to avoid charge build-up, and the needs for samples to be vacuum compatible so as to allow electron tunnelling to create images, the latter does not need the samples to be conductive nor vacuum environment, and imaging can be performed both in solid and liquid states even at low temperatures These simple features of AFM allows significant development to expand in many fields especially of materials science, chemistry, biology, and physics. A typical set-up of an AFM is depicted in Figure 1.11(A).

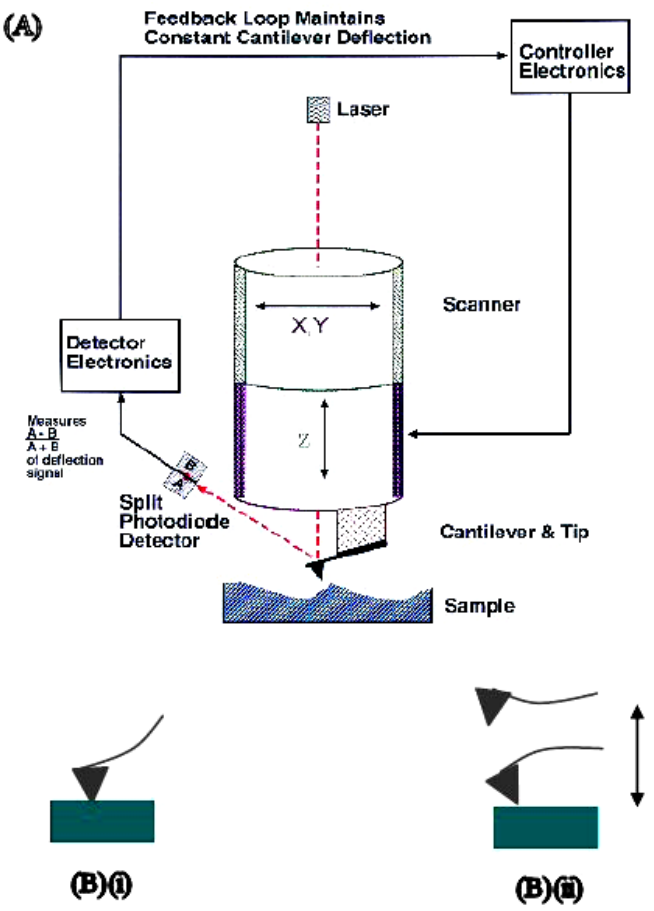

Figure 1.15 Schematic diagram of an AFM. The sample is placed on the piezoelectric scanner. A laser is reflected off the upper side of the cantilever and into a split photodiode via a mirror. In this way, vertical (z) and horizontal (y) deflection signals can be measured [18].

Contact mode and non-contact mode are two among few available scanning probes modes in AFM which have become commonplace in surface imaging. The working mechanism of the contact mode AFM is shown in Figure 115(B)(i).

Contact mode AFM is one of the most widely used method in scanning probes which works based on rastering a sharp tip across the sample. The force works on the tip is repulsive. Initially, the AFM tip needs to be moved manually very close to the vicinity of the sample. The piezoelectric scanner then will automatically adjust the position between the cantilever tip and the sample based on the pre-setup distance value

decided beforehand. Now that the sample is in direct contact with the sample surface, it will then be scanned by a piezoelectric scanner by means of either moving the sample or tip relative to each other. Every deflection resulted from the scanning causes the laser beam at the back of the cantilever tip to be reflected off to a split photodiode. This photodiode acts as a sensor which records all the deflections produced from the scanning. In order to maintain a constant distance between the cantilever tip and the sample, a feed loop is used in where the scanning direction is adjusted in the z direction. By having a feedback loop, damages caused to the sample from crashing of the cantilever tip could be minimized although cannot be totally eliminated. The measured cantilever deflections are used to generate a map of the surface topography. This technique has proven to be an effective method for imaging of biological samples. Although contact mode AFM offers fast scanning rate and proven to be very useful when having samples with rough surface area, often the force imposed end up causing damages or deformation of soft samples and distortion of the image as a consequence. This problem is always encountered with softer materials, such as biological samples, polymers, and even some seemingly hard materials, such as silicon wafers. This problem is however resolved by imaging in liquid form.

To overcome the problem that may arise from contact mode AFM, a so-called intermittent mode or tapping mode has been developed. The imaging principle is very similar to that of the previous but differs in terms of the way the cantilever tip oscillates. In tapping mode AFM, the tip is deflected at a certain intervals or resonant frequency, Figure 1.15B(ii). This way, the cantilever tip lightly taps the sample surface during rastering process and only touches the sample surface on a single oscillation. This method has proven to be a powerful tool when dealing with samples

that are prone to be damaged or loosely held to a surface. However, the difficulty to perform imaging in liquid form limits its advantages [19].

1.7. Innovation in Electrochemical Sensing

Electrochemical sensors have nowadays become an integral part in our everyday lives. Starting from the simplest disposable glucose sensor to the most complicated machines ever exist, they all differ in their designs and fabrication methods depending on the intended usage or purposes. Theoretically, an electrochemical sensor consists of two main elements, a receptor and a transducer. A receptor is normally the part having a direct contact with the sample. Very often, a receptor consists of a thin layer of film deposited on an inert substrate or electrode. The transducer, on the other hand, is a major element in any electrochemical sensor as it plays a major role in processing and converting any changes or parameters in the system into discernible signals, frequently in the form of current, voltage, or impedance/conductance. The recent rapid development in sensing field imposes a lot of impact on the construction of these sensors. In this section, a brief discussion on the general characteristics, elements and common methods indispensable in the construction of fundamental electrochemical sensing devices, with the emphasis on the sensor receptor will be discussed.

Currently, starting from the laboratory method to the industrial, there are varieties of options available for the fabrication of films. Thick films in general are defined as layers possessing a thickness of less than 0.1 μM. Thick-film technology normally is a major part inmicroelectronics, and normally refers to the screen printing technology in

where selected materials in paste form (sometimes called ink) are immobilized on a substrate with sieves to form a desired structure. The inks used to spread film pattern normally contains leads which may contain gold, platinum, palladium and glassy carbon particles. Usually, ceramic materials are chosen for thin films fabricated at high temperature. The film patterns are normally formed using CVD method. Meanwhile, thin-film fabrication normally utilizes the semiconducting and mechanical properties of highly purified crystalline silicon as the base. The manufacturing steps of thin-film may include covering by metallic layers, followed by the making of etching masks using photolithography, etching processes and covering of insulating layers. There are several deposition methods of materials onto substrates, for example via high vacuum deposition, sputter deposition or by chemical procedures such as CVD. A good example of thin film is the inter-digitated electrode of where the structure resembles an overlapping two combs.

In order for the receptor to interact with the target compound, the substrate or electrode surface will normally have to undergo two key processes, surface cleaning and surface modification. In this work, all the working electrodes (bppg carbon, GC and ITO) go through cleaning step either by polishing with micro-sized abrasives, followed by sonication. These treatments are essentials in electrochemical sensing in order to remove any impurities or adsorbed layers prior to usage. Subsequently, the pre-treated substrates will then undergo a modification procedure to provide the receptor base with functional groups or molecules for particular applications.

Ideally, the modified surface shall have a certain level of stability in order to be used repeatedly and durable for a certain length of time for sensing purposes.

Immobilization of chemical and biological compounds for surface modification has long been a useful method be it for quantitative or qualitative measurements. There are many methods available for surface modification such as adsorption, and covalent attachment at the surface. In this work, modification of working electrode surface was achieved *via* evaporation method and layer by layer deposition method, which will be discussed in detailed in the corresponding chapters. The usage of metallo-intercalators for binding of biological molecules such DNAs will also be presented in this work.

Regardless of types of electrochemical sensors, there are common facts that apply to them. First of all, sensors, in a broader sense shall interact with the target / sample directly at the surface. It shall also be emphasized that electrochemical sensors shall be able to convert or transform the chemical signals into electrical signals at a reasonable time length. Preferably, they shall exhibit certain level of repeatability to be able to work continuously.

In this work, focus of attention is first put on the usage of functional materials such as cobalt(II)phthalocyanine owing to its well known redox properties in the literature. The electrochemical properties of the said material is characterized in relation to the triple phase boundary graphite | 4-(-3-phenylpropyl) pyridine | aqueous electrolyte processses which leads to its application in CO_2 sensing. The next highlight is then directed to the new organic redox system observed in TODAQ. Previous studies of Anthraquinone derivaties have demonstrated their capability of exhibiting sensitivity towards proton as well as cation exchange properties. The immobilization of TODAQ in organic liquids coupled to the triple phase boundary process promotes the construction of a basic pH and cations sensing system. Then, a new type of thin film

is constructed from alternating functionalized positively charged carbon nanoparticles and negatively charged DNA target probe *via* layer by layer deposition method. The detection of dsDNA via this method will be shown. Following that, an elegant way of constructing an ammonia sensor by means of having an ionomer-matrix experimental setup using functional CNPs and ion exchangers for pH sensitive application will be discussed. Finally, fundamental properties of Prussian blue-decorated ion exchanger matrix system are studied, and feasible applications will be proposed.

1.8. References

[1] D. Pletcher, A First Course in Electrode Processes, Electrochemical Consultancy, 1991.

[2] H. Helmholtz, Ann. Phys. Und. Chem, Leipzig, 1853.

[3] R. P. Buck, J. Electroanal. Chem. 23 (1969) 219.

[4] A. M. Bond, Broadening Electrochemical Horizons, Oxford University Press, Oxford, 2002.

[5] R. G. Compton, C. E. Banks, Understanding Voltammetry, World Scientific, 2007.

[6] A. Fick, Philos. Mag. 10 (1855) 33.

[7] A. C. Fisher, Electrode Dynamics, Oxford University Press, 1996.

[8] M. J. Reynolds, C. Reynolds, S. Yates, G. Shul, J. Niedziolka, M. Opallo, F. Marken, New J. Chem. 30 (2006) 327.

[9] F. Marken, Webster, R. D. Webster, S. D. Bull, S. G. Davies, J. Electroanal. Chem. 437 (1997) 209.

[10] U. Schroder, R. G. Compton, F. Marken, S. D. Bull, S. G. Davies, S. Gilmour, J. Phys. Chem. B 105 (2001) 1344.

[11] J. C. Ball, F. Marken, F. L. Qiu, J. D. Wadhawan, N. Blythe, U. Schroder, R. G. Compton, S. D. Bull, S. G. Davies, Electroanal. 12 (2003) 1017.

[12] V. Mirceski, R. Gulaboski, F. Scholz, Electrochem. Commun. 4 (2002) 814.

[13] R. Gulaboski, F. Scholz, J. Phys. Chem. B 107 (2003) 5650.

[14] G. Bouchard, A. Galland, P. A. Carrupt, R. Gulaboski, V. Mirceski, F. Scholz, H. H. Girault, Phys. Chem. Chem. Phys. 5 (2003) 3748.

[15] F. Scholz, R. Gulaboski, K. Caban, Electrochem. Commun. 5 (2003) 929.

[16] http://www.asu.edu/courses/phs208/patternsbb/PiN/rdg/elmicr/elmicr.shtml Accessed 18 April 2012.

[17] http://www.siliconfareast.com/edxwdx.htm Accessed 18 April 2012.

[18] http://cse.lmu.edu/resources/MANE_Labs/Instruments/Atomic_Force_ Microscope_AFM_.htm Accessed 18 April 2012.

[19] http://asdlib.org/onlineArticles/ecourseware/Bullen/SPMModule_Basic TheoryAFM.pdf Accessed 18 April 2012.

Chapter 2

Introduction to Nanocarbon Materials

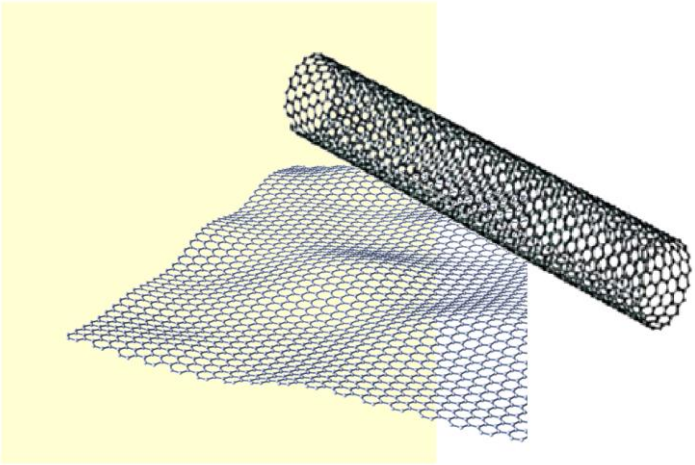

This chapter introduces the role of nano-carbon materials in electrochemistry and in particular in sensor development.

Contents

2.1. Introduction

Electroanalytical methods have proven to be an alternative yet effective method in electroanalysis, especially when it comes to the field of sensing and detection of active species mainly due to its low cost. As designing or selecting process of electrodes for real use can add to the manufacturing cost, a proper consideration is of indispensable element of all. The necessity to employ large scale of expensive materials such as gold and platinum can somehow lead to unbearable cost incurring. For this reason, the hunt for inexpensive but reliable materials is an endless and continuous journey to sustainable materials.

The urge for functional materials with enhanced physicochemical properties has led to the discovery of particles in the range of nanometer size called nanomaterials. Since its first discovery in 1857 by Michael Faraday [1], the buzz word "nanomaterials" has become commonplace in electroanalysis. The various intrinsic chemical as well as physical properties include its enhanced performance in mass transport, catalytic effect, high surface area, and maneuverability of control in different experimental environments. With current advance in nanomaterial research and technology, there is a variety of methods available for the synthesis of nanomaterials.

Today, nanomaterials exist in many forms which includes nanoparticles (NP), nanotubes (NT), nanofiber (NF) and nanowires(NW) and so on. Carbon-based materials, made entirely of carbon atoms, are one of the main highlights in nanomaterial study for the past few years due to its practical potential industrial applications including in electronics, aerospace, automobile, energy storage, sensing, coating and paintings, biomedical and so on. The many forms of carbon nanomaterials present offer a wide range of potentials especially in the field of electroanalysis as they can be tailor-made to suit the purposes or particular needs.

In this section, a review mainly on graphene, carbon nanotubes (CNTs), fullerenes, and carbon nanoparticles (CNPs) will be presented in conjunction with their significant contributions in electroanalytical chemistry as well as their applications in electrochemical sensing and detection. Their unique physicochemical properties, general fabrication methods, and development in electrochemical sensing will be discussed.

2.2. Graphenes

Graphene, the basic building block of other nanocarbon materials such as graphite, CNT, and fullerenes, can be simply described as a two-dimensional single layer of graphite [2] consist of sp^2-bonded carbon atoms densely packed in a hexagonal lattice. As carbon is the most abundant element on earth, graphene is an allotrope of the former alongside the very well studied diamond and graphite. The first attempt to fabricate graphene was carried out in 1975 by B. Lang where he showed that thermal decomposition of carbon on monocrystal platinum substrate resulted in the formation of single- and multi-layered graphite [3]. However, the difficulty of producing

graphite sheets with consistent properties and the lack of suitable applications of the material produced were the reasons for the study to be discontinued. On the 20th century, graphene was only considered as academic materials as scientists believed that two-dimensional materials would be thermodynamically unstable [4]. In 2004, Geim and Novoselov succeeded in isolating the single layered graphene, and the graphene crystal was first discovered using the very well known method called scotch-tape method [5]. They were crowned as Nobel Prize winners in 2010 not for their discovery of graphene, but for their ability in identifying an isolated single-layer graphene and for complete extensive studies on its fundamental properties including successful attempts for repeatable fabrication of graphene via exfoliation method [6].

Graphene was reported not to be completely flat, but in reality it is actually wavy due to the elimination effect of thermal fluctuations at temperature of absolute non-zero on the crystal surface [7]. In principle, graphene is defined as a monolayer of carbon atoms sheet, but studies also reported that graphene with double layer or more than two but less than ten layers with interplanar spacing of approximately 0.335 nm [8], exhibited similar with some degree of divergent properties relative to the former. However, the material is categorized as graphite when the number of carbon layers exceeds ten. Structurally graphene was reported to have two different types of edges which are referred as ‘armchair’ and ‘zigzag’, though a combination of these two is also possible [9]. On each edge, there is an unpaired electron which is available for binding with other reactants. However, the latter is reported to be stable in chemical reactivity as it has a triple covalent bond between the two open edge carbon atoms from a single hexagonal ring [10]. Meanwhile, the former posses a localized edge which further increases the local density of states near the Fermi level, and this energy level corresponds to the non-bonding

configurations [11]. The reactivity sequence of graphene with armchair edges is reported to be larger than that of the zigzag carbon. Theoretically, chirality and morphology of graphene edges impose a great effect on its electronic properties [12].

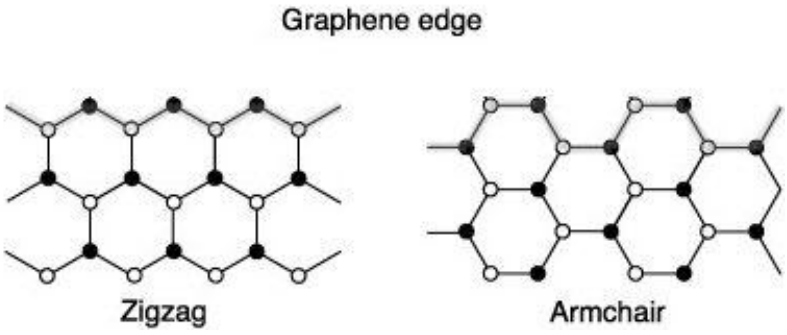

Figure 1. Graphene edge configurations [12].

There are few criteria to consider prior to using any carbon-based materials in any kind of electrochemical application. Characterization of some fundamental electrochemical performance of a carbon electrode shall include study on available potential window, the rate of electron transfer, redox potentials, electrical conductivities etc. Zhou *et al.* reported that graphene shows a wide electrochemical window of ca. 2.5 V in 0.1 M phosphate buffer solution pH 7.0 [13]. This value is almost as good as of that shown by graphite, glassy carbon (GC) and boron-doped diamond electrodes. A study on the charge transfer resistance on graphene electrode using AC impedance analysis revealed that graphene has smaller value compared to that of graphite and GC.

In order to investigate the reactivity (in this case refers to the electrode kinetics) at graphene electrode, a common bench mark system, $[Fe(CN)_6]^{3-/4-}$ and $Ru(NH)_3^{3+/2+}$ were employed and for both cases showed well-defined redox peaks [14,15,16]. Linear relationship between both anodic as well as cathodic current against square root of scan rate indicates that redox processes observed on graphene-based electrode is governed by diffusion controlled process [15]. The peak to peak separations (ΔEp) resulted for one electron transfer redox system using $[Fe(CN)_6]^{3-/4-}$ and $Ru(NH)_3^{3+/2+}$ are 61.5 – 73 mV (at 10 mV s^{-1}) [14,16,17,18] and 60 – 65 mV (at 100 mV s^{-1}) [16] respectively, are very close to the ideal value of 59 mV, indicating that fast electron transfer occurring between graphene electrode and redox species [17].

There have been numerous numbers of publications on the graphene production methods in the literature. To start with, an enhanced study on preparing a single layer graphene (SLG) as well as few-layer graphene was conducted by Novoselov *et al*. via exfoliation and cleavage method.[19]. Exfoliation in principal involves a repetition of peeling process. This so-called scotch tape method is still practically been used extensively by laboratories mainly in fundamental studies to fabricate excellent quality of pure graphene sheets, although unsuitable for production of large quantities. It was reported that an attempt to synthesize graphene by means of thermal chemical vapor deposition method was initiated by Somani et al. in 2006 [20]. Following this, a study on growing graphene layers using Ni substrates were reported. Using a mixture of methane, hydrogen and argon (CH_4: H_2: Ar = 50 : 65 : 200 standard cubic centimeters per minute) as the precursors, Kim et al. conducted CVD at 1000 °C [21]. The product was then rapidly cooled to room temperature using flowing argon gas (10 °C s^{-1}). This procedure of rapidly cooling is a very important element to constrain the formation of multilayer graphene sheets and for easiness

in transferring graphene layers from the Ni substrate [22]. In the same fashion to TCVD, Plasma Enhanced Chemical Vapour Deposition (PECVD) is an interesting method to produce carbon nanostructures. The sole difference between these two technique lies on the energy source used to evaporate the starting materials in the furnace. Instead of heat, basic operation of PEVCD depends on the plasma generation of the reacting gases by applying direct current (DC) or radio frequency (RF) between two electrodes. The energy generated then is transferred to the gas mixture, and this turn them into reactive radicals, ions, neutral atoms and molecules Also, unlike TCVD, no metal catalyst is needed in PEVCD. These atomic and molecular fragments interact with a substrate and, depending on the nature of these interactions, either etching or deposition processes occur at the substrate. Zhu *et al*. in his work revealed that formation of graphene layers via PEVCD is achievable regardless of types of substrates used [23].

One the most commonly used method to produce graphene is via chemical reduction of graphene oxide. Graphene oxide is known as an overlapping of layered structure, which contains epoxide functional groups along the basal plane and carboxyl moieties along the edges. It is normally produced by the oxidative treatment of graphite as established by Brodie [24], Hummers [25], and Staudenmeir [26]. GO is physically much lighter in color than pure graphite and is not conductive due to its loss of extended π-conjugated orbital system from oxidation. GO exhibits high affinity to water, thus its hydrophilicity can be used to dissolve it in water for thin layer fabrication. When dissolved in water, GO then contains covalent bond from oxygen and non-covalent bond with water molecules. Application of thermal treatment to GO solution causes it to expand and delaminate due to the evaporation of the intercalated water molecule accompanied

by the release of some gases as a result of pyrolysis process. It was reported that a method based on this hypothesis managed to produce monolayer graphene sheets [27].

The tremendous interest in graphene-based electrode has led to many applications in electrochemical sensing detection recently, especially for reactive small molecules. It was reported that Zhou *et al*. prepared single sheets of graphene via chemical reduced graphene oxide (CR-GO) method and later tested four different DNA bases, guanine (G), adenine (A), thymine (T) and cytosine (C) [13]. It was then showed that detection of single-stranded DNA (ssDNA) and double-stranded DNA (dsDNA) was also achieved using the same graphene-based electrode. Shan et al. reported the favorable interactions between the graphene-based electrode and glucose oxidase (GOD). In order for dehydrogenases to exhibit catalytic properties, it requires B-nicotine adenine dinucleotide (NAD^+) and its reduced form NADH as the cofactors. Oxidation of NADH which produces NAD^+ is an important element in the construction of biosensing devices for lactate, alcohol and glucose [28]. However, the high overvoltage value of the NADH oxidation and surface fouling due to the product accumulation at the working electrode limits the sensor performance [29]. Liu *et al*. added methylene green (MG) into GO solution prior to chemical reduction in order to obtained a well-dispersed CR-GO. Reduction of GO by hydrazine causes the CRG to bear positive charges. The non-covalently modified CGR electrode used in the study shows that the oxidation of MG-graphene occurs at a much lower potential of 0.14 V vs. Ag/AgCl [30]. Wang *et al*. reported that the differentiation between dopamine with two other coexisting compounds, ascorbic acid (AA) and uric acid (UA), using multilayer graphene nanoflake films (MGNF)s –based electrode was achieved with high selectivity and sensing senstivity range of 5 μM ~ 200 μM [31].

It was reported that graphene is not entirely flat but it possesses waves as any temperature greater than absolute zero can result in thermal energy. The strong carbon-carbon bonds keep them intact. This simple but yet groundbreaking experiment revealed that graphene was the thinnest and lightest material ever produced until now. Graphene has proven to be a very promising novel material for the new generation specifically as electronic material owing to its enhanced properties. To begin with, its high surface area provides lots of possibilities for target molecules or other reactants to bind with as it possesses active binding sites.

Graphene is continuously gaining tremendous attention for its amazing chemical and physical properties. It has been reported that graphene is harder than diamond, and currently the strongest material ever exist that it is 300 times stronger than steel. Studies also revealed that it is a better conductor than that of copper. Its transparency also adds to its unique characteristics as well as flexibility-wise.

2.3. Fullerenes

A molecule resembled a soccer-ball-shaped made of carbon atoms was first identified in 1985, by Kroto and Smalley [32]. It was named Buckminsterfullerene, after the American architect R. Buckminster Fuller, whose geodesic domes it resembles. Buckminsterfullerene takes a structure of a cage made up of 60 carbon atoms, consist of 20 hexagons and 12 pentagons. According to Euler's theorem, every member in the fullerene family has the 12 pentagons and m number (m = n-20 where n = number of carbon atoms in fullerene) of hexagons. C_{60} is a spherical particle with

radius of approximately 0.498 nm with great mechanical strength and flexibility, contains two unoccupied tetrahedral sites and one octahedral site. These sites cater sufficient spaces to provide for spheres with radius of 0.112 nm and 0.206 nm, accordingly [33]. It has been reported that fullerene is apt to form metal intercalated complexes, and prone to crystallize with the presence of solvent molecules trapped in its cage, for example, [C_{60}(γ-cyclodextrin)$_2$] and [C_{60}(1,4-hydroquinone)$_3$] [34]. C_{60}, the smallest of the fullerene group, is a very reactive molecule containing 30 π -bonds. These π -bonds of C_{60} resemble those electron-deficient of alkenes. For this reason, it would be fair to mention that C_{60} acts more like a superalkene due to its high reactiveness. The discovery of this C_{60} molecule is the key to open up a wider and brighter future field of carbon chemistry. All 60 carbon atoms in this molecule are held together by weak forces to result in it be readily soluble in liquid solvents such as benzene. Although other fullerenes with different sizes of carbon cages such as $C_{70,}$ C_{140}, and C_{160} and many other derivatives have also been reported, the overview of fullerenes and its fundamental with emphasis on C_{60} only will be presented.

In general, C_{60} can synthetically be produced in laboratories. In general, the most commonly used effective route is to synthesize is by means of transforming graphite into fullerenes via arc discharge method [35]. The best part of utilizing arc in helium flow at atmospheric pressure is the fact that vacuum is unnecessary. This simple process is normally followed by the reaction mixture will then undergoes a chromatography to purify the product. This method was proven to yield fullerenes ($C_{60)}$ with high purity [35]. However, extensive studies on fullerenes have revealed that they can also be found occasionally in nature [36].

Fullerenes are known to be heat resistant and dissolve at room temperature. Currently, there are huge amounts of patents for their commercial applications. Pure fullerenes are good electrical insulators, but shows high conductivity equivalent to that of metal when doped with metal from alkali group. It was reported that C_{60} when doped with potassium makes superconductors K_3C_{60} at 18 K, while when doped with rubidium makes Rb_3C_{60} at 30K [37]. Due to their size and porosity, fullerene is also a good candidate to be a catalyst in hydrocarbon upgrading, for instance, methane into higher hydrocarbons [38]. Fullerene has also being studied for application in pharmaceuticals owing to the fact that C_{60} derivatives are highly hydrophobic and act as antioxidant thus enable itself to be protease inhibitor [39]. It has also been reported that fullerene particles are very rigid and very flexible. These mechanical properties lead to many studies on their application as nanowires particularly for electrochemical sensing areas [40]. Fullerene is undoubtedly a promising functional material, but the real application or commercialization of fullerene-based patents and products is still far behind due to its high cost.

2.4. Carbon Nanotubes (CNTs)

A lattice made of 6-ring carbon atoms forms one graphene monolayer. If this monolayer is being rolled up, the resulting cylinder-shaped tube will be called single wall nanotube (SWNT), with a typical diameter of 1~1.5 nm [41], while carbon multiwalled nanotube (CMWNT) is made up from more than two concentric SWNTs inside one another [42], having diameters in the range of 2~50 nm with interspacing between individual layers of ~0.34 nm [43,44]. The two open ends of carbon nanotubes take the edge plane-like form, whereas the walls take the properties close to

that of basal plane-like. Typically, CNTs show large surface area of 200~300 m^2 per gram [45]. They have become a favorite research topic due to its unique structure and electrocatalytic properties. At present, there are three most well practiced methods to fabricate CNTs. They are arc-discharge, laser ablation, and CVD.

Carbon electrodes in general, and specifically CNTs, have been renowned as exceptional electrode materials owing to their excellent electrical and mechanical properties [46,47]. A single CNT is able to act like a metal, semi-metal and semiconductor thus widening its potential to be used as the replacement for silicon-based integrated circuits production, depending on how the graphene sheet is being rolled up. This is very important as their versatility to switch its electrical properties is a major driving force in the miniaturization of transistor size, thus further enhancing IC performance. Studies on its mechanical behavior revealed that CNTs exhibit outstanding tensile strength compared to any other existing materials [48]. This gives a huge impact on its application in many areas such as sensors, actuators, and battery technology. Many studies have shown that CNT edges are reactive and often functionalized to obtain functional groups such as –COOH, -OH, or –C=O. Other way of functionalizing of CNTs can be achieved via non-covalent bonding of the CNT sidewall. This method is particularly useful in binding small molecules and biomolecules, and also covering the sidewall with polymer chains [49].

The discovery of CNTs has imparted a huge impact in analytical chemistry, especially in designing electrochemical gas sensors, detectors, and biosensors. To begin with, the vast majority of CNT-based gas sensors working mechanism are based on the electrical resistance

changes upon binding with the analyte. In the same manner, detection of nitrogen dioxide [50], ammonia [51], hydrogen [52], and inorganic vapor [53] were successfully achieved. Coating of polymers such as polyethylyneimine, and Nafion, onto the CNT sidewalls resulted in detection of NO_2, and NH_3, respectively, with high sensitivity and high selectivity [54]. Detection of CO was performed using MWCNTs owing to their catalytic properties upon the oxidation of CO [55]. In another design, MWCNTs was immobilized between the interdigitated microelectrode gap for the detection of NH_3 [56]. Detection of other gaseous such as CO and CO_2 using MWCNT modified electrode were also reported via impedance metric method whereas impedance increment were observed in proportion to the partial pressure of respective gaseous analyte [57].

A wide potential range, inertness in most electrolyte solutions, and high surface area are their main attractions especially in electrochemical sensors. Most CNT-based biosensor works on the condition that the conventional working electrode is modified mainly via evaporation method in where CNTs suspension in bromoform [58], ethanol [59], or N,N-dimethylformide [60] will be left to dry to produce a new functional working electrode. Modifying working electrode with CNTs was shown to be effective in enhancing the reversibility of the electrode process, as reported for dopamine [58] and neurotransmitters [61]. In electrochemical biosensors, direct attachment of proteins such as cytochrome [62] and haemoglobin [63] onto the CNTs have been reported whereas direct electron transfer between CNTs electrodes and proteins was monitored. There are a few reports of CNTs-based modified electrodes on where enzymes such as glucose oxidase [64] and organophosphorus hydrolase [65] were bonded to the MWCNTs surface via adsorption methods. The usage of CNTs have also been reported for detection of DNA

hybridization [66]. Most of such biosensors typically are constructed by means of prior immobilization of single stranded DNA labeled with a redox active indicator onto the CNTs surface, followed by electrochemical measurements after a complementary form a DNA hybrid. In another approach, a nanoelectrode array consist of MWCNTs decorated with a probe molecule covalently to the MWCNTs ends, arranged side by side to each other, was used to detect the signals from the target molecules was also reported [67].

2.5. Carbon Nanoparticles (CNPs)

Nanoparticle (NP) study was initiated by Michael Faraday in 1847 where he discovered gold colloids. Ever since much work have been carried out mainly on metallic nanoparticles such as iron, silver, platinum, nickel, and copper. These nanoparticles were specifically studied as they show catalytic effect upon the production of other promising functional nanomaterial namely nanocarbons. On the other hand, carbon nanoparticles (CNPs) a member of nanocarbon materials, have drawn a great attention owing to its high surface area, easiness of functionalization, and inexpensiveness [83], CNPs can be considered as extraordinary materials from nanocarbon family as they exhibit combined properties that of other nanocarbon materials such as CNTs, fullerenes, or nanodiamonds (high active surface area, adsorptive, good electrical conductivity etc.). It has also been reported that CNPs can change their electrical properties from semimetal conductor provided the particle size is less than 1 nm in diameter [68]. It was reported that their high elasticity is useful for protective or biocompatible coatings purposes [69]. Their versatility and low cost therefore can be utilized in preparing electrochemically active surface for various electrochemical processes.

CNPs or carbon black or are sometimes referred to as furnace black, channel black, thermal black, or acetylene black, depending on the feedstock materials used in their production [70]. It has been reported that in year 2000 that the worldwide production of CNPs was approximately 6 million tons. The number keeps increasing as CNPs have found their application especially in the industry for consumer products. Carbon black is an important element in the production of reinforced rubbers (tires mainly) [71] and pigment materials (UV protection and light absorption) [72]. It was reported that the production of these carbon nanoparticles normally occur at elevated temperature as low as 1700 K up to 2500 K depending on the precursor materials and production methods being used [73]. Compared to soot, which is defined as impure carbon particles that contains inorganic residuals resulting from incomplete decomposition of carbononaceous materials by thermal treatment, carbon black which basically contains 97-99 % elemental carbon [74], on the contrary, are generally particles in nanoscale size produced by incomplete thermal decomposition of hydrocarbon feedstock, and often accompanied by other gaseous by-products such as H_2,O_2,H_2O and CH_4 and some other pollutants as well [75]. Vast majority of the CNPs nowadays are produced by means of three main methods which are CVD [76], arc discharge [77], and laser ablation [78]. Although other method such as shock wave method is also available [79].

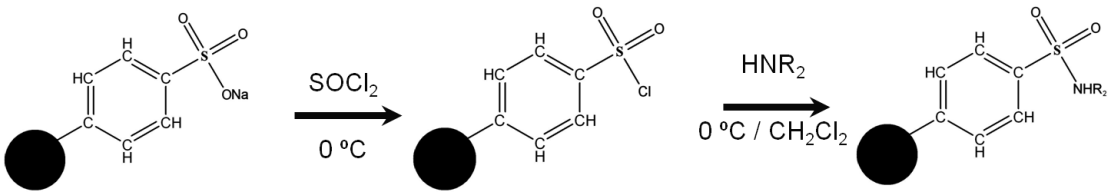

Figure 2.2. Reaction scheme for the formation of positively charged CNPs using Emperor 2000^{TM} CNPs as starting materials.

Emperor 2000^{TM} CNPs are commercially available hydrophilic CNPs possessing phenyl sulphonate groups on its surface, manufactured by Cabot Corporation®. It was reported that a working electrode modified with Emperor 2000^{TM} CNPs could be used to magnify the Faradaic current signal resulting from the irreversible electroreduction of H_2O_2 and other redox probes [80]. Using Emperor 2000^{TM} CNPs as the electrode surface modifier, detection of 2-hydroxy-4-methoxybenzophenone which is known as a sun blocker, and 5-chloro-2(2,4-dichloro-phenoxy)phenol or also known as triclosan which is the main ingredient in production of disinfectants, at lower concentrations has been reported [81]. In 2010, it has been demonstrated previously by Marken *et a*l., that Emperor 2000^{TM} can be functionalized by attaching diamines to the sulphonate group to produce a positively charged CNPs, see Figure 2.2 [82]. The success of modifying the former suggests that further functionalization is possible to produce more CNPs with different functional groups for specific electrochemical sensing purposes. In this work, in collaboration with Tony James group, using the previously synthesized positively charged CNPs as the starting materials an attempt to synthesize negatively charged CNPs was conducted [83]. The resulting surface-dopylated CNPs in combination with different types of ion exchanger was studied, and the application of the matrix in gas sensing will be discussed in detailed in the following chapter.

2.6. Contributions from this Thesis

Despite the vast potential of applications proposed for CNTs and fullerenes, there are still unresolved issues pertaining to them. Their relatively high cost in production, difficulty in mass production and complications in their purification processes as well as the necessity of conducting proper toxicity testing to ensure their safety aspects are taken care of, however, limits their current application hitherto.

On the contrary, the simplicity and low cost in bulk production of single layer or multi-layer graphene and CNPs make them excellent candidates as building blocks in electroanalytical studies. On this basis, in Chapter 5 and Chapter 6, CNPs-modified electrodes based experiments will be utilized in designing DNA-based assemblies with potential application in DNA sensing and an ammonia sensing systems based on dopylated carbon nanoparticles immobilsied onto ionomer spheres.

2.7. References

[1] M. Faraday, Philos. Trans. R. Soc. London 147 (1857) 145.

[2] P. Y. Huang, C. S. Ruiz-Vargas, A. M. Van Der Zande, W. S. Whitney, M. P. Levendorf, J. W. Kevek, S. Garg, Nature 469 (2011) 389.

[3] B. Lang, Surf. Sci. 53 (1975) 317.

[4] A. K. Geim, K. S. Novoselov, Nat. Mater. 6 (2007) 183.

[5] K. S. Novoselov, A. K. Geim, S. V. Morozov, D. Jiang, Y. Zhang, S. V. Dubonos, I. V. Grigorieva, A. A. Firsov, Science 306 (2004) 666.

[6] Scientific background on the Nobel Prize in Physics : Graphene, The Royal Swedish Academy of Sciences, Stockholm 2010.

[7] C. Day, A. Geim, K. Novoselov, Physics, 12 (2010) 2.

[8] H. P. Boehm, R. Setton, E. Stumpp, Pure Appl. Chem. 66 (1994) 1893.

[9] D. Aurbach, B. Markovsky, I. Weissman, E. Levi, Y. Ein-Eli: Electrochim. Acta 45 (1999) 67.

[10] K. Xu, P. D. Ye, J. Phys. Chem. C 114 (2010) 10505.

[11] K. Tanaka, S. Yamashita, H. Yamabe, T. Yamabe, Synth. Met. 17 (1987) 143.

[12] K. A. Ritter, J. W. Lyding, Nat. Mater. 8 (2009) 235.

[13] M. Zhou, Y. M. Zhai, S. J. Dong, Anal. Chem. 81 (2009) 5603.

[14] S. L. Yang, D. Y. Guo, L. Su, P. Yu, D. Li, J. S. Ye, L. Q. Mao, Electrochem. Commun. 11 (2009) 1912.

[15] W. J. Lin, C. S. Liao, J. H. Jhang, Y. C. Tsai, Electrochem. Commun. 11 (2009) 2153.

[16] L. H. Tang, Y. Wang, Y. M. Li, H. B. Feng, J. Lu, J. H. Li, Adv. Functional Mater. 19 (2009) 2782.

[17] N. G. Shang, P. Papakonstantinou, M. McMullan, M. Chu, A. Stamboulis, A. Potenza, S. S. Dhesi, H. Marchetto, Adv. Functional Mater. 18 (2008) 3506.

[18] J. F. Wang, S. L. Yang, D. Y. Guo, P. Yu, D. Li, J. S. Ye, L. Q. Mao, Electrochem. Commun.11 (2009) 1892.

[19] K. S. Novoselov, A. K. Geim, S. V. Morozov, D. Jiang, Y. Zhang, S. V. Dubonos, I. V.

Grigorieva, A. A. Firsov, Science 306 (2004) 666.

[20] P. R. Somani, S. P. Somani, M. Umeno, Chem. Phys. Lett. 430 (2006) 56.

[21] Q. Yu, J. Lian, S. Siriponglert, H. Li, Y. P. Chen, S. S. Pei, Appl. Phys. Lett. 93 (2008) 113103.

[22] K. S. Kim, Y. Zhao, H. Jang, S. Y. Lee, J. M. Kim, K. S. Kim, J. H. Ahn, P. Kim, J. Y. Choi, B. H. Hong, Nat. 457 (2009) 706.

[23] M. Y. Zhu, J. J. Wang, B. C. Holloway, R. A. Outlaw, X. Zhao, K. Hou, V. Shutthanandan, D. M. Manos, Carbon 45 (2007) 2229.

[24] B.C. Brodie, Ann. Chim. Phys. 59 (1860) 466.

[25] W. Hummers, R. Offeman Preparation of graphitic oxide J Am Chem Soc, 80 (1958) 1339.

[26] L. Staudenmaier, Ber. Chem. Ges. 31 (2006) 1481.

[27] H.C. Schniepp, J. L. Li, M. J. McAllister, H. Sai, M. Herrera-Alonso, D.H. Adamson, J. Phys. Chem. B 110 (2006) 8535.

[28] J. A. Cracknell, K. A. Vincent, F. A. Armstrong, Chem. Rev. 108 (2008) 2439.

[29] J. Wang, Electroanal. 17 (2005) 7.

[30] H. Liu, J. Gao, M. Q. Xue, N. Zhu, M. N. Zhang, T. B. Cao, Langmuir 25 (2009) 12006.

[31] Y. Wang, Y. M. Li, L. H. Tang, J. Lu, J. H. Li, Electrochem. Commun. 11 (2009) 889.

[32] H. W. Kroto, J. R. Heath,S. C. O'Brien, R. F. Curl RF, R. F. Smalley, Nature 318 (1985)162.

[33] A. Ikeda, Y. Suzuki Y, M. Yoshimura, S. Shinkai, Tetrahedron 54 (1998) 2497.

[34] K. E. Geckeler, S. Samal, Polymer International 48 (1999) 743.

[35] G. N. Churilov, Fullerenes, Nanotubes, Carbon Nanostruct.16 (2008) 395.

[36] R. Dagani, Chem. Eng. News 70 (1992) 6.

[37] M. J. Rosseinsky, A. P. Ramirez, S. H. Glarum, D. W. Murphy, R. C. Haddon, A. F. Hebard, T. T. M. Palstra, A. R. Kortan, S. M. Zahurak, A. V. Makhija, Phys. Rev. Lett. 66 (1991) 2830.

[38] N. F. Goldshleger, Fullerene Sci. Technol. 9 (2001) 255.

[39] I. C.Wang, L. A. Tai, D. D. Lee, P. P. Kanakamma, C. K. F. Shen, T. Y. Luh, C. H. Cheng, K. C. Hwang, J. Med. Chem. 42 (1999) 4614.

[40] Q. Bao, C. M. Li, L. Liao, H. Yang, W. Wang, H. Yu, T. Loh, K. P. Guo, Nanotechnology 20 (2009) 65203.

[41] A. Krishnan, E. Dujardin, T. W. Ebbesen, P. N. Yianilos, M. M. J. Treacy, Phys. Rev. 58 (1998) 14013.

[42] M. P. Siegal, D. L. Overmyer, P. P. Provencio, Appl. Phys. Lett. 80 (2002) 2171.

[43] S. Iijima, Nature 354 (1991) 56.

[44] B. S. Sherigara, W. Kutner, F. D. Souza, Electroanalysis 15 (2003) 753.

[45] G. G. Wildgoose, C. E. Banks, H. C. Leventis, R. G. Compton, Microchim. Acta 152 (2006) 187.

[46] G. G. Wildgoose, S. J. Wilkins, G. R. Williams, R. R. France, D. L. Carnahan, L. Jiang, R. G. Compton, Chem. Phys. 6 (2005) 352.

[47] R. N. Adams, Electrochemistry at Solid Electrodes, Marcel Dekker, New York 1969.

[48] J. P. Salvetat, G. A. D. Briggs, J. M. Bonard, R. R. Bacsa, A. J. Kulik, Phys. Rev. Lett. 82 (1999) 944.

[49] A. B. Kuzmenko, E. Van Heumen, F. Carbone, D. Van Der Marel, Phys. Rev. Lett. 100 (2008) 117401.

[50] Z. Wu, S. Pei, W. Ren, D. Tang, L. Gao, B. Liu, F. Li, C. Liu, H.Cheng, Adv. Mater. 21 (2009) 1756.

[51] M. Ishigami, J. H. Chen, W. G. Cullen, M. S. Fuhrer, E. D. Williams, Nano Lett. 7 (2007) 1643.

[52] D. Yu and F. Liu, Nano Lett. 7 (2007) 3046.

[53] K. A. Ritter and J. W. Lyding, Nat. Mater. 8 (2009) 235.

[54] M. Trojanowicz, Trac-Trends Anal. Chem. 25 (2006) 480.

[55] A. Incze, A. Pasturel, C. Chatillon, Appl. Surf. Sci. 177 (2001) 221.

[56] D. Aurbach, B. Markovsky, I. Weissman, E. Levi, Y. Ein-Eli, Electrochim. Acta 45 (1999) 67.

[57] K. Xu, P. D. Ye, J. Phys. Chem. C 114 (2010) 10505.

[58] J. H. Warner, M. H. Rümmeli, A. Bachmatiuk, B. Büchner, Nanotechnology 21 (2010) 325702

[59] A. Incze, A. Pasturel, C. Chatillon, Appl. Surf. Sci., 177 (2001) 221.

[60] P. Koskinen, S. Malola, H. Ha´kkinen, Phys. Rev. Lett. 101 (2008) 121.

[61] J. Ferna´ndez-Rossier, J. J. Palacios, Phys. Rev. Lett., 99 (2007) 177.

[62] F.L. Cheng, S. Du, B.K. Jin, Chin. J. Chem., 21 (2003) 436.

[63] Y.D. Zhao, Y.H. Bi, W.D. Zhang, Q.M. Luo, Talanta 65 (2005) 489.

[64] M.D. Rubianes, G.A. Rivas, Electrochem. Commun. 5 (2003) 689.

[65] M. Trojanowicz, A. Mulchandani, M. Mascini, Anal. Lett. 37 (2004) 3185.

[66] L. L. Song, X. H. Zheng, R. L. Wang, Z. Zeng, J. Phys. Chem. C 114 (2010) 12145.

[67] P. Koskinen, S. Malola, H. Hakkinen, Phys. Rev. Lett. 101 (2008) 115502.

[68] G. P. Lopinski, V. I. Merkulov, J. S. Lannin, Phys. Rev. Lett., 80 (1998) 4241.

[69] G. A. J. Amaratunga, M. Chhowalla, C. J. Kiely, I. Alexandrou, R. Aharonov, R. M. Devenish, Nature 383 (1996) 321.

[70] International carbon black directory and source book, 1999.

[71] K. Mustafa, M. Mustafa, M. A. Ahamad, J. Nat. Rubber Res., 12 (2009) 27.

[72] D. Li, G. Sun, Dyes Pigm. 72 (2007) 144.

[73] F. Fabry, G. Flamant, L. Fulcheri, Chem. Eng. Sci. 56 (2001) 2123.

[74] J. B. Donnet, R. C. Bansal, and M. J. Wang, Carbon black, Marcel Dekker, New York, ISBNO-8247-8975-X.

[75] J.B. Donnet, R.C. Banasal, M.J. Wang, Carbon Black—Science and Technology (2nd ed.) Marcel Dekker, New York 1993.

[76] J. Yu, Q. Zhang, J. Ahn, S. F. Yoon, R. Y. J. Li, B. Gan, K. Chew, K. H. Tan, Mater. Sci. Eng., B 90 (2002) 16.

[77] S. Iijima, Mater. Sci. Eng. B 19 (1993) 172.

[78] A. Al Khawwam, C. Jama, P. Goudmand, O. Dessaux, A. El Achari, P. Dhamelincourt, G. Patrat, Thin Solid Films, 408 (2002) 15.

[79] J. Deppe, A. Emelianov, A. Eremin, H. Jander, HG. Wagner, I. Zaslonko, Phys. Chem. 214 (2000) 129.

[80] S. M. Macdonald, K. Szot, J. Niedziolka, F. Marken, M. Opallo, J. Solid State Electrochem. 12 (2008) 287.

[81] L. Vidal, A. Chisvert, A. Canals, E. Psillakis, A. Lapkin, F. Acosta, K. J. Edler, J. A. Holdaway, F. Marken, Anal. Chim. Acta 616 (2008) 28.

[82] J. D. Watkins, R. Lawrence, J. E. Taylor, S. D. Bull, D. Steven, G. W. Nelson, W. Geoffrey, J. S. Foord, D. Wolverson, L. Rassaei, N. D. M. Evans, D. M. Nick, S. A. Gascon, S. A. Gascon, F. Marken, Phys. Chem. Chem. Phys. 12 (2010) 4872.

[83] N. B. Ibrahim, K. Lawrence, T. D. James, F. J. Xia, M. Pan, J. M. Mitchels, M. Marken, Sens. Actuators, B 161 (2012) 184

Chapter 3

Voltammetry of Cobalt(II)phthalocyanine (CoPc) at 4-(3-Phenylpropyl)pyridine Microdroplet | Aqueous Electrolyte | Electrode Triple Phase Boundary Interfaces

---

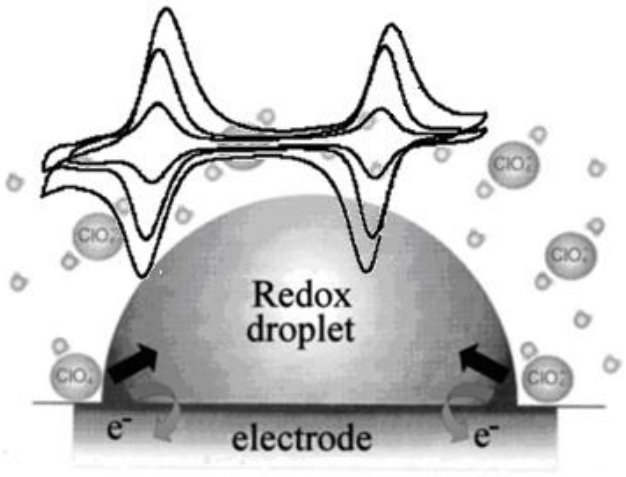

Publication: Parts of this work have been published in "Ion Transport Across Liquid | Liquid Interfacial Boundaries Monitored at Generator-Collector Electrodes" by A. Vuorema, H. Meadows, N. Bin Ibrahim, J. Del Campo, M. Cortina-Puig, M.Y. Vagin, A.A. Karyakin, M. Sillanpaa, F. Marken, Electroanalysis 22 (2010) 2889-2896.

Content

Abstract

Abstract

In this chapter, a novel way to detect CO_2 gas based on ion transfer processes at a triple phase junction graphite | 4-(3-phenylpropyl)pyridine | aqueous electrolyte is investigated. Cobalt(II)phthalocyanine (or Co(II)Pc) is readily dissolved in the organic 4-(3-phenylpropyl)pyridine microdroplet phase and it exhibits reduction and oxidation processes which are coupled to liquid | liquid ion transfer. Both cation transfer for Co(III/II) and cation transfer for Co(II/I) are observed. In order to maintain charge neutrality, each one-electron oxidation (or reduction) process is coupled to the expulsion (or insertion) of cations (here Li^+, Na^+, K^+, Ca^{2+}, Mg^{2+} or NH_4^+). The introduction of CO_2 into the triple phase boundary system results in different potential shifts for all cation types studied.

3.1. Introduction

3.1.1. Introduction to Metallophthalocyanine (MPc) Redox Systems

Metallophthalocyanines (MPcs) complexes are synthetically produced electrochemically active materials, structurally similar to that of porphyrins, with a wide range of interesting properties. MPcs have long been known as an important compound in the pigment and ink industry. However, their unique physicochemical properties have led them to be used in many applications such as photocopying, laser

printing, oil sweetening and in infrared devices. Previous studies on MPs have proven that compared to porphyrins, they can easily fabricated, and possesses better stability towards degradation [1,2,3,4]. Their ability to absorb visible light has led themselves to be a key element in the construction of solid state photovoltaic cells and as a sensitizer in large band gap semiconductors. Extensive studies have also shown that MPcs are excellent candidates as an electrochemical reaction catalyst [5] for oxidations of such as oxidations of thiols [6], sulphide ions [7], hydrazine [8], hydrogen peroxide [9], nitrite [10], and nitric oxide [11], while capable of reducing oxygen and carbon dioxide [12]. The main contributor for its electrocatalytic properties lies on the binding behaviour of the metal center with the ligand sphere (see Figure 3.1.)

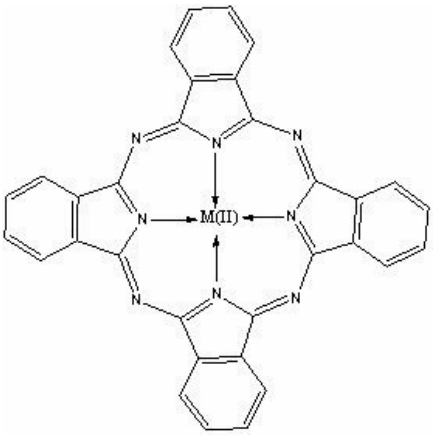

Figure 3.1. Molecular structure of metallophthalocyanine complexes

Many applications of MPcs as redox active materials in the aqueous solutions are based on the oxidation of either the metal center or the phthalocyanine ring. Typically, the oxidation state of the phthalocyanine ring is Pc^{2-}, and can be oxidized twice which can twice undergo ($Pc^{2-} \rightarrow Pc^{-} \rightarrow Pc^{0}$), meanwhile showing maximum number of up to four consecutive reduction processes ($Pc^{2-} \rightarrow Pc^{3-} \rightarrow Pc^{4-} \rightarrow Pc^{5-}$

→ Pc^{6-}). On the other hand, the metal center which consist of the transition metals, are also capable of showing reversible process. The ability of metal center to provide with redox processes is mainly due to its favourable interaction with the axial ligands from solvents, and these properties are often characterized using spectroelectrochemical methods.

The deposition method of MPcs plays an a very important effect inthe resulting physical properties. Previous studies revealed that MPcs which are only soluble in organic solvents are normally used in electrode modifications via adsorption [12,13,14,13] or casting [14] methods.

In this chapter, electrochemical processes are studied for a novel system, microdroplet of 4(-3-phenylpropyl)-pyridine (PPP) immobilized at a basal plane graphite electrode. The organic solvent PPP is a non-volatile, highly immiscible, and a suitable medium for water insoluble transition metal complexes such as those of porphyrins or phthalocyanines. It has been shown in the previous studies that cobalt(II)tetraphenylporphyrin (CoTPP) possesses a well known redox system [15] associated with naturally occurring vitamin B12 or cobalamin systems [16,17,18], which show electrocatalytic properties in hydrophobic environment [19]. CoTPP is known to be selectively soluble in certain organic solvents and totally insoluble in aqueous solutions. On this basis, the redox system of cobalt(II)phthalocyanine is selected and investigated under triple phase boundary conditions in the absence and in the presence of carbon dioxide. The effects of varying the aqueous solution containing different types of electrolyte cations are investigated.

3.1.2. Introduction to Electrode - Liquid - Liquid Triple Phase Boundary Redox Processes

Redox processes at triple phase boundary systems are of interest in a range of technologies in particular in fuel cell processes [20]. The particular case of electrode | liquid | liquid line interfaces has been studied over the past decade [21] and applications have been suggested in particular in sensing [22]. When oil droplets are deposited onto the electrode surface ion transfer into the organic oil phase is possible and in particular with ionophores like boronic acids [23] facilitated and selective ion transfer becomes possible. One benefit of this approach is due to the removal of interferences which are not able to cross the liquid | liquid phase boundary.

For gas sensing applications electrode | liquid | liquid triple phase boundary systems have not been previously investigated. In this chapter a metal complex based on a phthalocyanine is studied with the ability to undergo both oxidation (coupled to anion transfer) and reduction (coupled to cation transfer). Processes are investigated first under inert atmosphere and then under CO_2.

3.2. Experimental

3.2.1. Reagents

Typically, 4 mg of cobalt(II)phthalocyanine (Co(II)Pc) was dissolved in 80 mg 4-(3-phenylpropyl)pyridine (see Figure 3.1) then added to 10 mL acetonitrile to provide deposition solution. Fresh solutions were made for each set of testing, as the solutions in acetonitrile were only stable for several hours before the complex would precipitate. Deionised water was taken from an Elgastat filter system (Elga, Bucks, UK) with a resistivity of not less than 18 MΩ cm and was used to prepare 0.1 M aqueous electrolyte solutions of $LiClO_4$, $KClO_4$, $NaClO_4$, $Ca(ClO_4)_2$, $Mg(ClO_4)_2$, or NH_4ClO_4. Chemical reagents used were of purest commercially available grade.

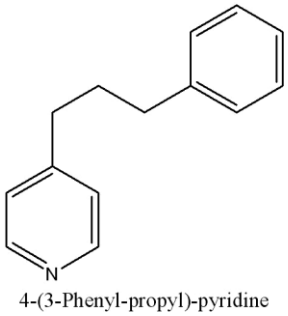

Figure 3.1. Molecular structure of PPP.

3.2.2. Instrumentation

Voltammetric measurements were conducted with a μ-Autolab potentiostat system (Eco Chemie, The Netherlands) in a conventional three-electrode electrochemical cell. Experiments were performed in staircase voltammetry mode with platinum gauze counter and saturated calomel reference electrode (SCE, REF401, Radiometer). A 4.9 mm diameter basal plane pyrolytic graphite electrode (Pyrocarbon, Le Carbone, UK) was used as the working electrode. The electrode was cleaned by polishing on a fine carborundum paper after each use. Aqueous solutions were thoroughly de-aerated

with nitrogen gas (BOC) prior to conducting experiments. All experiments were performed at a temperature of 22 ± 2°C.

For Scanning Electron Microscopy (SEM), a Leo 1530 system was used. Samples were prepared by scratching and gold sputter coating prior to analysis. The surface composition of the modified electrodes were analyzed by energy dispersive X-ray (EDX) analyzer. The operating voltage of electronic beam was 20 keV for morphological observation and 16 keV for EDX analysis.

3.2.3. Procedures

All experiments were conducted using a 4.9 mm diameter basal plane pyrolytic graphite electrode. Typically 10 μL of the deposition solution was placed onto the basal plane pyrolytic graphite electrode surface and after evaporation of the acetonitrile phase an electrochemically active microdroplet deposit of PPP with dissolved CoPc remained [24].

3.3. Results and Discussion

3.3.1. CoPc Microdroplet Voltammetry I.: Effects of the Deposition Volume, Scan Rate, and Concentration

Initially, the behaviour of Co(II)Pc dissolved in 4-(3-phenylpropyl)-pyridine (or PPP) is investigated in the form of microdroplets immobilised on graphite and immersed in aqueous 0.1 M $NaClO_4$. The schematic drawing in Figure 3.2.A describes the situation where reactive edges, the triple phase boundary, are formed between the electrode surface, the aqueous phase, and the organic phase. In Figure 3.2.B typical cyclic voltammograms are shown. There are two types of processes: the oxidation at 0.2 V vs. SCE (see equation 3.1) and the reduction at -0.7 V vs. SCE (equation 3.2).

$$Co(II)Pc(oil) + ClO_4^-(aq) \leftrightarrow Co(III)Pc^+(oil) + e^- + ClO_4^-(oil) \quad (3.1)$$

$$Co(II)Pc(oil) + e^- + Na^+(aq) \leftrightarrow Co(I)Pc^-(oil) + Na^+(oil) \quad (3.2)$$

The oxidation is associated with the transfer of the anion, Perchlorate, from the aqueous phase into the organic PPP phase. Similarly, the reduction is associated with the transfer of the cation, here Na^+. By changing the amount of deposit on the electrode surface the size and shape of voltammetric responses is affected. In Figure 3.2.C it can be seen that increasing the amount of deposit at the electrode surface initially causes an increase and then a decrease in peak current data. This and the considerable broadening of the voltammetric signals at higher levels of deposit indicate formation of bigger droplets and "flooding" of the electrode surface leading to passivation. The optimum deposition volume appears to be 10 μL.

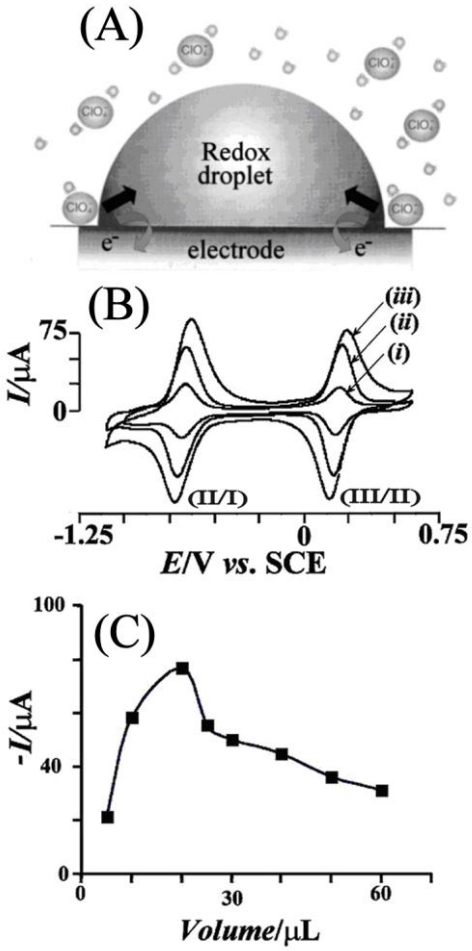

Figure 3.2. (A) Schematic drawing of a redox active microdroplet deposited onto an electrode. Electron transfer and ion transfer are coupled at the triple phase boundary. (B) Cyclic voltammograms (scan rate 0.05 Vs^{-1}) for a deposition volume of (i) 5 μL, (ii) 10 μL, and (iii) 20 μL) of a solution of 84 mM Co(II)Pc in 4-(3-phenylpropyl)-pyridine, immobilized onto a 4.9 mm diameter basal plane pyrolytic graphite electrode and immersed in aqueous 0.1 M $NaClO_4$ solution. (C) Plot of reduction peak versus deposition volume.

Figure 3.3.A shows typical voltammograms obtained to explore the effect of scan rate on the voltammetric signals. Well defined voltammograms for both reduction and oxidation are observed over a range of scan rates (from 5 to 100 mV s^{-1}) and the linear

increase in the peak current (see Figure 3.3.B) is consistent with quick bulk electrolysis of the content of microdroplets deposited on the basal plane pyrolytic graphite electrode.

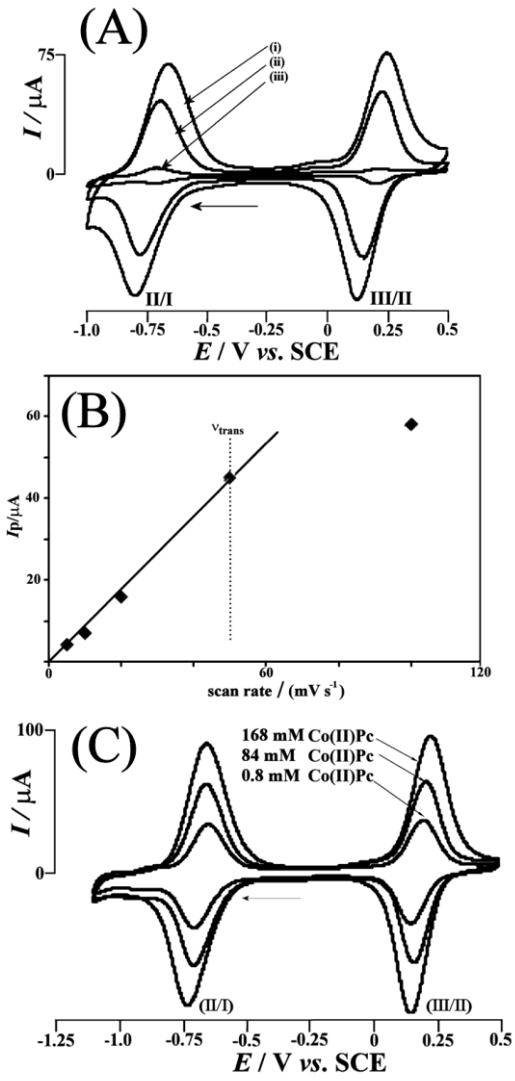

Figure 3.3. (A) Cyclic voltammograms (scan rate of (i) 0.1 Vs^{-1}, (ii) 0.05 Vs^{-1}, and (iii) 0.01 Vs^{-1}) for the reduction / oxidation of a 80 nL deposit of a solution of 84 mM Co(II)Pc in 4-(3-phenylpropyl)pyridine, immobilized onto a 4.9 mm diameter bppg electrode and immersed in aqueous 0.1 M $NaClO_4$ solution. (B) Plot of reduction peak current versus scan rate. (C) Cyclic voltammograms (scan rate 0.05 V s^{-1}) for the reduction / oxidation of 168 mM Co(II)Pc, 84 mM Co(II)Pc, and 42 mM Co(II)Pc in 80 nL 4-(3-phenylpropyl)-pyridine, immobilized onto a 4.9 mm diameter basal plane pyrolytic graphite electrode and immersed in aqueous 0.1 M $NaClO_4$ solution.

The peak-to-peak separation between reduction and oxidation responses for Co(II/I) and Co(III/II) systems decreased from ca. 100 mV to 82 mV and down to 15 mV for

scan rates of 100 mV s^{-1}, 50 mV s^{-1}, and 20 mV s^{-1}, respectively. Integration of the current under the peaks for each case suggested absence of loss mechanisms and full chemical reversibility.

The shape of the voltammetric response for the immobilized organic phase is almost symmetric and bell-shaped for thin films (finite diffusion), but a distinct diffusion tail is observed for thicker film deposits (semi-infinite diffusion). The transition from finite to semi-infinite diffusion characteristics can be observed when the scan rate was varied. The plot in Figure 3.3.B demonstrates how the cathodic peak current is proportional directly to scan rates whereas at higher scan rates proportionality to the square root of scan rate was observed. The transition point (or transition scan rate ν_{trans}) in diffusion characteristics can be obtained from this plot (see dotted line).

The concentration of Co(II)Pc in PPP has a considerable effect on the voltammetric characteristics. Figure 3.3.C shows cyclic voltammograms obtained for the reduction and oxidation of 168 mM Co(II)Pc, 84 mM Co(II)Pc, and 42 mM Co(II)Pc deposited onto a bppg electrode. Under these conditions, both the peak currents and the charge under the peaks are approximately proportional to the concentration of Co(II)Pc within the microdroplet up to high concentrations (linear up to ca. 100 mM).

The most interesting feature of the triple phase boundary redox processes investigated here is the coupled transfer of electrons and ions (both cations and anions). Therefore, in the next section the effect of the supporting electrolyte on the ion transfer is investigated.

3.3.2. CoPc Microdroplet Voltammetry II.: Effects of the Supporting Electrolyte

In order to investigate the effect of the electrode | liquid | liquid ion exchange process coupled to the electron transfer, experiments in different concentrations and types of aqueous electrolytes were conducted. Figure 3.4.A shows the effect of changing the $NaClO_4$ solution concentration on oxidation and reduction responses for the Co(II)Pc redox system.

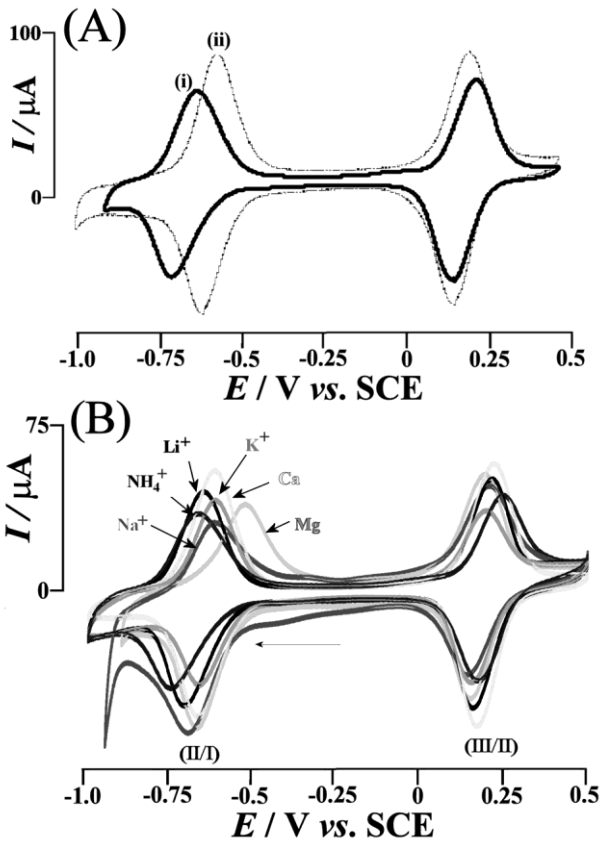

Figure 3.4. (A) Cyclic voltammograms (scan rate 0.05 Vs^{-1}) for the reduction / oxidation of 80 nL deposit of a solution of 84 mM Co(II)Pc in 4-(3-phenylpropyl)-pyridine, immobilized onto a 4.9 mm diameter basal plane pyrolytic graphite electrode, and immersed in aqueous (i) 0.1 M and (ii) 1.0 M $NaClO_4$ solution. (B) Cyclic voltammograms (scan rate 0.05 V s^{-1}) for the reduction / oxidation of 80 nL deposit of a solution of 84 mM Co(II) Pc in 4-(3-phenylpropyl)-pyridine, immobilized onto a 4.9 mm diameter bppg electrode, and immersed in aqueous 0.1 M solutions of $NaClO_4$, $KClO_4$, $LiClO_4$, $Mg(ClO_4)_2$, $Ca(ClO_4)_2$, and NH_4ClO_4.

In the presence of more sodium ions, Na^+, the reduction of Co(II/I) becomes more facile and therefore the reduction is detected at less positive potential. The oxidation process, Co(III/II), is proposed to be accompanied by the transfer of an anion from the aqueous phase into the organic phase. In contrast, the charge balance during reduction, Co(II/I), is achieved via transfer of a metal cation from the aqueous phase into the organic phase. It was observed that the midpotential of Co(II/I)Pc redox process in 0.1 M $NaClO_4$ solution shifted to a more positive potential in 1 M $NaClO_4$ solution. This can be explained from the Nernst equation, which predicts that when the cation concentration in the electrolyte solution is increased, a shift towards more positive potential value is expected. The same argument is valid for the Co(III/II) redox system, where the same shift of midpotential value is expected in the opposite direction. Experimentally, the total shift of Co(II/I) and Co(III/II) midpoints is ca. 120 mV consistent with the Nernst equation prediction, however, the shift appears to be dominated by the Co(II/I) system (see Figure 3.4.A). This is caused here by perchlorate affecting the reference electrode.

Figure 3.4.B shows the voltammetric responses obtained for the reduction and oxidation of Co(II)Pc system in aqueous 0.1 M solutions of $NaClO_4$, $KClO_4$, $LiClO_4$, $Mg(ClO_4)_2$, $Ca(ClO_4)_2$, and NH_4ClO_4. Almost all Co(III/II) redox processes tested in various electrolyte solutions appeared superimposed at a midpoint potential of 0.210 V vs. SCE which is consistent with the reversible transfer of ClO_4^-. The voltammetric responses for the Co(II/I) system, which are coupled to cation transfer, show a distinct shift for each type of cation used. The reduction potential of Co(II/I) seemed to have varied over different types of cations used, while the reduction potential of Co(III/II) almost remained unchanged.

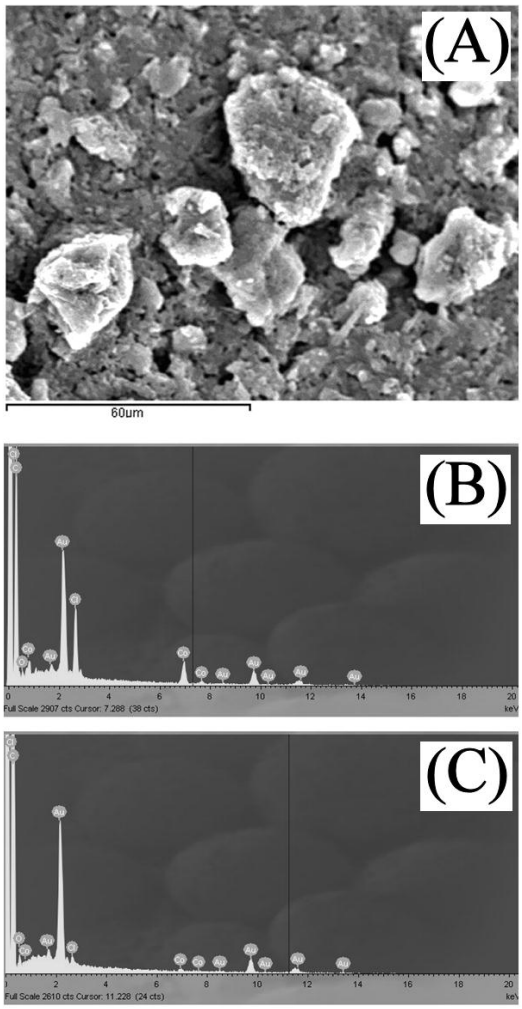

Figure 3.5. (A) Typical SEM image of the graphite surface with deposits formed from 84 mM Co(II)Pc in 4-(3-phenylpropyl)-pyridine immobilized onto a 4.9 mm diameter basal plane, dipped into 0.1 M $NaClO_4$ solution, and oxidised at 0.5 V vvs. SCE. (B) EDX spectrum for an oxidised deposit containing $Co(III)Pc^+$ and ClO_4^-. (C) EDX spectrum for a deposit containing Co(II)Pc.

The surface of the electrode was investigated with scanning electron microscopy (SEM) and energy dispersive x-ray spectroscopy (EDX). The image in Figure 3.5.A reveals particulate materials, possibly mixed with graphite. The EDX spectrum in Figure 3.5.B shows the presence of Co(III) and ClO_4^-, while Figure 3.5.C shows the

presence of Co(II) without ClO_4^- microdroplets consistent with the proposed anion transfer process.

3.3.3. CoPc Microdroplet Voltammetry III.: Effects of Carbon Dioxide

Given the sensitivity to cation transfer, it was envisaged that CO_2 could have an interesting effect on the Co(II/I)Pc redox process by changing the ability of the cation to transfer. CO_2 gas when bubbled through the aqueous electrolyte solution is likely to be enriched in the organic phase where solubility can be substantially higher. The following Figure 3.6 shows the voltammetric responses of Co(II)Pc immersed in electrolytes containing different cations in the absence and presence of carbon dioxide. In each case, a potential shift can be seen resulting from the introduction of carbon dioxide into the redox system. The effect for potassium containing electrolyte is most dramatic. The shift of the midpoint potential (ca. 0.238 V) is accompanied by a change in the shape of the voltammogram. It is suggested that a fast equilibrium of Co(I)Pc binding to CO_2 explains the potential shifts during the reduction of Co(II). The mechanism is coupled to cation transfer in this system (see equations 3.3 to 3.5).

$$Co(II)Pc(oil) + e^- + M^+(aq) \leftrightarrow Co(I)Pc^-(oil) + M^+(oil) \quad (3.3)$$

$$Co(I)Pc^-(oil) + CO_2 \leftrightarrow Co(I)Pc(CO_2)^-(oil) \quad (3.4)$$

$$Co(I)Pc(CO_2)^-(oil) + M^+(oil) \leftrightarrow Co(I)Pc(CO_2)^-M^+(oil) \quad (3.5)$$

As suggested in equation (3.3) the reduction of Co(II)Pc is accompanied by a cation transfer from the aqueous solution into the organic phase. The $Co(I)Pc^-$ resulting from the reduction process is then proposed to interact with CO_2 to produce an adduct, possibly $Co(I)Pc(CO_2)^-$ with CO_2 bound to the metal centre (see equation 3.4). The

resulting ion pair in the organic phase is likely to form the neutral complex (equation 3.5).

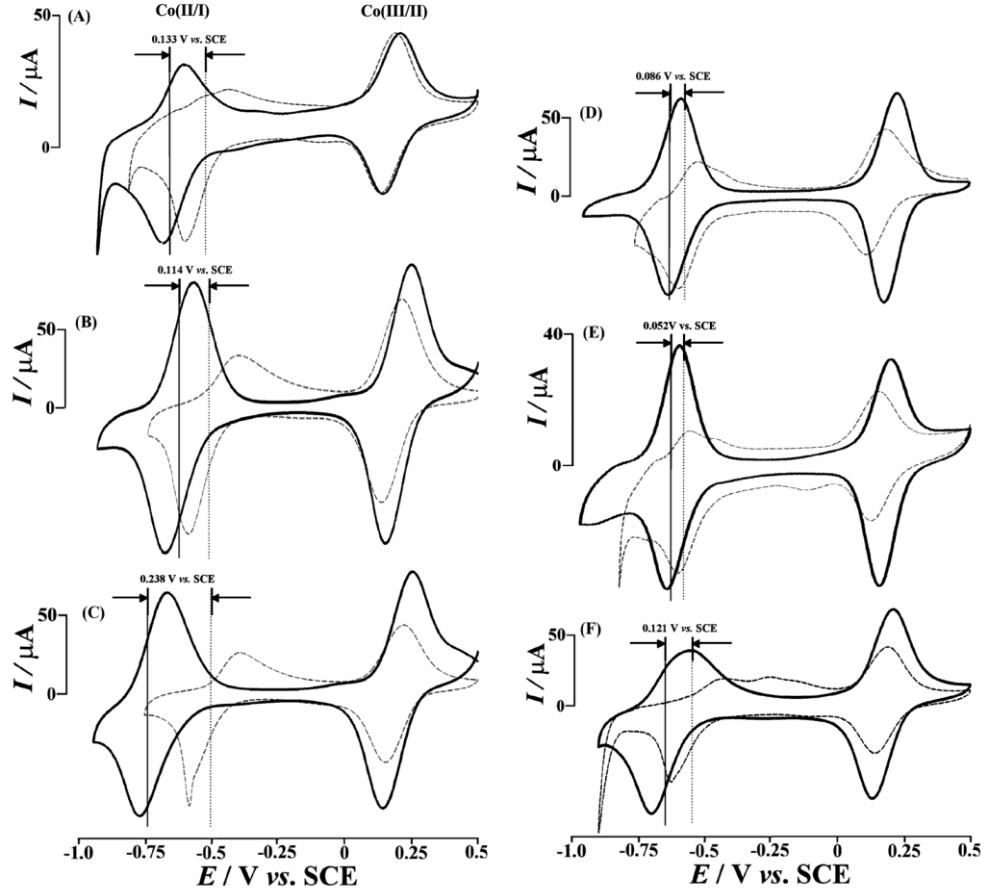

Figure 3.6. (A) Cyclic voltammograms (scan rate 0.05 V s^{-1}) for the reduction / oxidation of 80 nL deposit of a solution of 84 mM Co(II)Pc in 4-(3-phenylpropyl)-pyridine immobilized onto a 4.9 mm diameter bppg electrode and immersed in aqueous 0.1 M solutions of (A) $LiClO_4$, (B) $NaClO_4$, (C) $KClO_4$, (D) $Mg(ClO_4)_2$, (E) $Ca(ClO_4)_2$, and (F) NH_4ClO_4 in the absence and presence (dotted lines) of CO_2.

Table 3.1 summarized the midpotential shifts for the reduction / oxidation processes of Co(II)Pc. From the table, it was discovered that the largest midpotential shift change of 0.238 V vs. SCE was obtained when potassium ion was used as the transferring cation. In contrast to that, Ca^{2+} exhibited the smallest amount of

midpotential shift of 0.052 V vs. SCE under the same conditions. Potassium also exhibits the most negative midpoint potential which is indicative of the highly hydrophilic nature of this cation.

Table 3.1. Midpoint potential data obtained from cyclic voltammograms (scan rate 0.05 V s^{-1}) for the reduction / oxidation of 80 nL deposit of a solution of 84 mM Co(II)Pc in 4-(3-phenylpropyl)pyridine, immobilized onto a 4.9 mm diameter basal plane pyrolytic graphite electrode, and immersed in aqueous 0.1 M solutions of $NaClO_4$, $KClO_4$, $LiClO_4$, $Mg(ClO_4)_2$, and $Ca(ClO_4)_2$ in the absence and in the presence of CO_2.

	$E_{mid[N2]}$ (*E*/V vs. SCE)	$E_{mid[CO2]}$ (*E*/V vs. SCE)	ΔE_{mid} (*E*/V vs. SCE)
Li^+	-0.678	-0.545	0.133
K^+	-0.768	-0.530	0.238
Na^+	-0.659	-0.546	0.114
Mg^{2+}	-0.641	-0.555	0.086
Ca^{2+}	-0.595	-0.647	0.052
NH_4^+	-0.662	-0.541	0.121

3.4. Conclusions

Well-defined peaks of reduction and oxidation of Co(II)Pc were obtained in the cyclic voltammetric measurements. It was shown that the presence of CO_2 facilitated the cation transfer based on the shifts of reduction process for Co(II)Pc to $Co(I)Pc^-$. This process was measured in the presence of different types of cations in the electrolyte

solutions with potassium showing the biggest effect. The combination of processes at the triple phase boundary has enabled a simple methodology of carbon dioxide detection system to be developed. However, the CO_2 pressure dependence and the effect of interferences are still not established.

3.5. References

[1] C.P. Perollier, A.B. Sorokin, Chem. Commun. 14 (2002) 1548-1549.

[2] B. Meunier, A. Sorokin, Acc. Chem. Res. 30 (1997) 470-476.

[3] A. Sorokin, J. Amer. Chem. Soc. 118 (1996) 7410-7411.

[4] N. Grootboom, T. Nyokong, J. Mol. Catal. A-Chem. 179 (2002) 113-123.

[5] J.H. Zagal, Coord. Chem. Rev. 119 (1992) 89-136.

[6] X.H. Qi, Electroanalysis, 3 (1991) 119-124.

[7] Y.H. Tse, Anal. Chem. 67 (1995) 981-985.

[8] P. Ardiles, J. Mol. Catal. A-Chem. 165 (2001) 169-175.

[9] F. Mizutani, S. Yabuki, S. Iijima, Electroanalysis, 7 (1995) 706-709.

[10] C.A. Caro, F. Bedioui, J.H. Zagal, Electrochim. Acta 47 (2002) 1489-1494.

[11] M. Pontie, H. Lecture, F. Bedioui, Sens. Actuators B-Chem. 56 (1999) 1-5.

[12] H. Aga, A. Aramata, Y. Hisaeda, J. Electroanal. Chem. 437 (1997) 111-118.

[13] D. Schlettwein, T. Yoshida, J. Electroanal. Chem. 441 (1998) 139-146.

[14] S.L. Vilakazi, T. Nyokong, Polyhedron, 17 (1998) 4415-4423.

[15] D.G. Davis, The Porphyrins. D. Dolphin (ed.) Vol. 5., London: Academic Press, 1978.

[16] R. Banerjee, S.W. Ragsdale, Ann. Rev. Biochem. 72 (2003) 209-247.

[17] Y. Hisaeda, Coord. Chem. Rev. 198 (2000) 21-37.

[18] D. Schlettwein, T. Yoshida, J. Electroanal. Chem. 441 (1998) 139-146.

[19] C. Shi, F.C. Anson, Inorg. Chem. 40 (2001) 5829-5833.

[20] F. Marken, J.D. Watkins, A.M. Collins, Phys. Chem. Chem. Phys. 13 (2011) 10036-10047.

[21] C.E. Banks, T.J. Davies, R.G. Evans, G. Hignett, A.J. Wain, N.S. Lawrence, J.D. Wadhawan, F. Marken, R.G. Compton, Phys. Chem. Chem. Phys. 5 (2003) 4053-4069.

[22] N. Katif, R.A. Harries, A.M. Kelly, J.S. Fossey, T.D. James, F. Marken, J. Solid State Electrochem. 13 (2009) 1475-1482.

[23] A.M. Collins, J.D. Watkins, N. Katif, Y.J. Huang, Y.B. Jiang, T.D. James, S.D. Bull, F. Marken, Chem. Commun. 47 (2011) 12002-12004.

[24] F. Marken, J. Electroanal. Chem. 437 (1997) 209-218.

Chapter 4

N,N,N',N'-Tetra-Octyl-2,7-Diamino-9,10-Anthraquinone (TODAQ) Liquid-Liquid Redox Chemistry in a N-Octyl-Pyrrolidone (NOP) Microdroplet: pH and Cation Sensitivity

---

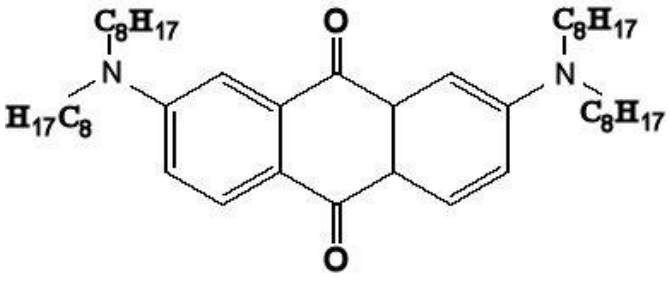

Acknowledgement: James E. Taylor and Dr. Stephen D. Bull are gratefully acknowledged for synthesis of TODAQ.

Content

Abstract

Basal plane pyrolitic graphite (bppg) electrodes are employed immobilized with a redox active species, N,N,N',N'-tetra-octyl-2,7-diamino-9,10-anthraquinone (TODAQ) immobilized within a water-insoluble organic phase of N-octyl-2-pyrrolidone (NOP), and immersed into aqueous electrolyte. TODAQ is shown to undergo a two-electron - two-proton redox process similar to conventional anthraquinone systems but with purely organic phase based reactivity. The effect of pH and other metal cations is investigated and a surprising metal binding effect is observed. A switch from proton transfer to cation transfer with formation of a new solid phase is suggested. The potential for application in pH sensing is discussed.

4.1. Introduction

4.1.1. Introduction to pH Sensors

pH measurements is one of the key steps in any chemical reactions. Not only in academia, it is also widely important in industry. Nowadays, pH sensors exist in many forms from the most simplest pH strips for home diagnostics to the expensive glass membrane pH meters with complex and multiple functions. Despite the advance and

enhanced performance of glass membrane pH sensors, it is vulnerable to colloids and is cannot be cleaned. Other typical pH sensors in general are constructed based on potentiometric method [1,2,3,4,5,6,7], but their efficiency is always affected by its instability and or/drift, hence require constant recalibrations[8].

Potential drift has been known as a major problem in many commercial pH sensors. In order to overcome this issue, a method based on measuring the difference between two potential peaks has been suggested. The first involves the usage of alkylferrocene which is the pH insensitive part, followed by the second, the pH sensitive alkylthiol counterpart [9]. Studies following this aim on designing a pH probe with enhanced performance using various types of functional materials with redox active properties, sensitive to pH changes. Although it contributes in solving issues present in self-assembled monolayer-based designs, the requirement of having many components mixed in segregated compartments led to a major problem at the manufacturing stage. For this reason, there is always an urge of developing new types of pH measuring devices.

Up to date, sequential studies have been targeted at producing single component pH sensors which contain both pH sensitive and insensitive properties. e.g. polymeric molecule [10]. To a large extent, these kinds of compounds proved to be capable of providing with better stability compared to conventional systems, there were still inherent drawbacks when measurement were conducted in many different aqueous solutions [11].

This report examines the possibility of developing a pH sensing probe based on the redox chemistry of a new type of anthraquinone derivative, N,N,N',N'-tetra-octyl-2,7-diamino-9,10-anthraquinone (TODAQ). It has been shown previously that the application of derivatization of carbon particles by anthraquinoine by chemical, and, anthraquinone-ferrocene film electrodes have resulted in a sensitive reagentless pH probe [12,13]. The use of TODAQ in microdroplets of oil offers potential benefits such as a separate organic reaction zone free of hydrophilic interferences, insensitivity to colloids, and ease of fabrication and use.

4.1.2. Introduction to Anthraquinone Redox Systems

Anthraquinones (AQs) have hystorically been used as dyes. They have a structure that resembles to that of anthracene. Many studies on Anthraquinone derivatives have been mainly focused on their potential use in chemistry, biochemistry and pharmacology. It has been reported that AQs are capable of binding to nucleotides, thus being used in protein purification process via affinity technique [14]. In recent development, it was reported that both synthetic and natural AQ derivatives have been used for medical purposes, such as anticancer drugs and antitumor agents [15]. In biological electron transport, AQs plays an important role in cellular respiration [16], while been popularly used in industry as redox catalyst [17,18]. In general, the reduction anthraquinone is always represented as showing single voltammetric signal eventhough is based on the two electrons two protons reactions in aqueous phase (see equation 4.1)

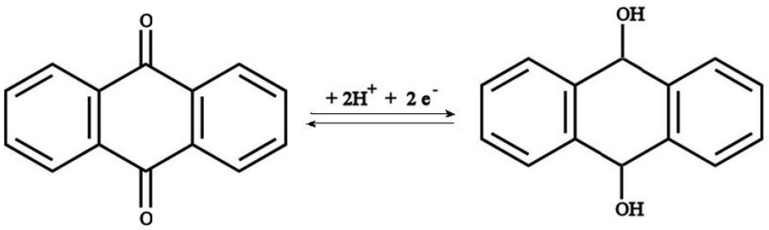

(4.1)

This equation is considered valid for redox processes in aqueous or biphasic media for the new anthraquinone derivative, N,N,N',N'-Tetra-Octyl-2,7-Diamino-9,10-Anthraquinone (TODAQ) used here. A similar compound has been studied for example by Shamsipur et al. [19]. This molecule has been designed (see Figure 4.1) to be extremely hydrophobic with four octyl-groups to achieve (i) high solubility in the organic phase, (ii) negligible solubility in the aqueous phase, and (iii) no tendency to crystallise.

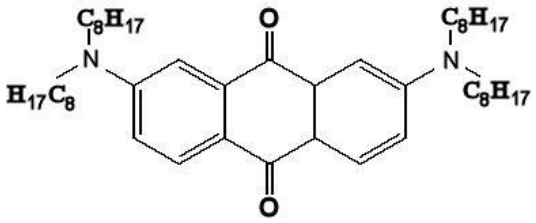

Figure 4.1. Molecular structure of N,N,N',N'-tetra-octyl-2,7-diamino-9,10-anthraquinone or TODAQ

4.2. Experimental

4.2.1. Chemicals

Chemical reagents such as N-Octyl-2-pyrrolidone (NOP), phosphoric acid and NaOH were purchased from Aldrich and used without further prurification. Solution were prepared by dissolving 4 mg N,N,N',N'-tetra-octyl-2,7-diamino-9,10-anthraquinone (TODAQ) in 80 mg N-Octyl-2-pyrrolidone (NOP) by gentle agitation and heating. Filtered and demineralized water was taken from an Elgastat filter system (Elga, Bucks, UK) with a resistivity of not less than 18 MΩ cm resistivity.

Typically, 4 mg of N,N,N',N'-Tetra-Octyl-2,7-Diamino-9,10-Anthraquinone (TODAQ) was dissolved in 80mg N-Octyl-2-pyrrolidone (NOP) then added to 10 ml acetonitrile (50-fold dilution) to provide deposition solutions. Deionised water was taken from Elgastat filter system (Elga, Bucks, UK) with a resistivity of not less than 18 MΩ cm and was used to prepare 0.1 M aqueous electrolyte solutions of $Zn(NO_3)_2$, NH_4NO_3, $Ba(NO_3)_2$, or $NaNO_3$. Chemical reagents used were of purest commercially available grade.

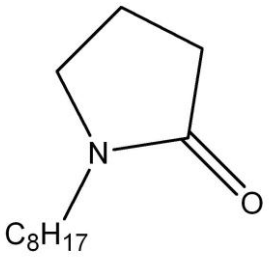

1-Octyl-pyrrolidin-2-one

Figure 4.2. Molecular structure of the solvent N-Octyl-2-pyrrolidone or NOP.

4.2.2. Working Electrode Preparation

All experiments were conducted using a 4.9 mm diameter basal plane pyrolytic graphite electrode. Typically 10 μL of the deposition solution was placed onto the basal plane pyrolytic graphite electrode surface and after evaporation of the acetonitrile phase an electrochemically active microdroplet deposit remained [20].

4.2.3. Instrumentation

Voltammetric measurements were conducted with a μ-Autolab potentiostat system (Eco Chemie, The Netherlands) in a conventional three-electrode electrochemical cell. Experiments were performed in staircase voltammetry mode with platinum gauze counter and saturated calomel reference electrode (SCE, REF401, Radiometer. A 4.9 mm diameter basal plane pyrolytic graphite electrode (Pyrocarbon, Le Carbone, UK) was used as the working electrode. The electrode was cleaned by polishing on a fine carborundum paper after each use. The counter electrode (used to provide the current) was platinum gauze with an SCE reference electrode (used to control the potential). Aqueous solutions were thoroughly de-aerated with argon (BOC) prior to conducting experiments, at temperature of 22 ± 2°C.

For Scanning Electron Microscopy (SEM), a Leo 1530 system was used. Samples were prepared by scratching and gold sputter coating prior to analysis. Atomic force microscopy images were obtained with a Digital Instruments Nanoscope IIIa Multimode Scanning Microscope in the AFM tapping mode. The AFM tips were AC240TS from Olympus. The surface composition of the modified electrodes were analyzed by energy dispersive X-ray (EDX) analyzer. An AMRAY 1810 type SEM

equipped with Link ISIS micro-analyzer was used. The operating voltage of electronic beam was 20 keV for morphological observation and 16 keV for EDX analysis.

4.3. Results and Discussion

4.3.1. TODAQ Voltammetry I.: Effects of Deposition Volume, Scan Rate, and Phosphate Buffer Solution pH

The cyclic voltammetric response of TODAQ immobilized in NOP on a bppg electrode in a 0.1 M phosphate buffer solution pH 7 at various scan rates (10, 100, 200, and 500 mV s^{-1}) are shown in Figure 4.2A. A reduction wave is initially observed at -0.81 V *vs.* SCE with a corresponding oxidation peak at -0.47 V *vs.* SCE consistent with anthraquinone reduction and oxidation. A plot of reduction peak current against square root of scan rate (Figure 4.3B) shows a linear trend over the range of scan rates studied in good agreement with a diffusion-based redox process Most likely here is the diffusion of redox active TODAQ in the NOP microdroplet environment. In Figure 4.2C the reduction peak current increases as the deposition volume is increased from 5 to 20 μL. However, when deposition volume was further increased (more than 20 μL), a decrease in the total charges under the peaks was observed. This can be explained with the depletion of triple phase boundary zone due to the increasing microdroplet sizes and finally a "flooding" of the graphite surface with loss of activity.

In order to determine that cation insertion only occurs at the triple phase boundary, an experiment without the usage of NOP as the organic phase was performed. In this case, the redox active material, TODAQ was immobilized onto the bppg surface in

the form of microcrystals and immersed into aqueous 0.1 M phosphate buffer solution pH 7 at 10 mV s^{-1} (see Figure 4.2.D). The reduction of TODAQ was proven to have occurred despite the absence of NOP as the organic phase. This suggests that electrochemically driven protonation of TODAQ was also possible in solid microcrystalline form. The TODAQ crystals are likely to be "soft" and proton insertion may be facile.

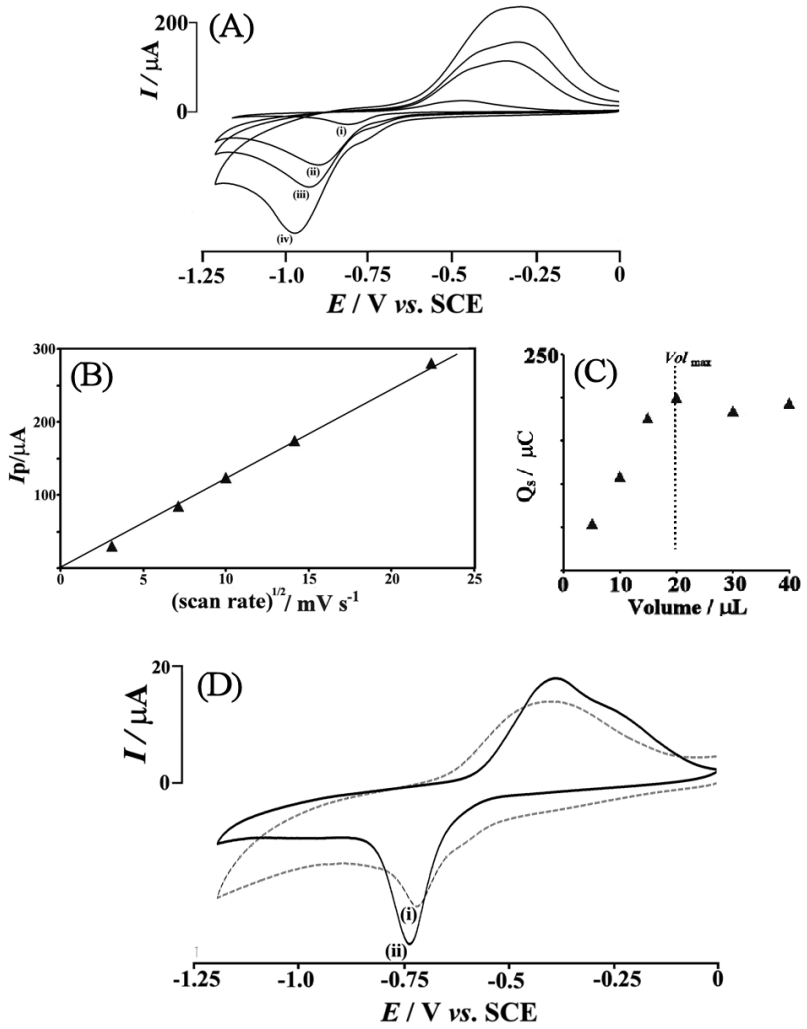

Figure 4.2. (A) Cyclic voltammograms (scan rates (i) 10, (ii) 100, (iii) 200, and (iv) 500 mV s^{-1} for the reduction of 74 nL deposit of 82 mM TODAQ immobilized in NOP microdroplets onto a 4.9 mm diameter bppg electrode, and immersed in aqueous 0.1 M $NaNO_3$. (B) Plot of the cathodic peak current *vs*. root square of scan rate. (C) Plot of the charge under the peak versus the volume of deposit. (D) Cyclic voltammogranms of 74 nL deposit of 82 mM TODAQ in NOP immobilized onto bppg (i) without and (ii) with NOP in 0.1 M phosphate buffer pH 7 aqueous solution.

Next, the effect of pH is investigated. The corresponding cyclic voltammograms in a selected pH range (from pH 2 to pH 10) were recorded for the immobilized TODAQ in NOP on a bppg electrode and are shown overlaid in Figure 4.3.A. As the pH increases, the peak potential shifts towards more negative values thereby making the reduction of the TODAQ more difficult as is expected based on the Nernst equation. The corresponding plot of reduction peak potential versus pH for main reduction wave for nine different pH values studied is given in Figure 4.3.B. In between the range of pH 2 and pH 8, a linear response with a corresponding gradient of ca. 58 mV per pH unit was obtained, which is consistent with a 2-electron 2-proton transfer, and also consistent with previous studies of anthraquinone derivates for example at mercury electrodes [12,13,21,22]. Meanwhile, at higher pH values (pH 9 and 10), an almost plateau-like response was observed. Given the nature of this biphasic process, this is surprising because a charge transfer of cations or anions across the water-organic interface must occur to maintain charge neutrality. If protons don't transfer, probably other cations in the buffer solution can transfer in competition. In general, the overall reaction scheme for TODAQ redox system in the presence of phosphate buffer can be proposed in two different range, acidic (below pH 8) and alkaline (pH 8 and above), as shown in equations 4.2 and 4.3, respectively.

$$\text{pH} > 8 : \text{TODAQ(oil)} + 2\,M^{+}\text{(aq)} + 2\,e^{-} \rightarrow \text{TODAQ}^{2-}\text{(oil)} + 2\,M^{+}\text{(oil)} \quad (4.2)$$

$$\text{pH} < 8 : \quad \text{TODAQ(oil)} + 2\,H^{+}\text{(aq)} + 2\,e^{-} \rightarrow \text{TODAQH}_2 \quad (4.3)$$

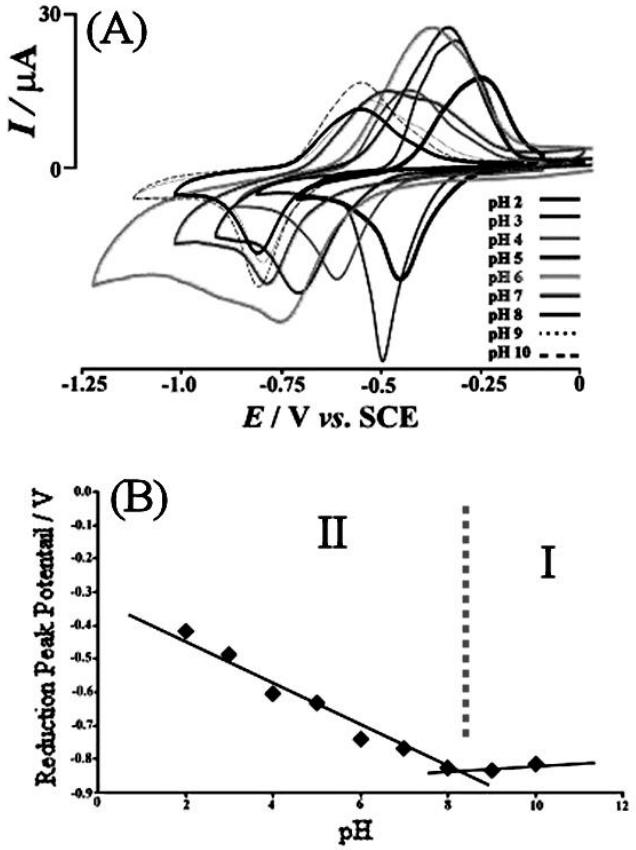

Figure 4.3. (A) Cyclic voltammograms (scan rate 50 mV s^{-1}) detailing the effect of pH values on 74 μL of 82 mM TODAQ immobilized in NOP microdroplets onto a 4.9 mm diameter bppg electrode in 0.1 M phosphate buffer solutions between pH 2 and pH 10. (B) Plot of reduction peak potential against pH for TODAQ immobilized on bppg.

4.3.2. TODAQ Voltammetry II.: Effects of the Type and Concentration of Supporting Electrolyte

Figure 4.4.A below corresponds to voltammograms recorded for the reduction of TODAQ in NOP in three different concentrations of phosphate buffer pH 4 solution. As the PBS concentration was raised from (i) 0.01 M, (ii) 0.1 M, and (iii) 1 M, respectively, it was observed that the voltammograms became more peak-shaped and better defined. This suggests that transfer of proton from the aqueous solution into the

microdroplets is facilitated by the excess presence of proton within the electrolyte. This again is a surprising result given that the activity of protons is not changed (the midpoint potential remains approximately constant). The interfacial process and the interaction of cations with the TODAQ molecule at the liquid – liquid interface could be crucial here.

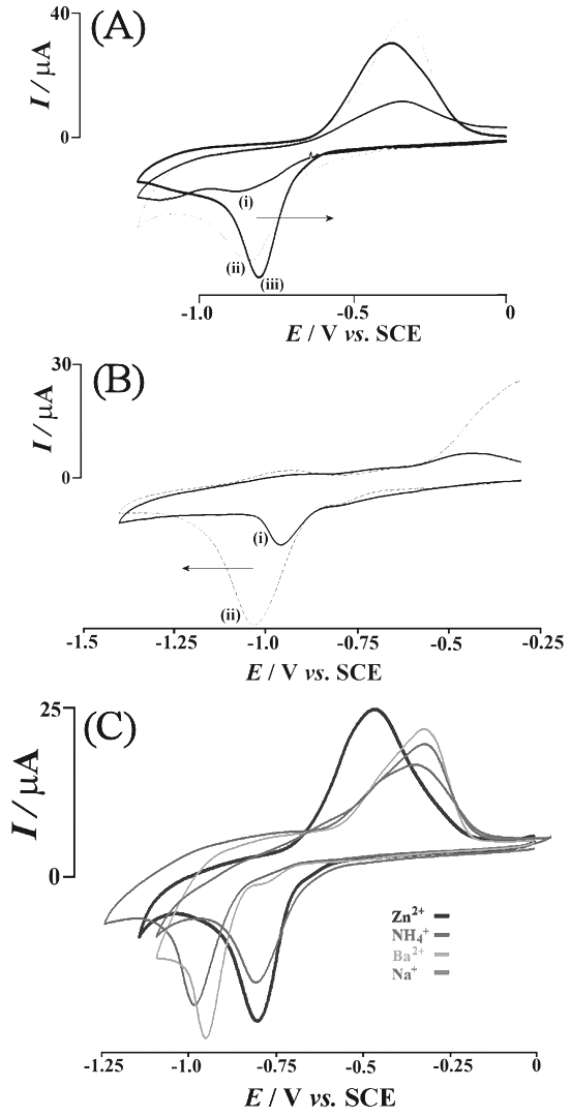

Figure 4.4. (A) Effect of concentration of supporting electrolyte solutions on cyclic voltammograms (at scan rate of 50 mV s^{-1}) for the reduction of 74 nL of 82 mM TODAQ immobilized in NOP microdroplets onto a 4.9 mm diameter bppg electrode in (i) 0.01 M and (ii) 0.1 M and (iii) 1 M phosphate buffer solution pH 4. (B) As above, in (i) 0.1 M and (ii) 1.0 M NaCl aqueous solution. (C) Effect of concentration of electrolyte solutions containing Zn^{2+}, NH_4^+, Ba^{2+} or Na^+ ions on the reduction potential of 74 nL of 82 mM TODAQ immobilized in NOP microdroplets onto a 4.9 mm diameter bppg electrode at scan rate of 50 mV s^{-1}.

Next, the effect of NaCl electrolyte concentration is investigated. In Figure 4.4.B cyclic voltammograms for TODAQ reduction in 0.1 M and in 1.0 M NaCl are shown. Again a pronounced effect is observed and well-defined voltammetric responses are obtained at higher activity. The interaction of Na^+ with TODAQ at the liquid-liquid interface may be crucial in both cases. This kind of interfacial complex could be a crucial intermediate that needs to be present in significant amounts at the location of the three phase boundary for the process to be efficient. This TODAQ – Na^+ interfacial complex could then be reduced to the $TODAQ^-$ - Na^+ ion pair, which then allows hopping of electrons and formation of the product leuco-TODAQ.

To explore this triple phase boundary reactivity in more detail, further experiments with a wider range of cations have been conducted. Figure 4.4.C shows data overlaid for cyclic voltammograms recorded in Zn^{2+}, NH_4^+, Ba^{2+}, and Na^+ solution. Voltammetric responses under these conditions are very stable over consecutive potential cycles. The cations Zn^{2+} and NH_4^+ appear particularly effective in enhancing the cathodic response. Zn^{2+} is likely to coordinate to the N,O-binding site more strongly. NH_4^+ appears to provide conditions for almost reversible cation transfer. One central question in these experiments is the type of product formed in the NOP microdroplets. Therefore additional experiments with EDX elemental analysis were conducted.

The microdroplets formed by the solvent evaporation processes were characterized by the SEM and EDX with and without Zn^{2+} cations present. The SEM (see Figure 4.5.A) of non-volatile liquids is very difficult and often only “halos” of deposits are visible.

Here, some evidence for deposits between the graphite surface features is seen as brighter features. More importantly, the EDX spectrum is indicative of some insertion of Zn^{2+} ion from the aqueous solution into the microdroplet on the bppg electrode. This signal is not found on all parts of the graphite electrode surface, but it is very clear (see Figure 4.5.B).

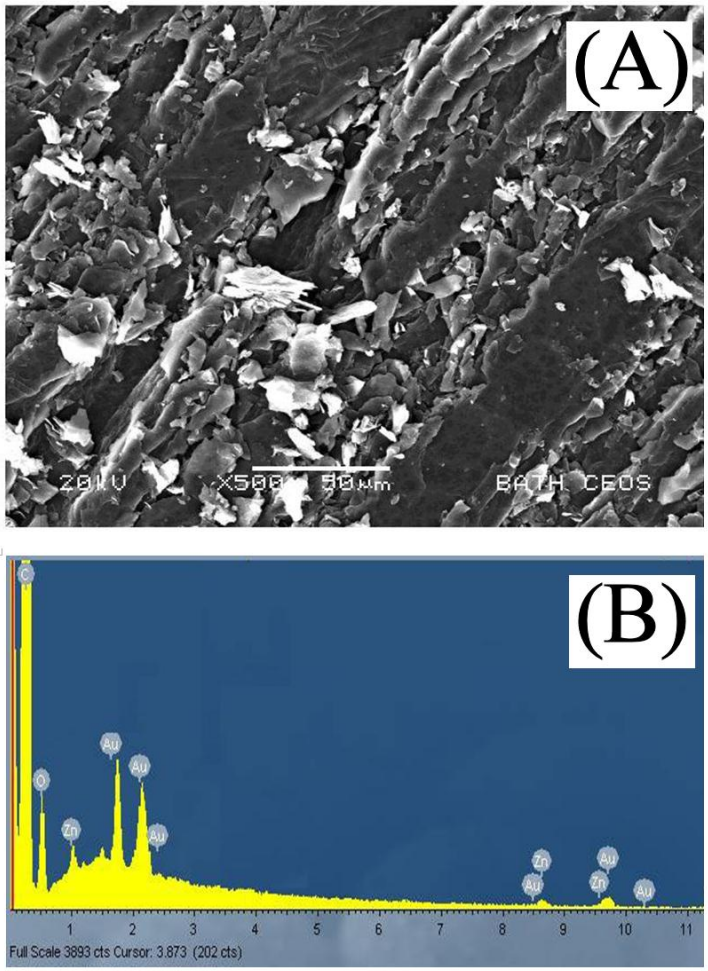

Figure 4.5. (A) SEM micrograph of TODAQ/NOP microdroplets on bppg electrode . (B) EDX chart of TODAQ deposit in (A) 0.1 M $Zn(NO_3)_2$ solution..

These results imply that the transfer of both protons (at more acidic pH) and other cations (at more alkaline pH) is possible. Coordination to one or more molecules of

TODAQ can help solubilising the hydrophilic cations in the highly hydrophobic environment (see equation 4.4).

$$TODAQ(oil) + Zn^{2+}(aq) + 2\,e^{-} \leftrightarrow TODAQ^{2-}(oil) + Zn^{2+}(oil) \qquad (4.4)$$

This type of process could be relevant for example in the uptake of cations into cell membranes and cation effects on ubiquinone Q10 reactivity have been reported under similar conditions [23].

4.4. Conclusions

The electrochemical characterization of N,N,N',N'-tetra-octyl-2,7-diamino-9,10-anthraquinone (TODAQ) as a possible pH probe is reported. It was found that the most well-defined Nernstian electrochemical signal for the anthraquinone derivative studied was between pH 2 and pH 8. The resulting peak potential data were shown to produce a stable linear response with a slope of ca. 58 mV per unit at room temperature.

The sensitivity to other cations such as Zn^{2+} or Na^{+} was unexpected and it could be useful. Usually, ionophors need to be present to select certain cations in sensing processes, but here the complex formation seems to be direct to the electrochemically active TODAQ reagent. In future, derivatives could be designed to enhance this effect and to trigger cation binding over a wider pH range and at lower cation concentration.

The "cross-sensitivity" of redox processes at liquid-liquid interfaces is of considerable interest and effects of electrolyte concentration on reduction responses observed here

may be a good model system. The transfer of electrons and cation at the triple phase boundary involves intermediates and in particular in 2-electron processes. The lifetime of intermediates may be crucial for charge hopping and effective cation transfer. The observed effects are reminiscent to those for cation interaction with lipid membranes and further study will be required to unravel the details with respect to existence of intermediates.

4.5. References

[1] Q. Cheng, A. Brajter Toth, Anal. Chem. 68 (1996) 4180-4185.

[2] J. Tkac, Bioelectrochem. 56 (2002) 23-25.

[3] Y. Cui, Science, 293 (2001) 1289-1292.

[4] C.N. Aquino Binag, Chem. Mater. 8 (1996) 2579-2585.

[5] S. Komaba, Electrochim. Acta, 42 (1997) 383-388.

[6] J. Janata, Chem. Rev. 90 (1990) 691-703.

[7] Y.L. Liu, J. Amer. Chem. Soc. 119 (1997) 8720-8721.

[8] M. Stredansky, Anal. Chim. Acta, 415 (2000) 151-157.

[9] J.J. Hickman, Science, 252 (1991) 688-691.

[10] K.L. Robinson, N.S. Lawrence, Anal. Chem. 78 (2006) 2450-2455.

[11] K.L. Robinson, N.S. Lawrence, Electrochem. Commun. 8 (2006) 1055-1061.

[12] V.G.H. Lafitte, Electrochem. Commun. 10 (2008) 1831-1834.

[13] I. Streeter, J. Solid State Electrochem. 8 (2004) 718-721.

[14] V. Ova, J. Chromatog. B-Anal. Technol. Biomed. Life Sci. 715 (1998) 273-281.

[15] S. Routier, Anti-Cancer Drug Design 13 (1998) 407-415.

[16] S.B. McLoughlin, C.R. Lowe, Enzyme Microbial Technol. 20 (1997) 2-11.

[17] A. Salimi, Electroanalysis 11 (1999) 114-119.

[18] A. Salimi, Pol. J. Chem. 72 (1998) 2573-2582.

[19] M. Shamsipur, K. Alizadeh, S. Arshadi, J. Mol. Struct.-Theochem. 758 (2006) 71-74.

[20] F. Marken, J. Electroanal. Chem. 437 (1997) 209-218.

[21] M. Shamsipur, J. Electroanal. Chem. 600 (2007) 345-358.

[22] G.G. Wildgoose, Talanta 60 (2003) 887-893.

[23] I. Bogeski, R. Guaboski, R. Kappl, V. Mirceski, M. Stefova, J. Petreska, M. Hoth, J. Amer. Chem. Soc. 133 (2011) 9293.

Chapter 5

DNA - Carbon Nanoparticle Conjugate Films

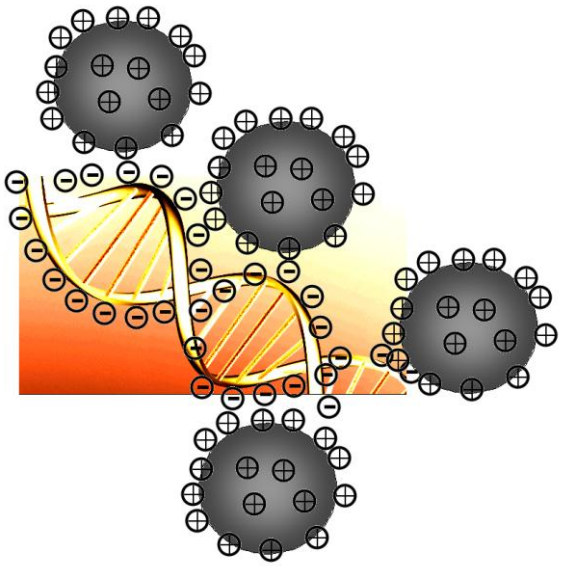

Acknowledgement. Positively charged carbon nanoparticles were synthesized and provided by John D. Watkins and Kate Lawrence. ITO junction electrodes were prepared by Charles Y. Cummings. DNA samples were provided by Dr. Paul Davies. Dr. Sara E.C. Dale and Prof. Simon Bending are acknowledged for help with AFM.

Abstract

In this chapter, an electrochemical DNA sensing strategy for the detection of DNA hybridization is reported based on a positively functionalized carbon nanoparticle material conjugated with either poly-adenylic acid or dsDNA from calf thymus. Electrodes are assembled on ITO electrode substrates. The layer-by-layer growth of films and electrochemical characterisation without/with methylene blue intercalator are reported. Next, an ITO junction electrode is modified with carbon nanoparticles and poly-adenylic acid and then the oligonucleotide T5 is shown to interact to change the nano-scale resistivity of the film.

Content

5.1. Introduction

5.1.1. Introduction to Label-free DNA Sensors

Electronic sensor chips are currently the main means used in the detection of specific DNA consequences. The DNA detection is normally achieved via the hybridization of two complementary DNA molecules. The classical approach prior to DNA detection is the preparation of the DNA probe, which generally carried out by immobilizing a single stranded DNA (ssDNA) molecule on a substrate, which will then undergo interacts with the target molecule (complementary DNA molecule). Hybridization event eventually induces molecular changes, and very often, hybridization detection is characterized by fluorescence techniques [1,2], quartz crystal microbalance (QCM) [3,4], surface plasmon resonance spectroscopy (SPR) [5], atomic-force microscopy (AFM) [6], and electrochemical techniques.

Although there are many well-established methods in detecting DNA hybridization event, most of the well-known means are normally complicated multi-steps and time-consuming, and most strikingly incur high cost. In contrast to these, with the recent advance in electrochemical methods [7,8] the detection DNA hybridization process can be monitored and measured at a short timescale, and surprisingly simple and can be done at a low cost. Electrochemical methods offers a lot better in terms of the potential of further miniaturization of hybridization sensors thus perfectly fits the demand at industrial scale. Very often, the hybridization reaction involves the usage of redox active materials attached to the electrode surface.

There are many organic compounds with redox active properties such as methylene blue, daunomycin, or Hoechst [9 , 10 , 11 , 12 , 13]used in the detection DNA hybridization. Cobalt, osmium and ruthenium-based metal complexes are also known to be [14,15,16] amongst the regular detection markers. In another way, redox active enzymes can also be attached covalently to the target molecule so that a sensitive hybridization sensing mechanism can be accomplished [17,18,19,20,21].

Although the presence of redox indicators or intercalators are helpful in the hybridization sensing, they can also complicate the detection process as they might give rise to the interference in the sensing responses. Therefore, a label-free detection systems are preferable so as to obtain a fast but yet economical method. Direct detection of hybridization reaction utilizing for example the direct oxidation process of DNA bases [22,23,24] have been reported without the usage of electroactive markers. Other available alternatives methods involves the measurements of conductance or resitance [25,26,27,28,29], and capacitance [30] changes. It has been reported that the electrical resistance and capacitance are useful sensitive parameters at the electrode surface and will allow for the construction of DNA hybridization biosensors with enhanced performance to be achieved.

5.1.2. Nanoparticles in DNA Sensing

Generally, a biosensor consists of two main parts, which is first the bioreceptor, which interacts with the tarhet analyte, and a transducer, which converts the recognition event into measureable electronic signals [31]. In electrochemical DNA sensors, the transducer is normally made of either gold or glassy carbon electrode. Consequently,

a DNA probe will be then immobilized onto the electrode surface to form a bio-regocnition layer. The durability and sensitivity of DNA sensors are determined by the immobilization method of these DNA probes. Currently, available immobilization methods include physical adsorption, covalent binding and electrochemical polymerization.

In order to to able to interpret the hybridization signals correctly, these responses need to be amplified. One of the most promising materials that can be used as signals amplifier are the nanocarbons which include nanoparticles [32,33,34], nanotubes [35,36,37] and nanowires [38,39], which have proven to aid in the recent development of bio-molecule and gene detection. For example, an electrochemical DNA biosensor based on the multi-layered films, produced by layer by layer (LbL) deposition method, immobilized on the MWCNTs and CNPs have been suggested [40]. The promoted means was reported to be able to produce films with great stability and provides with effective way in the biosensor construction.

5.1.3. Nanoparticle Immobilization Methods: Layer by layer Techniques

Decher et al. invented the layer by layer (LbL) deposition method [41,42,43,44]. Following the establishment of this technique, many studies have been reported focusing on various LbL films preparation. In this work, the modification of working electrode is achieved by means of the electrostatic interaction. Alternation between positively and negatively charged materials enables the control of film thickness and offers freedom in layering sequences.

Unlike other film fabrication methods, LbL is a very simple means as it only requires beakers and tweezers, therefore cost reduction can be achieved. With various types of available materials LbL offers a wide range of options in terms of the selection of film materials. Poly-electrolytes [45,46,47,48] such poly-(allylamine hydrochloride) (PAH), poly-(diallyldimethylammonium chloride) (PDDA), and poly-(ethyleneimine) (PEI) are among common materials used as film starting materials. Others such as poly-(p-phenylenevinylene) (PPV), applied in light-emitting diodes [49,50]and poly-(amidoamine)dendrimer (PAMAM) and its metal derivatives [51,52] were also reported. Due to its nature, most of the biomolecule solutions are normally negatively charged. Therefore very often, LbL seembly involving these materials are achieved via electrostatic mode, such as in the case of proteins [53,54,55,56,57,58,59,60], DNA [61,62,63,64,65,66,67,68,69] and charged poly-saccharides [70,71,72,73,74,75,76].

In this study, a thin nanofilm was formed based on the deposition of functionalized nanoparticles [77] / poly-adenylic acid by means of LbL method onto ITO and ITO junction electrodes. Next, films from carbon nanoparticles and dsDNA are investigated. The conductive film enables inter-particle electron hopping to occur. The DNA probe immobilized on the ITO junction surface is then hybridized with the complementary DNA target to result in changes in inter-particle spacing of the nano-film. The DNA hybridization event is monitored electrochemically by generator-collector mode bipotentiostat. Preliminary results suggests that the change in inter-particle spacing resulted from the DNA hybridization cause a change in the resistivity across the ITO junction electrode

5.2. Experimental

5.2.1. Materials and Reagents

The functionalized carbon nanoparticle was performed in collaboration with by John Watkins and James Taylor. The probe ssDNA (polyadenylic acid) and 5mer target ssDNA (T5) were purchased from Eurofins (MWG Operon,GmbH). All other reagents used were of the highest grade commercially available and were applied without additional purification. All solutions were prepared with deionised water taken from an Elgastat filter system (Elga, Bucks, UK) with a resistivity of not less than 18 MΩ cm.

5.2.2. Procedures and Methods

Cleaning of the ITO Electrodes. Prior to deposition, the ITO or ITO junction electrode (in collaboration with Charlie Cummings) surface were washed with ethanol and water, dried, and treated at 500 °C in air for 30 minutes to remove any organic materials on the surface.

Preparation of Deposition Solutions. For deposition 4 mg sulphonamide-functionalized carbon nanoparticles (in collaboration with John Watkins) were added into 4 mL distilled water. The resulting solution/suspension was initially sonicated for 1 hour (in a low lower cleaning bath, Fisher FB11012) and then shaken vigorously prior to each use. For preparation of poly-adenylic acid solution (DNA probe), typically 4 mg of poly-adenylic acid were added into 4 mL phosphate buffer solution. For preparation of Oligo-nucleotide T5 (target probe), 0.16 mg of oligo-nueleotide T5 was added into 4 mL phosphate buffer solution.

Modification of ITO Electrodes. A clean ITO or ITO junction electrode is first dipped into a positively charged carbon nanoparticle solution for 2 minutes followed by rinsing and drying. It was then dipped into a negatively charged polyadenylic acid solution for two minutes followed by rinsing and drying. These procedures were repeated over several times to give multi-layer deposits of carbon nanaoparticles with approximately 1 nm thickness per layer (by AFM, vide infra).

Voltammetric Measurements. For electrochemical measurements a PSTAT 30 bipotentiostat system (Autolab, Echochemie, Netherlands) was employed. In electrochemical experiments a conventional three-electrode cell with platinum wire counter and saturated calomel reference (SCE, REF401, Radiometer, Copenhagen) were employed. AFM images were obtained with the Asylum Research MFP-3D stand alone microscope. The AFM tips were AC240TS from Olympus.

Microscopic Imaging. For Scanning Electron Microscopy (SEM), a Leo 1530 system was used. Samples were prepared by scratching and gold sputter coating prior to analysis. Atomic force microscopy images were obtained with a Digital Instruments Nanoscope IIIa Multimode Scanning Microscope in the AFM tapping mode. The AFM tips were AC240TS from Olympus. The surface composition of the modified electrodes were analyzed by energy dispersive X-ray (EDX) analyzer. An AMRAY 1810 type SEM equipped with Link ISIS micro-analyzer was used. The operating voltage of electronic beam was 20 keV for morphological observation and 16 keV for EDX analysis. The surfaces of the EDX samples were scratched prior to measurements.

5.3. Results and Discussion I.: Poly-Adenylate – CNP Films

The thin layer was fabricated by applying the positively charged carbon nanoparticles (ca. 9-18 nm diameter) followed by alternating rinse and cycles using negatively charged. These layer-by-layer deposits become visible to the naked eye after ca.20 to 40 deposition cycles (see Figure 5.1.A. An AFM image of a 20-layer deposit is shown in Figure 5.1.B. The relationship between the thickness of film and number of deposition volume is shown in Figure 5.1.C. The average height for each deposit was observed as 1 nm per layer. The AFM image suggested that the film was unevenly grown due to the distribution of particles sizes. The AFM proved that the fabrication of nanofilms of the nanoparticles and DNA on the ITO electrode surface by layer-by-layer deposition technique was achieved.

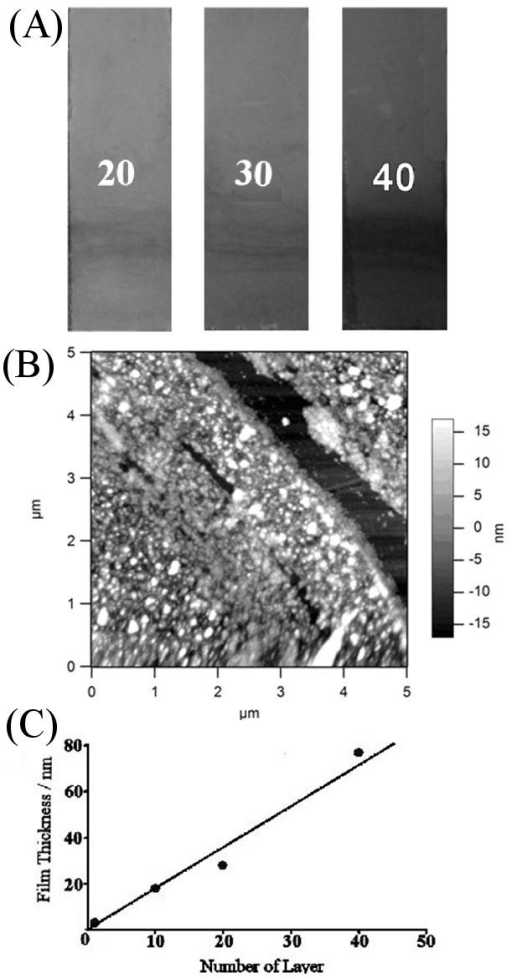

Figure 5.1. (A) Color change with increment of deposition numbers of layer by layer films of poly-adenylic acid-carbon nanoparticles on ITO. (B) AFM image and profile for 20-layer film formed by alternating deposition of positively and negatively charged carbon nanoparticles, and (C) Film thickness versus number of layer estimated from AFM profiles.

Initially, cyclic voltammograms were obtained for carbon nanoparticles deposited onto ITO electrodes (see Experimental). The capacitive current response was measured as a function of the number of layer deposited in aqueous 0.1 M phosphate buffer pH 7. Data in Figure 5.2.A show well-defined capacitive current responses over a potential range between 0.0 V and 0.6 V *vs.* SCE.

A linear relationship between capacitance and the number of layers deposited was observed (see Figure 5.2.B). This suggests that the layer by layer deposition process

occurs continuously for at least 40 layers and that the electrical conductivity in film deposits is good.

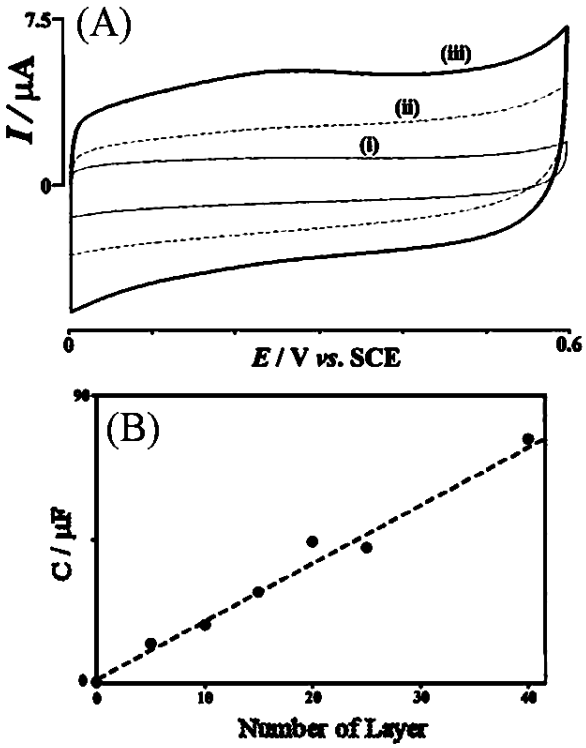

Figure 5.2. (A) Cyclic voltammograms (scan rates 50 mV s^{-1})) obtained for films of (i) 20, (ii) 30, and (iii) 40 times deposition of carbon nanoparticles deposited onto an ITO electrode and immersed into aqueous 0.1 M phosphate buffer pH 7. (B) Plot of capacitance (at 0.3 V *vs.* SCE) versus number of layers deposited onto ITO electrode surface.

5.4. Results and Discussion II.: dsDNA – CNP Films

Next, similar layer by layer deposition experiments are performed with calf thymus dsDNA to investigate the effect of the hybridization (more rigid dsDNA) on the structure and reactivity of films. AFM imaging revealed a similar deposition process with "patchy" films building up in every deposition cycle.

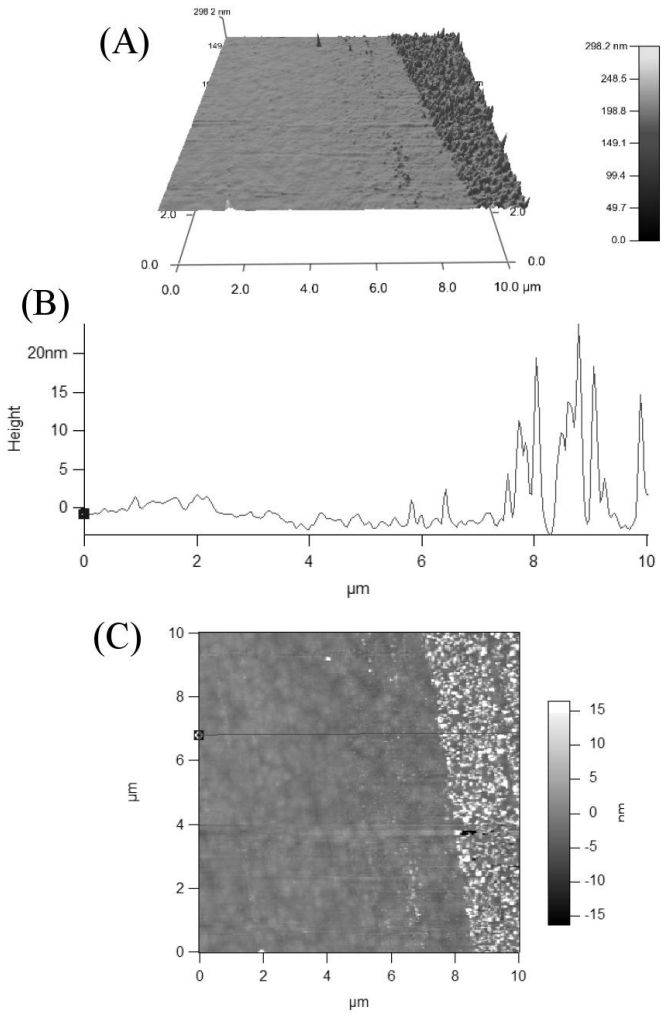

Figure 5.3. (A) AFM topography image for a 20-layer film of dsDNA with carbon nanoparticles. (B) Cross-sectional view. (C) AFM (top-view) of the 20-layer film deposit.

The increase in height of these films in average was again ca. 1 to 1.5 nm per layer. However, the films are clearly highly structured and additional AFM images (see Figure 5.4) clearly reveal carbon nanoparticles assembling around individual DNA strands to form aggregates.

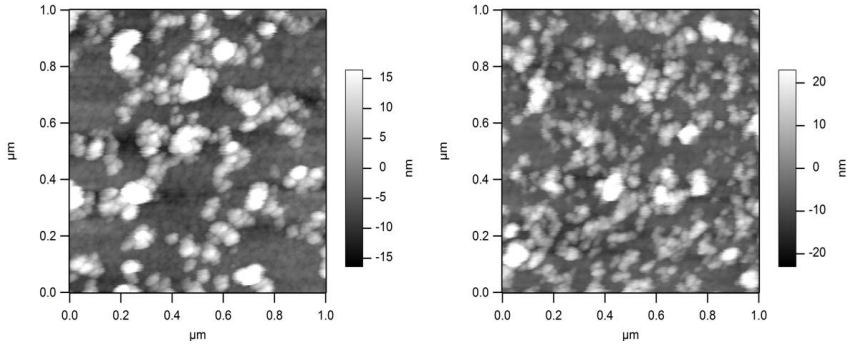

Figure 5.4. AFM topography images for dsDNA from calf thymus layer by layer deposited with positive carbon nanoparticles. The assembly of carbon particles with individual dsDNA strands is clearly observed.

Electrochemical responses for these dsDNA – CNP films are dominated by the capacitance response for the carbon. Figure 5.5.A shows typical voltammetric signals and the plot in Figure 5.5.B summarises the data. The magnitude of the capacitive signal is very similar for poly-adenylic acid and dsDNA conjugates with CNPs.

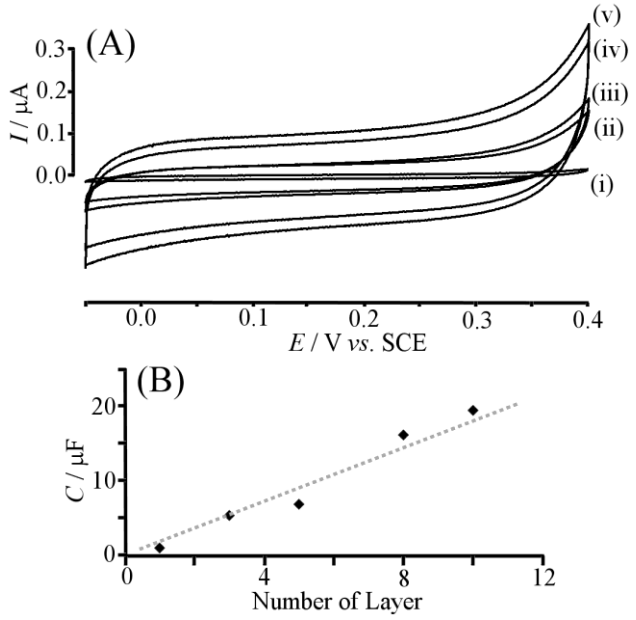

Figure 5.5. (A) Cyclic voltammograms (scan rate 10 mVs^{-1}) for (i) 1-layer, (ii) 3-layer, (iii) 5-layer, (iv) 8-layer, and (v) 10-layer films of dsDNA-CNP films. (B) Plot showing the capacitance as a function of number of layers.

Next, the interaction of the film with a typical "intercalator" or redox indicator is investigated. Figure 5.6 shows cyclic voltammograms for the reduction of adsorbed methylene blue at pH 7 in phosphate buffer solution. A typical 2-electron 2-proton reduction consistent with literature reports [78] is observed at a midpoint potential of ca. -0.23 V vs. SCE (see equation 5.1).

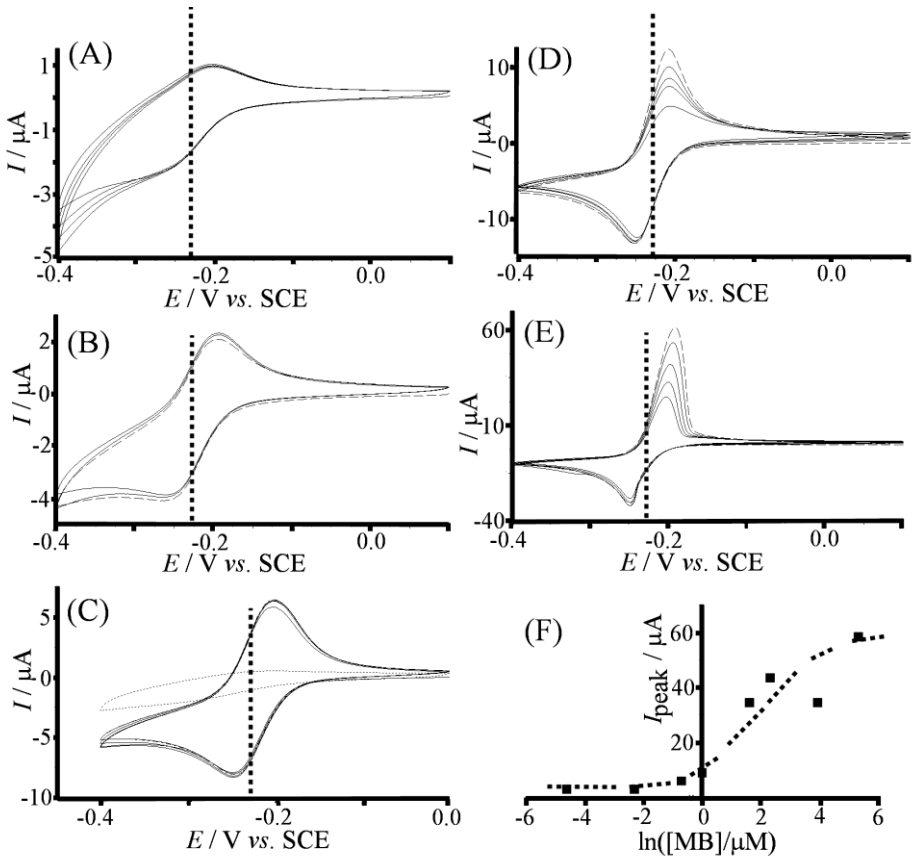

Figure 5.6. Cyclic voltammograms (scan rate 10 mVs^{-1}) for the reduction of methylene blue from (A) 1, (B) 5, (C) 10, (D) 50, (E) 200 μM solution into a 10 layer dsDNA-CNP film on ITO and immersed into 0.1 M PBS pH &. (F) Plot of the anodic peak current versus logarithm of methylene blue concentration.

These voltammetric responses are very stable in consecutive potential cycles indicating a strong bond between DNA and methylene blue. At higher concentrations of methylene blue (see Figure 5.6.E) the shape of the voltammetric response becomes asymmetric indicative of "solid state" conversion conditions with interactions between methylene blue molecules in a highly saturated film sample. The anodic peak currents can be taken as a measure of the amount of methylene blue adsorbed into the dsDNA-CNP film and a plot of the peak current versus logarithm of concentration is shown in Figure 5.6.F. The behaviour is approximately Langmuirian with a binding constant $K_{MB} = \frac{[MB_{bound}]}{[MB_{solution}]\times[empty\ sites]}$ of ca. 1.3×10^5 M^{-1}. This value is consistent with strong binding probably dominated by electrostatic interaction.

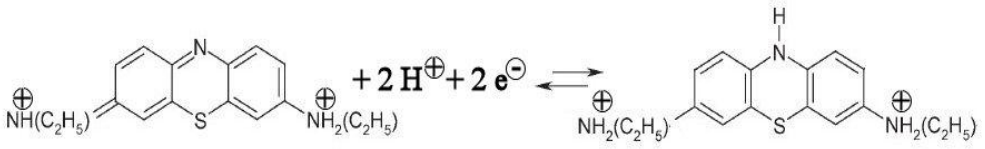

(5.1)

5.5. Results and Discussion III.: Junction Experiments

In order to explore potential for hybridisation sensing without label or redox probe a conductivity probe is developed. The gap size of the ITO junction electrode fabricated by focused ion beam etching was characterized using the fitted SEM. From Figure 5.7.B, it was observed the approximate gap size of the ITO junction is ca. 400 nm.

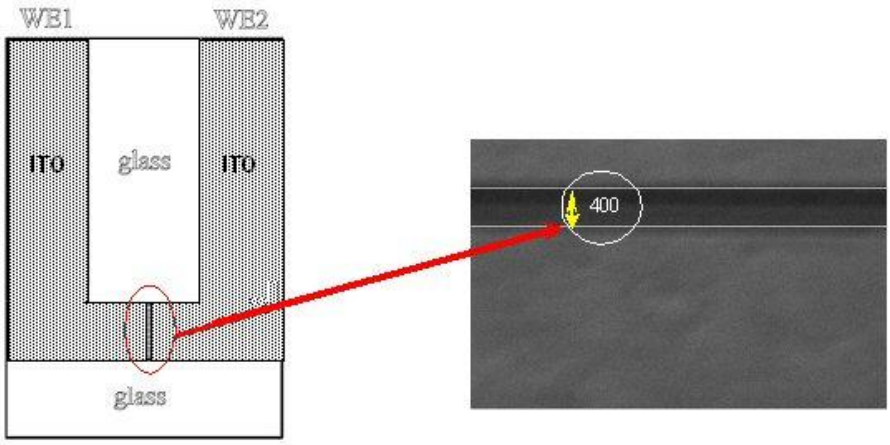

Figure 5.7. (A) Illustration of ITO junction electrode and (B) nano gap size.

The purpose of having positively charged carbon nanoparticles deposited onto the ITO electrode is to serve as an electrical conducting support for the DNA before and after hybridisation. Here poly-adenylic acid is studied when interacting with T5 as complementary probe. In principle, prior to hybridization of DNA, the positively charged carbon nanoparticles was assumed to be electrostatically bound to the negatively charged target DNA. When the DNA hybridization takes place, the formation of double helix between the probe and the complementary target ssDNA is predicted to cause the inter-particle spacing in the nanofilm structure to change (see Figure 5.8.A. In other words, in order for current to flow electrons have to move from one particle to another particle. By having the inter-particle to be further separated, the facility of electron transfer will be reduced. Therefore, an increment in electrical resistance measured between the adjacent ITO junction electrodes is expected. This was confirmed by the collector mode voltammetric response obtained after the hybridization occurred to have resulted in an increase in the electrical resistance value from 60 G Ω to 110 G Ω as shown in Figure 5.8.B.

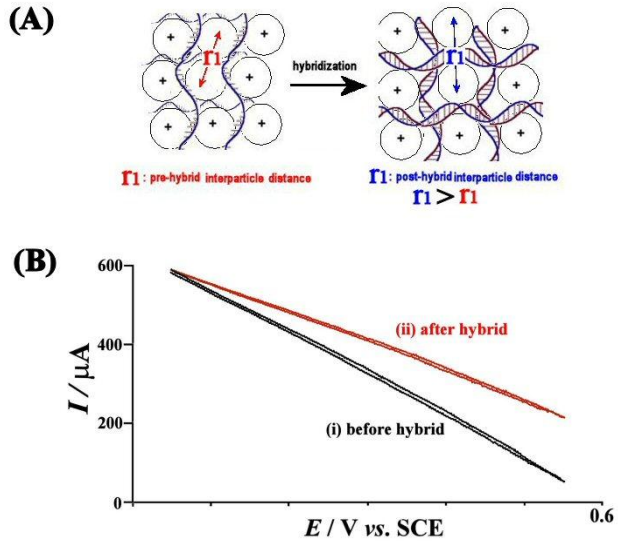

Figure 5.8. (A) Inter-particle spacing effect from DNA hybridization event. (B) Cyclic voltammograms for hybridization of complementary target probe (poly-adenylic acid with oligo-nucleotide T5) in aqueous 0.1 M phosphate buffer at an 15 layered-ITO junction electrode with the collector held at a potential of 0.1 V *vs*. SCE (scan rate 10 mV s^{-1}).

The experimental results reported here are preliminary in nature and the new hybridization detection system will have to be studied for a wider range of DNA samples to verify the sensitivity and specitivity of this approach.

5.6. Conclusions

Films of DNA with positively charge carbon nanoparticles have been assembled on ITO electrodes. A novel electrode system with two coupled working electrodes has been developed. ITO junction electrode modified with alternated positively charged carbon nanoparticles and negatively charged DNA target probe *via* LbL deposition technique were immersed in aqueous 0.1 M phosphate buffer pH 7 and studied by generator-collector mode cyclic voltammetry. The effect of number of deposition layers has been investigated. The novel electrode system reveals a high sensitivity for

DNA hybridization processes at ITO junction reaction zones. The new modified electrode will allow label-free DNA sensing to be further investigated.

5.7. References

[1] J. Reichert, Anal. Chem. 72 (2000) 6025.

[2] T.A. Taton, G. Lu, C.A. Mirkin, J. Amer. Chem. Soc. 123 (2001) 5164.

[3] F. Caruso, Anal. Chem. 69 (1997) 2043.

[4] F. Patolsky, A. Lichtenstein, I. Willner, J. Amer. Chem. Soc. 123 (2001) 5194.

[5] B.P. Nelson, Anal. Chem. 73 (2001) 1.

[6] Z.L. Zhang, Anal. Bioanal. Chem. 381 (2005) 833.

[7] J.J. Gooding, Electroanalysis, 14 (2002) 1149.

[8] T.G. Drummond, M.G. Hill, J.K. Barton, Nature Biotechnology, 21 (2003) 1192.

[9] A. Erdem, Anal. Chim. Acta, 422 (2000) 139.

[10] K. Hashimoto, K. Ito, Y. Ishimori, Anal. Chim. Acta, 286 (1994) 219.

[11] K. Hashimoto, K. Ito, Y. Ishimori, Anal. Chem. 66 (1994) 3830.

[12] S.O. Kelley, Bioconjugate Chem. 8 (1997) 31.

[13] D. Ozkan, Electrochem. Commun. 4 (2002) 796.

[14] K. Maruyama, Sens. Actuators B-Chem. 76 (2001) 215.

[15] A.B. Steel, T.M. Herne, M.J. Tarlov, Anal. Chem. 70 (1998) 4670.

[16] J. Wang, Anal. Chem. 68 (1996) 2629.

[17] G.U. Flechsig, T. Reske, Anal. Chem. 79 (2007) 2125.

[18] M. Trefulka, Electroanalysis, 19 (2007) 1281.

[19] T. Ihara,. Nucleic Acids Res. 24 (1996) 4273.

[20] O. Panke, A. Kirbs, F. Lisdat, Biosens. Bioelectron. 22 (2007) 2656.

[21] F. Patolsky, Langmuir, 15 (1999) 3703.

[22] E. Palecek, Anal. Chim. Acta, 469 (2002) 73.

[23] J. Wang, A.B. Kawde, Analyst, 127 (2002) 383.

[24] H.H. Thorp, Trends Biotechnol. 16 (1998) 117.

[25] M.Y. Vagin, A.A. Karyakin, T. Hianik, Bioelectrochem. 56 (2002) 91.

[26] S.L. Pan, L. Rothberg, Langmuir, 21 (2005) 1022.

[27] J. Wang, Anal. Chim. Acta, 402 (1999) 7.

[28] T.Y. Lee, Y.B. Shim, Anal. Chem. 73 (2001) 5629.

[29] H. Cai, Electroanalysis, 15 (2003) 1864.

[30] C. Berggren, Electroanalysis, 11 (1999) 156.

[31] K.J. Odenthal, J.J. Gooding, Analyst, 132 (2007) 603.

[32] J. Wang, Electroanalysis, 16 (2004) 928.

[33] A. Erdem, Electrochem. Commun. 7 (2005) 815.

[34] L. Authier, Anal. Chem. 73 (2001) 4450.

[35] M.L. Pedano, G.A. Rivas, Electrochem. Commun. 6 (2004) 10.

[36] J. Wang, G.D. Liu, M.R. Jan, J. Amer. Chem. Soc. 126 (2004) 3010.

[37] J. Li, Nano Lett. 3 (2003) 597.

[38] Z. Li, Nano Lett., 4 (2004) 245.

[39] M.A. Lapierre-Devlin, Nano Lett. 5 (2005) 1051.

[40] H.Y. Ma, Electroanalysis, 10 (2008) 1220.

[41] G. Decher, J.D. Hong, Makromol. Chem.-Macromol. Symp. 46 (1991) 321.

[42] G. Decher, J.D. Hong, Ber. Bunsen-Ges. Phys. Chem. Chem. Phys. 95 (1991) 1430.

[43] G. Decher, J.D. Hong, J. Schmitt, Thin Solid Films, 21 (1992) 831.

[44] Y. Lvov, G. Decher, H. Mohwald, Langmuir, 9 (1993) 481.

[45] G. Decher, Y. Lvov, J. Schmitt, Thin Solid Films, 244 (1994) 772.

[46] D. Korneev, Physica B, 213 (1995) 954.

[47] N.G. Hoogeveen, Langmuir, 12 (1996) 3675.

[48] W. Chen, T.J. McCarthy, Macromol. 30 (1997) 78.

[49] A.C. Fou, J. Appl. Phys. 79 (1996) 7501.

[50] W.B. Stockton, M.F. Rubner, Macromol. 30 (1997) 2717.

[51] J.A. He, Chem. Mater. 11 (1999) 3268.

[52] A.J. Khopade, F. Caruso, Langmuir, 18 (2002) 7669.

[53] M. Onda, Japan. J. Appl. Phys. 2-Lett. 36 (1997) L1608.

[54] F. Caruso, Langmuir, 14 (1998) 4559.

[55] Y.M. Lvov, J. Amer. Chem. Soc. 120 (1998) 4073.

[56] M.K. Beissenhirtz, F.W. Scheller, F. Lisdat, Anal. Chem. 76 (2004) 4665.

[57] P.L. He, N.F. Hu, J.F. Rusling, Langmuir, 20 (2004) 722.

[58] N. Sultana, J.B. Schenkman, J.F. Rusling, J. Amer. Chem. Soc. 127 (2005) 13460.

[59] T.G. Shutava, D.S. Kommireddy, Y.M. Lvov, J. Amer. Chem. Soc. 128 (2006) 9926.

[60] Z.M. Qi, Adv. Funct. Mater. 16 (2006) 377.

[61] X.D. Chen, J. Lang, M.H. Liu, Thin Solid Films 409 (2002) 227.

[62] A. Ishibashi, Chem. Phys. Lett. 419 (2006) 574.

[63] A.P.R. Johnston, Langmuir 22 (2006) 3251.

[64] J. Lang, M.H. Lin, J. Phys. Chem. B 103 (1999) 11393.

[65] L.Q. Luo, Biophys. Chem. 94 (2001) 11.

[66] X.Y. Shi, R.J. Sanedrin, F.M. Zhou, J. Phys. Chem. B 106 (2002) 1173.

[67] F. Yamauchi, Biomater. 27 (2006) 3497.

[68] G. Decher, Biosens. Bioelectronics, 9 (1994) 677.

[69] Y. Lvov, G. Decher, G. Sukhorukov, Macromol. 26 (1993) 5396.

[70] Y. Lvov, J. Biomater. Sci.-Polym. Ed. 9 (1998) 345.

[71] A. Voigt, Ind. Engineer. Chem. Res. 38 (1999) 4037.

[72] X.P. Qiu, Langmuir 17 (2001) 5375.

[73] T. Serizawa, M. Yamaguchi, M. Akashi, Biomacromol. 3 (2002) 724.

[74] C.A. Constantine, J. Amer. Chem. Soc. 125 (2003) 1805.

[75] B. Thierry, Biomacromol. 4 (2003) 1564.

[76] T.G. Shutava, Y.M. Lvov, J. Nanosci. Nanotechnol. 6 (2006) 1655.

[77] J.D. Watkins, R. Lawrence, J.E. Taylor, S.D. Bull, G.W. Nelson, J.S. Foord, D. Wolverson, L. Rassaei, N.D.M. Evans, S.A. Gascon, F. Marken, Phys. Chem. Chem. Phys. 12 (2010) 4872.

[78] J.E. Halls, C.Y. Cummings, J. Ellis, L.L. Keenan, D. Jiang, A.D. Burrows, F. Marken, Mol. Cryst. Liq. Cryst. 554 (2012) 12.

Chapter 6

Surface-Dopylated Carbon Nanoparticles Sense Gas-Induced pH Changes

---

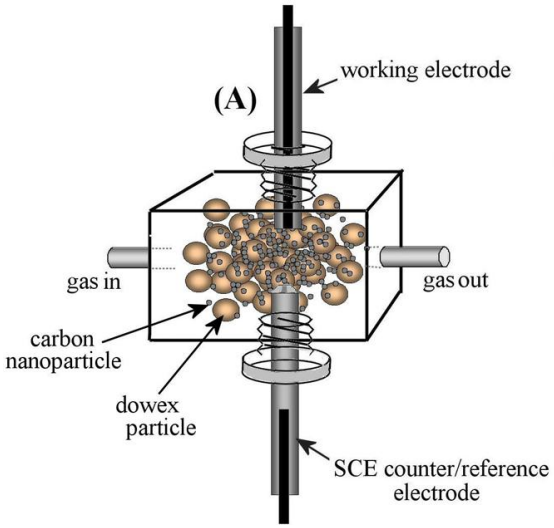

This work is published in:
Surface-dopylated carbon nanoparticles sense gas-induced pH changes, Norahim Bin Ibrahim, Katherine Lawrence, Tony D. James, Fengjie Xia, Mu Pan, Shichun Mu, John M. Mitchels, Frank Marken, *Sensors and Actuators B: Chemical*, 161 (2012) 184.

Acknowledgements
The synthesis of DOPA-modified carbon nanoparticles was carried out by Katherine Lawrence. Help with imaging and microscopy by John Mitchels is acknowledged.

Content

Abstract

Abstract

This chapter describes the surface-modification of carbon nanoparticles of ca 9-18 nm diameter (Emperor 2000). Covalent linking L-dopa-boc (boc-protected L-3,4-dihydroxyphenylalanine) with a surface coverage of approximately 100 per particle (or 3 × 10^{13} cm^{-2}) is achieved. In solution environments these redox-active nanoparticles provide chemically stable and pH-sensitive voltammetric responses (reversible 2-electron 2-proton oxidation) over a pH range from 2 to 12.

When mixed into Dowex 50 Wx4 cation exchanger or Dowex 50 1x2 anion exchanger and placed in contact with a glassy carbon electrode in a flow of humidified gas, the L-dopa-boc-modified carbon nanoparticles provide pH-sensitive surface probes to monitor the surface conditions. In a two-terminal cell it is demonstrated that gas flow measurements are possible with both modified cation and anion exchanger particles in contact to glassy carbon electrodes. The anion exchanger particles allow pH control after pre-conditioning in phosphate buffer. Loading-dependent sensitivity to ammonia gas is investigated and high sensitivity to ammonia is observed for Dowex 50 1x2 anion exchanger pre-equilibrated in phosphate buffer pH 3 and decorated with L-dopa-boc-modified carbon nanoparticles. Responses are observed with sequential injections of 1 cm^3 ammmonia into a gas flow-through device.

6.1. Introduction to Hydroquinone/Quinone Redox Systems

Many types of pH sensitive redox systems are known and in particular quinone-hydroquinone redox systems with pH dependence are ubiquitous in nature [1]. L-Dopa (3,4-dihydroxyphenylanaline or S-2-amino-3-(3,4-dihydroxyphenyl) propanoic acid) plays a special role as a redox active amino acid derivative with functions ranging from anti-oxidant [2], metal complexant [3], melanin precursor [4], to biological (marine) adhesive [5]. The chiral nature of L-dopa has been exploited recently to probe chiral electrode processes [6]. The effect of pH on the dopa redox reactivity has been studied by Brun and Rosset [7] and a transition from chemically reversible to irreversible oxidation has been observed due to a cyclisation reaction and formation of a leuco-dopachrome intermediate (see Figure 6.1) at lower proton activities [8]. Nucleophilic attack of the reactive dopaquinone has also been reported with water [9], nitrite [10], and with thiol derivatives [11]. L-Dopa is an important analytical target [12], but it also has been used to make sensor devices [13] and to detect metals such as aluminium [14,15]. There have been several examples of pH probe designs based on quinone-hydroquinone type redox systems [16,17] in particular based on anthraquinones [18]. A combination of a pH-dependent redox system and a pH-independent redox system has been proposed for reference-free pH measurements [19].

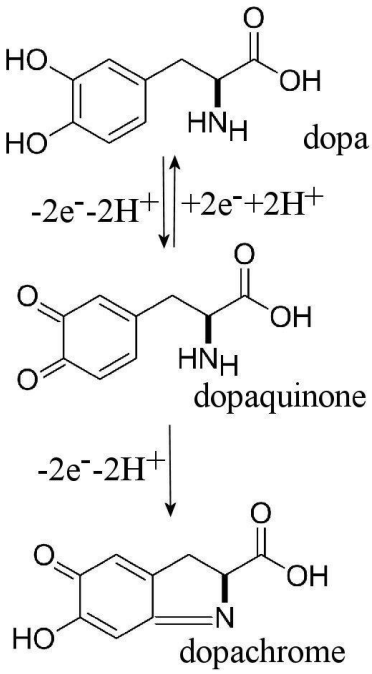

Figure 6.1. Reaction scheme for L-dopa oxidation.

In order to employ quinone-hydroquinone or other pH-dependent redox systems at an electrode surface, immobilisation onto an appropriate substrate is required. Several types of carbon substrates have been used as substrate materials including glassy carbon [20,21], graphite [22], carbon spheres [23], carbon nanotubes [24], and carbon nanoparticles [25]. Carbon nanoparticles (CNPs) combine high surface area (high immobilisation density [26]), versatile surface chemistry, and low cost. For example, industrial pigment materials such as Emperor 2000 (Cabot Corp.) carbon nanoparticles are readily available as starting materials and readily surface functionalised via sulfonate functional groups [27]. The reaction with thionylchloride followed by amines has been shown to open up a range of functionalisation opportunities [28]. In this chapter amide coupling chemistry is developed to connect L-dopa-boc units covalently to the surface amine functionalities of these carbon nanoparticles.

6.2. Introduction to Ammonia Sensing

Ammonia sensors have been reported for gas media based on for example oxide films [29,30] and for aqueous media based on direct detection [31,32] or based on indirect detection with immobilised anthraquinones [33]. Here, proof-of-principle experiments are reported for an ammonia gas induced effect on a L-dopa-boc sensed pH change at the electrode | aqueous electrolyte | gas triple phase boundary. In order to investigate the effect of gas pH (e.g. introducing ammonia) on the electrochemical response of dopa-boc functional groups on the surface of carbon nanoparticles, a two-terminal cell is employed. Figure 6.2.A shows a drawing of the glassy carbon working electrode in contact to the dowex ion exchanger particles, which carry the aqueous electrolyte phase and provide the electrical connection to the counter-reference electrode. The L-dopa-boc-functionalised carbon nanoparticles are distributed over the dowex surface and allow direct contact to the working electrode surface (see Figure 2B).

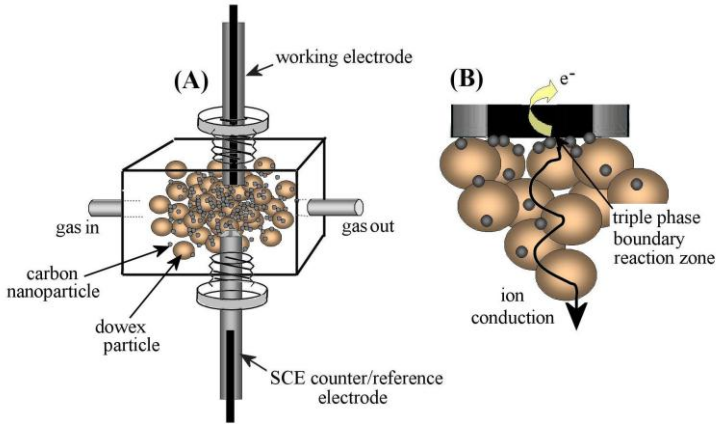

Figure 6.2. (A) Schematic drawing of the two-terminal electrochemical cell with carbon nanoparticle decorated Dowex ion exchanger particles acting as electrolyte and support for the redox system. (B) Scheme of the carbon nanoparticles in contact to the glassy carbon electrode surface, the ion conducting particles, and the surrounding gas phase.

Flow of gas through this cell is initially limited to argon (humidified with 80% relative humidity by flowing through saturated ammonium sulphate solution [34]) to allow L-dopa-boc electrochemistry to be studied as a function of the pH (imposed by pre-treatment of the ion exchanger in buffer). Finally, injection of small doses of ammonia is shown to change L-dopa-boc reactivity to provide a highly sensitive probe for ammonia exposure.

6.3. Experimental Methods

6.3.1. Chemicals

Dowex 50 Wx4 cation exchanger and Dowex 50W 1x2 anion exchanger, phosphoric acid, NaOH, thionylchloride, ethylenediamine, ammonium sulphate, L-dopa, were obtained from Aldrich and used without further purification. Emperor 2000^{TM} carbon nanoparticles were obtained from Cabot Corporation. Argon (Pureshield, BOC) was used for de-aeration of solutions. Demineralised and filtered water was taken from a Thermo Scientific water purification system (Barnstead Nanopure) with 18.2 MΩcm resistivity.

6.3.2. Instrumentation

A microAutolab III potentiostat system (EcoChemie, The Netherlands) was employed in electrochemical measurements. A 3 mm diameter glassy carbon disc electrode (BAS, US) or a Dropsense screen printed carbon disc electrode (Dropsense) were the working

electrode and a KCl-saturated calomel electrode (SCE, Radiometer) was the counter-reference. In solution experiments a platinum wire served as counter electrode. A custom-made PEEK cell with gas in and outlet (see Figure 1.5) was used with a wash bottle to pre-saturate argon with 80% relative humidity [35]. Scanning electron microscopy (SEM) and transmission electron microscopy (TEM) images were obtained on JEOL JSM6301F field emission scanning electron microscope (FESEM) and JEOL JEM1200EXII TEM systems, respectively.

6.3.3. Procedures

Boc Protection of L-Dopa. L-dopa (4 g, 20.3 mmol) was dissolved in dioxane (40 mL), 1 M sodium hydroxide (28 mL) and water (25 mL). Boc-anhydride (1.1 eq, 4.87 g, 22.3 mmol) was dissolved in 10 mL of dioxane and added to the orange L-dopa solution. This was stirred for 1 h, after which the pH was adjusted to between pH 9 and 10 by adding 1 M sodium hydroxide dropwise and testing with indicator paper. The black solution was stirred for 18 h, overnight. The resulting solution was concentrated by rotary evaporation before being acidified to pH 2 using 1 M hydrochloric acid. This was extracted four times using ethyl acetate. The organic layers were combined and dried using magnesium sulphate. The magnesium sulphate was removed by filtration and the remaining solvent was removed by rotary evaporation. The solid product (see structure 1 in Figure 3) was placed under high vacuum to ensure product was completely dry. The product was a brown solid (4.28 g, 71 %). $[M+Na]^+$ = 320.1110 and $[M+H]^+$ = 298.1291. The mass of M ($C_{14}H_{19}NO_6$) expected is 297.1212, mass spectrometry confirmed the expected formula with a mass accuracy of 4.5 ppm for $[M+H]^+$ and 1.9 ppm for $[M+Na]^+$. δH (300

MHz, DMSO-d_6): 1.31 (9H, s, Boc), 2.72 (2H, m, Ar$C\underline{H_2}$R), 3.95 (1H, m, Ar$CH_2C\underline{H}$(NHBoc)R), 6.44 (2H, d, Ar-$\underline{H_2}$H), 6.51 (1H, s, Ar-$H_2\underline{H}$), (6.92 (1H, d, N$\underline{H}$Boc confirmed by HMQC), 8.68 (1H, broad s, COO$\underline{H}$). δC (75 MHz, DMSO-d_6) confirmed by pendant: 28.52 (Boc $\underline{C}H_3$ groups), 36.23 (R$\underline{C}H_2$R), 55.94 (R$\underline{C}$HR), 78.35 (RO$\underline{C}C_3H_9$), 115.61 – 120.13 (3 Ar-$\underline{C}$H), 129.06 – 145.19 (3 Ar-$\underline{C}$), 155.80 (RHN$\underline{C}$(O)OR), 174.16 (R$\underline{C}$OOH).

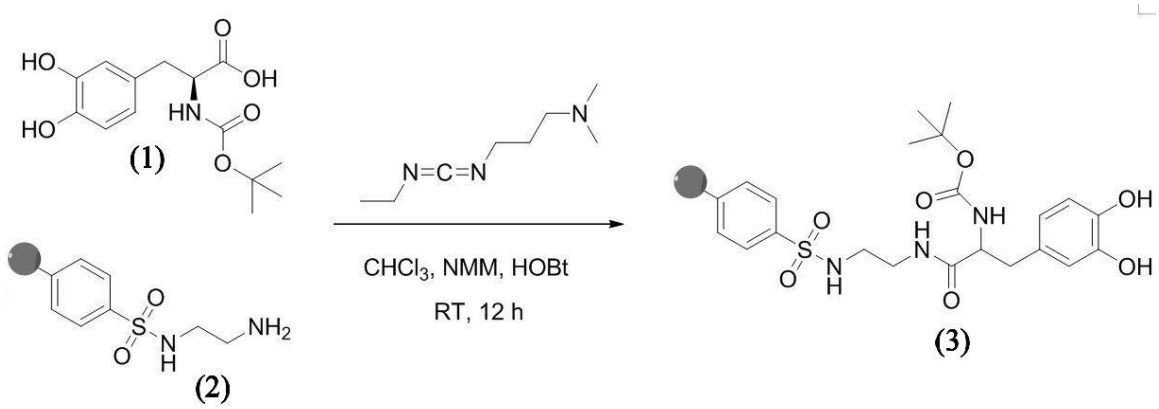

Figure 6.3. Reaction scheme for the formation of dopa-modified carbon nanoparticles and molecular structures for (1) boc-protected dopa, (2) ethylenediamine-modified Emperor 2000 carbon nanoparticle, and (3) dopa-modified carbon nanoparticle.

Ethylenediamine Modified Carbon Nanoparticles. (a) Emperor 2000 carbon nanoparticles (5 g) were sonicated in dry dichloromethane for 30 minutes after which the flask was degassed with nitrogen and placed in an ice bath to reduce the temperature to 0°C. Thionylchloride (50 mL, 0.69 mol) was added drop-wise to the cooled suspension under continuous stirring. The suspension was left to stir for 18 h, allowing to warm to room temperature. Excess dichloromethane and thionyl chloride were removed by rotary evaporation. (b) A clean and oven-dried round bottom flask was charged with

ethylenediamine (50 mL, 0.75 mol). To this, dichloromethane was added (150 mL) and the temperature was cooled to around 0°C using an ice bath. The chlorinated nanoparticles from part (a) were added in small portions to the cooled ethylenediamine and dichloromethane. This was removed from the ice bath and allowed to warm to room temperature over 2 h. Excess amine and dichloromethane were removed by rotary evaporation to give viscous black oil. Excess 1 M hydrochloric acid was added to the oil to yield a black solid that was collected by Büchner filtration. The solid was washed repeatedly with dichloromethane before being placed in a dessicator to dry.

Dopylation of Carbon Nanoparticles. An oven-dried round bottom flask was charged with boc-protected dopa (297 mg, 1 mmol). To this, N-methylmorpholine (1.08 mL, 10 mmol), hydroxybenzotriazole (135 mg, 1 mmol) and 1-ethyl-3-(3-dimethylaminopropyl) carbodiimide (155 mg, 1 mmol) were added and dissolved under nitrogen to form an orange solution. A portion of ground ethylenediamine-modIfied nanoparticles were added to the reaction mixture, this was stirred overnight for 18 h at ambient temperature. The resulting suspension was diluted in chloroform (300 mL). The black solid product was obtained by Büchner filtration.

6.4. Results and Discussion

6.4.1. Formation of L-Dopa-Boc-Modified Carbon Nanoparticles and Voltammetric Characteristics in Aqueous Media

A peptide coupling reaction using a carbodiimide activating agent was used (1-ethyl-3-(3-dimethylaminopropyl) carbodiimide [EDCI], see Figure 6.3). The L-dopa was boc-protected to ensure that the L-dopa solely reacted with the terminal amine on the nanoparticle, rather than form a polypeptide with other molecules of L-dopa.

The successful surface-functionalisation was confirmed by electrochemical methods. The modified nanoparticles (30 mg) were dispersed into 10 cm^3 water and deposited onto a carbon electrode using a pipette. Typically, 30 µL of the suspension were deposited and placed in an 80°C oven for 10 minutes to evaporate solvent. Cyclic voltammograms were recorded in aqueous 0.1 M pH 2 phosphate buffer solution (see Figure 6.4.A). A redox response was observed with an oxidation peak at 0.63 V vs. SCE and reduction peak at approximately 0.30 V vs. SCE consistent with the expected response for dopa-boc. The midpoint potential was $E_{mid} = ½(E_p^{ox}+E_p^{red}) = 0.47$ V vs. SCE very close to that reported previously for dopa at pH 2 in aqueous media [36].

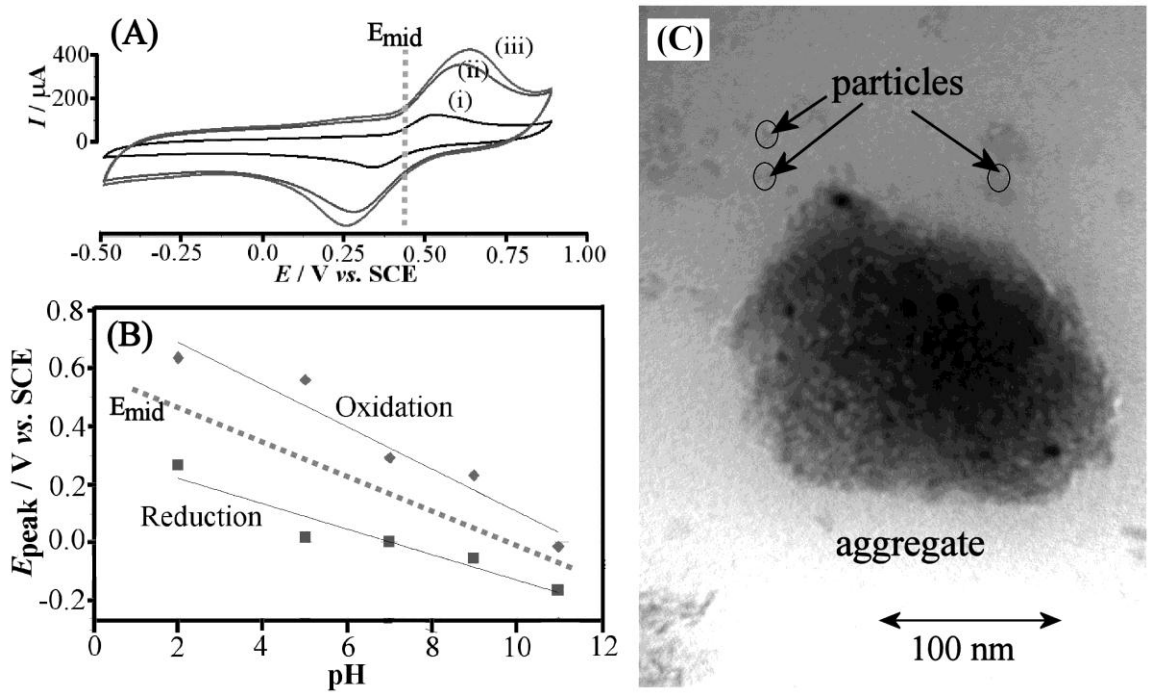

Figure 6.4. (A) Cyclic voltammograms (scan rate 50 mVs^{-1}) for the oxidation of L-dopa-boc modified carbon nanoparticles (i) 15 μg, (ii) 30 μg, and (iii) 60 μg immobilized on a 3 mm diameter screen printed carbon electrode and immersed in aqueous 0.1 M phosphate buffer pH 2. (B) Plot of the peak potentials and the midpoint potential as a function of pH. (C) TEM image of modified carbon nanoparticle aggregates of ca. 100 nm diameter.

The charge under the dopa-boc oxidation peak does vary to some extent due to the formation of carbon nanoparticle aggregates (and due to some carbon nanoparticle aggregates falling off the electrode), but assuming a 0.8 mC charge for the oxidation of 30 μg material and assuming a diameter of approximately 10 nm (see Figure 4C) allows the surface coverage to be estimated as ca. 100 L-dopa-boc per carbon nanoparticle.

Next, the dopa-boc-modified nanoparticles were investigated as a function of pH and Figure 6.4.B shows a plot of midpoint potentials versus pH. An approximately linear

correlation is observed with Nernstian slope consistent with a 2-electron 2-proton redox process. Importantly, the irreversible follow-up reaction to form dopachrome (Figure 6.1) appears to be suppressed by the boc-protection of the amine. Some variations in the peak potentials for oxidation and reduction are observed due to (i) problems of loss of particles into the aqueous solution phase and (ii) some more minor effects of buffer capacity on the peak position [26].

6.4.2. Voltammetric Characterisation of L-Dopa-Boc-Modified Carbon Nanoparticles in Contact to Humidified Dowex Media

In experiments with Dowex polymer media the carbon nanoparticles are immobilised at the interface between the working electrode and the ion exchanger particles. Therefore losses of L-dopa-boc-modified nanoparticles can be avoided and a constant amount of redox active material can be maintained at the electrode surface in close contact to the gas phase. In a typical experiment, an amount of carbon nanoparticles (for example 0.05 wt% loading) is mixed with the ion exchanger particles (pre-treated in buffer solution and dried) with mortar and pestle. SEM images of the particles of Dowex 50W 1x4 with about 200-300 μm diameter and of Dowex 50W 1x2 of typically 200 μm diameter are shown in Figure 5. The presence/location of carbon nanoparticles at a loading of 0.05 wt% (giving visibly black materials) is not resolved by SEM (see Figure 6.5.E,F) or TEM. Small features at the Dowex sphere surfaces are due mainly to small amounts of salt extrusions. The carbon nanoparticles of typically 9-18 nm diameter are likely to be

embedded into the Dowex particle surfaces or "smeared" over the polymer particle in the grinding process.

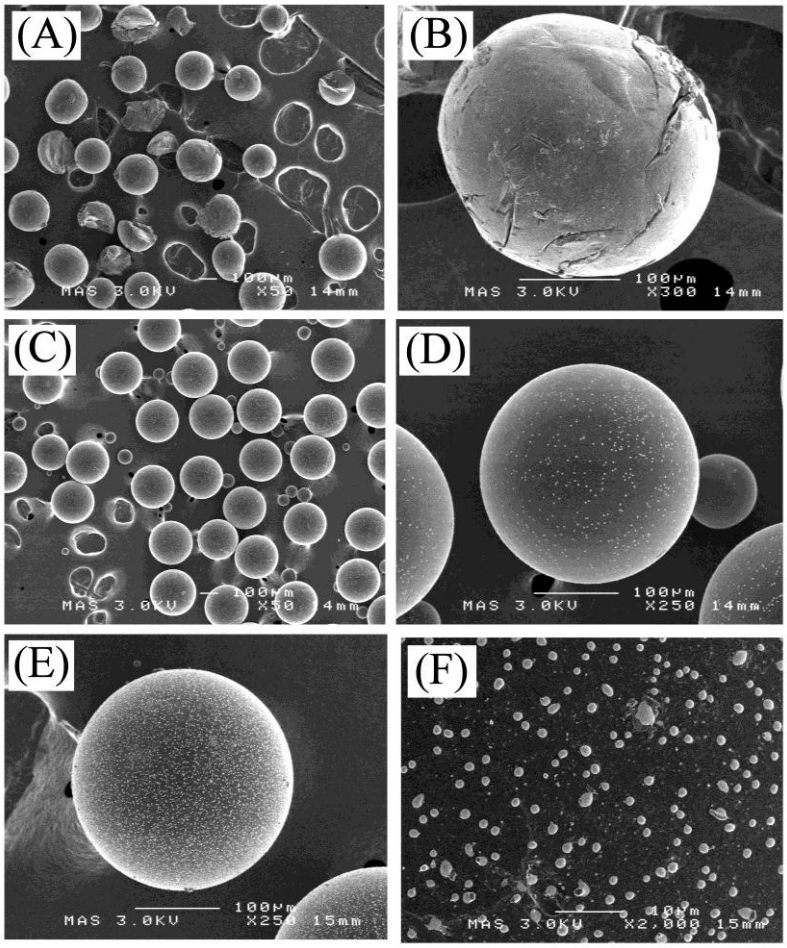

Figure 6.5. SEM images for (A,B) Dowex 50Wx4 particles after buffer treatment, (C,D) Dowex 1x2 particles after buffer treatment, and (E,F) Dowex 1x2 particles with 0.05 wt% loading of L-dopa-boc-modified carbon nanoparticles.

The Dowex/carbon nanoparticle mixture is placed into the electrochemical cell (see Figure 6.2.A) between counter-reference and working electrode. A flow of humidified argon (ca. 80 % relative humidity by passing argon through saturated $(NH_4)_2SO_4$ [35]) is used to maintain stable conditions in the cell. After a 10 minute equilibration measurements are performed in cyclic voltammmetry mode.

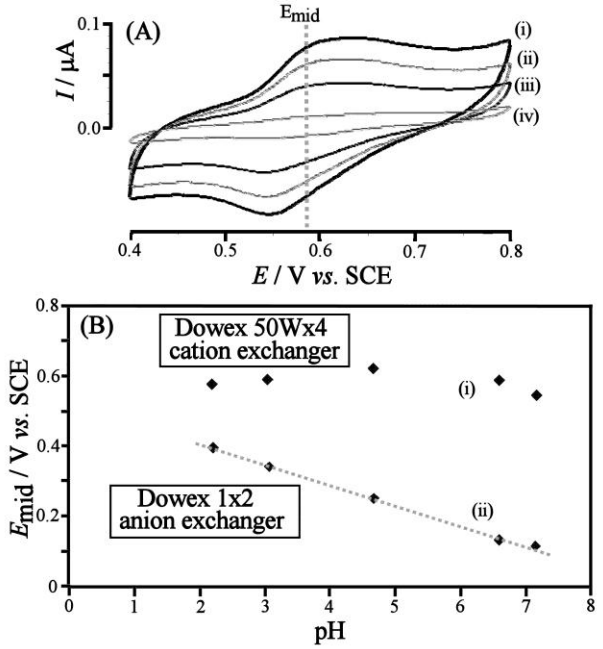

Figure 6.6. (A) Cyclic voltammograms (scan rate (i) 10, (ii) 8, (iii) 5, and (iv) 1 mVs^{-1}) for L-dopa-boc-modified CNPs (0.01 wt% loading) on Dowex 50Wx4 pre-treated in PBS pH 2.2. (B) Plot of the midpoint potentials for dopa-boc-modified CNPs for two different ion exchangers and as a function of pre-treatment pH.

Figure 6.6.A shows a typical set of voltammograms obtained for 0.01 wt% loading of L-dopa-boc-modified CNPs with Dowex 50Wx4 cation exchanger. The oxidation and reduction peaks are clearly observed with a midpoint potential of ca. 0.59 V vs. SCE. Experiments recorded as a function of scan rate showed linearity of peak current with scan rate in agreement with a surface-immobilised redox system. The effect of the pH of the pre-treatment solution for the ion exchanger is shown in Figure 6.6.B. A highly reproducible Nernstian dependency is observed for the Dowex 1x2 anion exchanger in agreement with phosphate anion immobilisation to maintain pH. This dependency is also in good agreement with the solution data (see Figure 6.4.B).

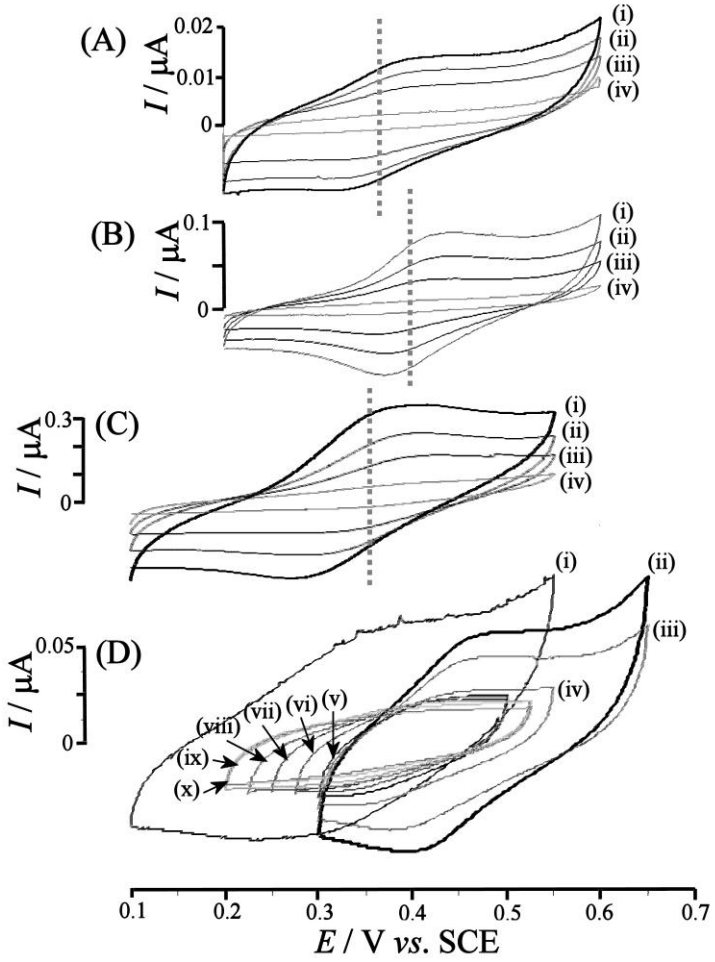

Figure 6.7. (A) Cyclic voltammograms (scan rate (i) 10, (ii) 8, (iii) 5, and (iv) 1 mVs^{-1}) for the oxidation of L-dopa-boc-modified CNPs (loading 0.08 wt% in Dowex 50 1x2 pH 3) in 80% humid argon. (B) As before with 0.16 wt% loading. (C) As before with 0.32 wt% loading. (D) Cyclic voltammograms (scan rate 10 mVs^{-1}) for the oxidation of L-dopa-boc-modified CNPs (loading 0.08 wt% in Dowex 50 1x2 pH 3) initial cycle (i) in 80% humid argon followed by measurements every 10 minutes (ii) to (x) in dry argon.

Perhaps surprisingly, the Dowex 50Wx4 cation exchanger particles appear to maintain a highly acidic environment (extrapolation of the data for Dowex 1x2 allows the pH to be estimated as -1) even when treated in milder buffer solution (see Figure 6.7.B). This is

explained by the absence of a buffer system other than the sulfonic acid groups in the ion exchanger.

The effect of CNP loading is demonstrated in Figure 6.7.A-C. Variation in peak currents of ca. +/- 50% for repeat experiments with the same loading of carbon nanoparticles are observed (probably due to effects of CNP distribution at the Dowex particle surface), but a general trend is seen for higher loading causing a higher peak current (see Figure 6.7.A-C). The area under the oxidation peak can be integrated (e.g. 4 μC for 0.32 wt% loading in Figure 6.7.C) and the number of active carbon nanoparticles evaluated (ca. 10^{11} for data in Figure 6.7.C corresponding to only 2% active electrode coverage). In all cases sub-mono-layer coverage is observed indicating that only individual "dots" of carbon are active and there is no conductivity across the dowex particle surfaces.

The effect of humidity on the cyclic voltammetry data is shown in Figure 6.7.D. Switching argon gas flow from 80% humidity to dry argon causes a slow change with a decrease in both capacitive background current and L-dopa-boc oxidation response. However, the midpoint potential appears stable (apart from the first switch in humidity level) and the L-dopa-boc response remains measurable over prolonged times.

6.4.3. Voltammetry of L-Dopa-Boc-Modified Carbon Nanoparticles in Contact to Humidified Dowex Media as a Tool for Ammonia Sensing

In order to explore the effect of ammonia on the L-dopa-boc oxidation response an experiment was performed with a syringe injection of 1 cm^3 quantities of ammonia into

the argon flow (ca. 60 cm^3 min^{-1}). To improve the sensitivity of the measurement differential pulse voltammetry scans were performed (see Figure 8).

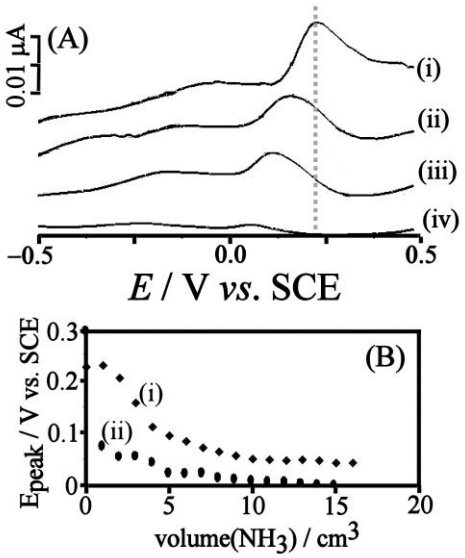

Figure 6.8. (A) Differential pulse voltammogram (scan rate 10 mVs^{-1}, step potential 1.06 mV, amplitude 25 mV) for L-dopa-boc-modified carbon nanoparticle oxidation in Dowex 50 1x2 (0.1 wt% loading) for (i) 0, (ii) 3, (iii) 4, and (iv) 9 cm^3 ammonia injection. (B) Plot of the midpoint potential versus volume of injected ammonia for (i) loading 0.1 wt% and (ii) loading 0.01 wt% (gas flow rate 60 cm^3 min^{-1}).

Initially, a stable peak signal is observed at ca. 0.25 V vs. SCE. At low carbon nanoparticle loading (see plot for 0.01 wt% in Figure 6.8.B(ii) an immediate drop in midpoint potential and in peak current are observed. With a higher loading of carbon nanoparticles (see Figure 8A) a gradual shift of the L-dopa-boc peak and a weakening of the peak are observed upon sequential injection of ammonia into the argon flow.

The shift in the midpoint potential is indicative of a shift in local pH at the Dowex - working electrode interface. Comparison with the calibration plot in Figure 6.8.B suggests a final pH reaching 8 to 9. The additional drop in current is consistent with the irreversible reaction of the dopaquinone, here probably with free ammonia (e.g. nucleophilic addition of ammonia to dopaquinone), to give more complex surface species without redox activity in the potential range covered in these measurements.

In summary, the surface-immobilised L-dopa-boc on carbon nanoparticles, which are immoblised onto Dowex ion exchanger particles, provides a sensitive tool for detecting ammonia or other pH-affecting gases. The methodology could be of wider applicability when the chemical selectivity of surface reactions (e.g. L-dopaquinone with other air-borne nucleophiles) could be exploited with electrochemical product detection. The effective chemical stabilisation of the L-dopa redox system by the boc protection group together with the convenient potential range will allow similar sensors to be operated in real gas media, e.g. in the presence of dioxygen, and under conditions of fluctuating humidity.

6.5. Conclusion

It has been shown that L-dopa-boc-modified carbon nanoparticles can be employed as redox probes in pH sensing. An electrochemical cell with Dowex ion exchanger electrolyte particles was introduced with carbon nanoparticles immobilised at the electrode surface – ion exchanger interface. L-Dopa-boc oxidation was detected over a 2

to 12 pH range and Dowex 50 1x2 has been demonstrated to allow control of the local pH at the electrode. Although most experiments were performed with 80% relative humidity under argon, it has been shown that sensitivity of the device towards humidity changes is acceptable. Injection of ammonia into the argon gas flow has been employed to cause pH changes at the electrode surface as monitored by the L-dopa-boc oxidation differential pulse peak potential. Sensitivity levels of 1 cm^3 ammonia (or ca. 33000 ppm short term exposure) are readily achieved in particular at lower L-dopa-boc-modified carbon nanoparticle loadings. In future, this device concept will be of wider use and potentially important for cases where chemical selectivity in gas sensing is required. For example, specific surface immobilised receptor groups could be developed to allow disease bio-marker detection in breath or environmental pollutant detection in urban or office areas.

6.6. References

[1] M. Uchimiya, A.T. Stone, Chemosphere 77 (2009) 451-458.

[2] B.K. Glod, K.I. Stanczak, A. Wozniak, W. Pakszys, Acta Chromato. 14 (2004) 142-148.

[3] F.N. Rein, R.C. Rocha, H.E. Toma, J. Inorg. Biochem. 85 (2001) 155-166.

[4] T.E. Young, J.R. Griswold, M.H. Hulbert, J. Org. Chem. 39 (1974) 1980-1982.

[5] P.A. Brooksby, D.R. Schiel, A.D. Abell, Langmuir 24 (2008) 9074-9081.

[6] T. Nakanishi, M. Matsunaga, M. Nagasaka, T. Asahi, T. Osaka, J. Amer. Chem. Soc. 128 (2006) 13322-13323.

[7] A. Brun, R. Rosset, J. Electroanal. Chem. 49 (1974) 287-300.

[8] X.Q. Liu, Z.L. Zhang, G.J. Cheng, S.J. Dong, Electroanalysis 15 (2003) 103-107.

[9] J.Y. Li, F.J. Zhang, B.M. Christensen, J. Electroanal. Chem. 412 (1996) 19-29.

[10] M. Rafiee, L. Khalafi, Electrochim. Acta, 55 (2010) 1809-1813.

[11] G.N.L. Jameson, J. Zhang, R.F. Jameson, W. Linert, Org. Biomol. Chem. 2 (2004) 777-782.

[12] J. Mathiyarasu, L. Nyholm, Electroanalysis, 22 (2010) 449-454.

[13] M.D. Rubianes, A.S. Arribas, E. Bermejo, M. Chicharro, A. Zapardiel, G. Rivas, Actuators B-Chem. 144 (2010) 274-279.

[14] F.P. Zhang, S.P. Bi, J.R. Zhang, N.S. Bian, F. Liu, Y.Q. Yang, Analyst, 125 (2000) 1299-1302.

[15] F.P. Zhang, S.P. Bi, H.Z. Li, Y.J. Chen, L.M. Dai, Electroanalysis, 13 (2001) 1054-1058.

[16] Q. Li, H. Li, J. Zhang, Z.H. Xu, Sens. Actutors B-Chem. 155 (2011) 730-736.

[17] H. Dussel, S. Komorsky-Lovric, F. Scholz, Electroanalysis, 7 (1995) 889-894.

[18] G.G. Wildgoose, M. Pandurangappa, N.S. Lawrence, L. Jiang, T.G.J. Jones, R.G. Compton, Talanta, 60 (2003) 887-893.

[19] N.S. Lawrence, M. Pagels, S.F.J. Hackett, S. McCormack, A. Meredith, T.G.J. Jones, G.G. Wildgoose, R.G. Compton, L. Jiang, Electroanalysis, 19 (2007) 424-428.

[20] M.A. Ghanem, J.M. Chretien, A. Pinczewska, J.D. Kilburn, P.N. Bartlett, J. Mater. Chem. 18 (2008) 4917-4927.

[21] K. Tammeveski, K. Kontturi, R.J. Nichols, R.J. Potter, D.J. Schiffrin, J. Electroanal. Chem. 515 (2001) 101-112.

[22] P. Abiman, G.G. Wildgoose, R.G. Compton, J. Phys. Org. Chem. 21 (2008) 433-439.

[23] M. Pandurangappa, T. Ramakrishnappa, R.G. Compton, Carbon, 47 (2009) 2186-2193.

[24] E.L.S. Wong, R.G. Compton, J. Phys. Chem. C, 112 (2008) 8122-8126.

[25] L. Vidal, A. Chisvert, A. Canals, E. Psillakis, A. Lapkin, F. Acosta, K.J. Edler, J.A. Holdaway, F. Marken, Anal. Chim. Acta, 616 (2008) 28-35.

[26] J.D. Watkins, K. Lawrence, J.E. Taylor, T.D. James, S.D. Bull, F. Marken, 23 (2011) 1320-1324.

[27] M. Amiri, S. Shahrokhian, E. Psillakis, F. Marken, Anal. Chim. Acta, 593 (2007) 117-122.

[28] J.D. Watkins, R. Lawrence, J.E. Taylor, S.D. Bull, G.W. Nelson, J.S. Foord, D. Wolverson, L. Rassaei, N.D.M. Evans, S.A. Gascon, F. Marken, Phys. Chem. Chem. Phys. 12 (2010) 4872-4878.

[29] M. Stankova, X. Vilanova, J. Calderer, E. Llobet, J. Brezmes, I. Gracia, C. Cane, X. Correig, Sens. Actuators B-Chem. 113 (2006) 241-248.

[30] Cheng-Wei Lin, Huey-Ing Chen, Tai-You Chen, Chien-Chang Huang, Chi-Shiang Hsu, Rong-Chau Liu, Wen-Chau Liu, Sens. Actuators B: Chem. (2011) article in press, doi:10.1016/j.snb.2011.07.041.

[31] B.A.L. de Mishima, D. Lescano, T.M. Holgado, H.T. Mishima, Electrochim. Acta, 43 (1998) 395-404.

[32] M.C. Buzzeo, D. Giovanelli, N.S. Lawrence, C. Hardacre, K.R. Seddon, R.G. Compton, Electroanalysis, 16 (2004) 888-896.

[33] T. Ramakrishnappa, M. Pandurangappa, D.H. Nagaraju, Sens. Actuators B-Chem. 155 (2011) 626-631.

[34] D.R. Lide (ed.), Handbook of Chemistry and Physics, 74th ed., CRC Press, London, 1993, 15-25.

[35] S.E.C. Dale, C.Y. Cummings, F. Marken, Electrochem. Commun. 13 (2011) 154-157.

[36] A. Afkhami, D. Nematollahi, L. Khalafi, M. Rafiee, Internat. J. Chem. Kin. 37 (2005) 17-24.

Chapter 7

Surface Electrochemistry at Dowex Ionomer | Glassy Carbon | Gas Interfaces

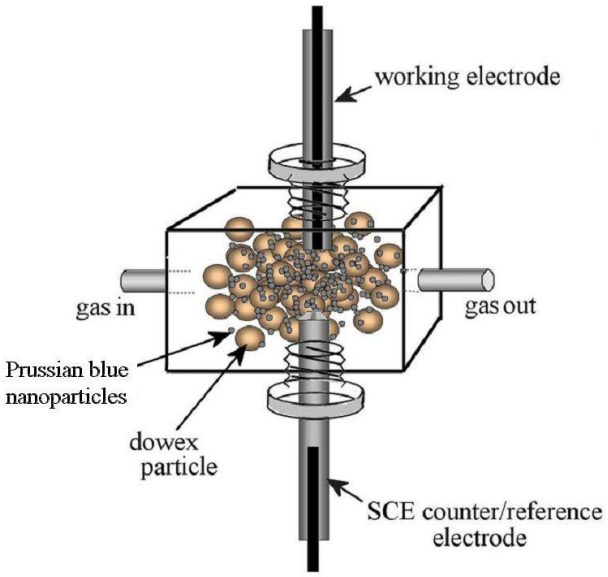

Acknowledgements
Collaboration and discussion with Dr. Sara E.C. Dale are gratefully acknowledged. We thank Dr. Andrew D. Burrows for providing a sample of $Co(phen)_3(PF_6)_2$.

Content

Abstract

This chapter focuses on the immobilisation of redox systems onto the surface of Dowex ionomer spheres and the study of redox processes which are of potential use in gas sensing. The "salt cell" device with a working and a counter/reference electrode terminal is employed with a humid gas flow. The $Co(phen)_3(PF_6)_3$ (phen = 1,10-phenanthroline) redox active metal complex is immobilised on Dowex 50 W 1x4 cation exchanger and investigated by cyclic voltammetry. A reversible Co(III/II) processes is observed and enhanced in the presence of 4-(3-phenyl-propyl)-pyridine. Next, Prussian blue is formed on the surface of Dowex 50W 1x2 anion exchanger and investigated as a function of potential. The stabilising effect of acidic pH on the $K(Fe[Fe(CN)_6])$ to $Fe[Fe(CN)_6]$ redox system is reported based on cyclic voltammetry and differential pulse voltammetry. Implications for future gas sensing devices are discussed.

7.1. Introduction to Prussian Blue and Ionomer | Electrode | Gas Interfaces

The joint interface of an electrode, ion conductor, and gas offers an interesting reaction environment with applications in gas sensing. In the previous chapter the use of Dowex ionomer materials was developed and the contact to the electrode was used for ortho-quinol/one redox chemistry under well defined pH and gas phase conditions. This idea is develop further in this chapter by introducing a well-known surface electrocatalyst, Prussian blue [1].

Prussian blue has been established in particular for hydrogen peroxide detection [2] and for biosensors [3]. The work by Karyakin et al. [4] suggests that extremely low detection limits are accessible. However, Prussian blue and its analogs [5] have been beneficial in a much wider range of applications [6]. Prussian blue can be formed in a layer-by-layer deposition process [7], by potential cycling [8], or by assembly from nanoparticles [9].

In this chapter, first Dowex 50 Wx4 ionomer particles with cation exchanger properties are studied and it is shown that metal complexes such as $Co(phen)_3^{3+}$ (of potential use in thiol, H_2S, or DNA sensing [10]) can be immobilised. Electrochemical signals are obtained in the presence of humid argon. Next, Dowex 50W 1x2 particles with anion exchanger capability are employed to first bind $Fe(CN)_6^{4-}$ which is then reacted with Fe^{3+}

to give a Prussian blue surface layer. The effect of pH on stability and signal are investigated. The system is promising for future sensor development.

7.2. Experimental Methods

7.2.1. Chemicals

Dowex 50 Wx4 cation exchanger and Dowex 50W 1x2 anion exchanger, phosphoric acid, NaOH, $K_4Fe(CN)_6$, and $Fe(NO_3)_3$ were obtained from Aldrich and used without further purification. Argon (Pureshield, BOC) was used for de-aeration of solutions. Demineralised and filtered water was taken from a Thermo Scientific water purification system (Barnstead Nanopure) with 18.2 MΩcm resistivity.

7.2.2. Instrumentation

A microAutolab III potentiostat system (EcoChemie, The Netherlands) was employed in electrochemical measurements. A 3 mm diameter glassy carbon disc electrode (BAS, US) was the working electrode and a KCl-saturated calomel electrode (SCE, Radiometer) was the counter-reference. A custom-made PEEK cell with gas in and outlet (see Figure 1) was used with a wash bottle to pre-saturate argon with 80% relative humidity [11].

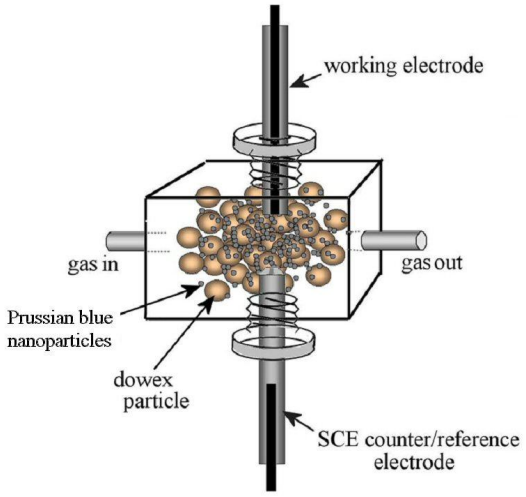

Figure 7.1. Schematic drawing of the gas flow cell with Dowex particles acting as the solid electrolyte. Redox systems are immobilised onto Dowex by mechanical grinding or by surface precipitation.

7.2.3. Procedures

The modification of the Dowex ion exchanger particles with redox active materials was performed in two different approaches:

A: for solid materials, such as $Co(phen)_3(PF_6)_2$, the ion exchanger and redox active solid (0.05 wt%) were placed into a mortar and pestle and gently ground together. In some cases an additional liquid, 4-(3-phenyl-propyl)-pyridine) was added (1 wt%).

B: the immobilization of Prussian blue followed a surface-precipitation approach. Dowex 50 1x2 anion exchanger was first placed into aqueous 20 mM $K_4Fe(CN)_6$ for 5 minutes followed by filtration and washing with distilled water (yellow coloration). The particles are then placed into aqueous 20 mM $Fe(NO_3)_3$ for 5 minutes followed by filtration and washing with distilled water (green coloration). Finally, the particles are placed into

aqueous 0.1 M phosphate buffer at the desired pH for 5 minutes followed by filtration and washing with distilled water. When dried, a green solid is obtained and used in "salt cell" electrochemistry. Figure 7.2. shows a typical optical microscopy image of Dowex microparticles.

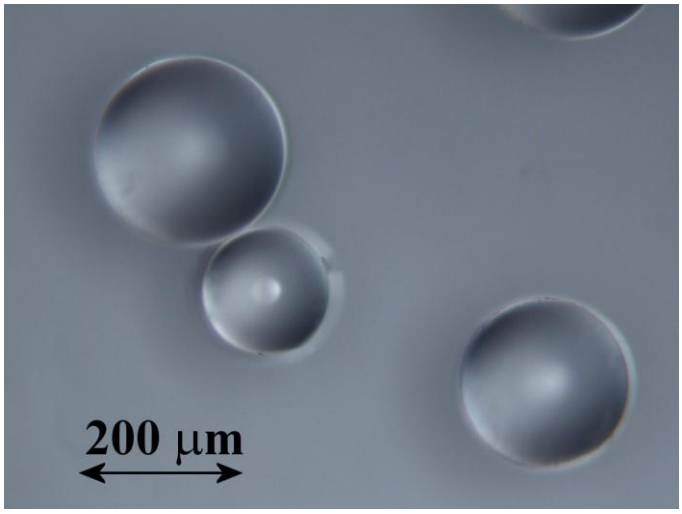

Figure 7.2. Optical microscopy image of Dowex 50 ion exchanger micro-particles used as solid electrolyte between working electrode and counter-reference electrode.

7.3. Results and Discussion

7.3.1. Voltammetric Characteristics of $Co(phen)_3^{3+/2+}$ Absorbed into Acidic Dowex 50 W×4

Initially, a well-known redox system with reversible one-electron transfer (see equation 1) is investigated. The redox-active metal complex $Co(phen)_3^{2+}$ has been studied previously [12] and employed for example as intercalator into DNA [13], for the catalytic reduction of carbon dioxide [14], and for the electroanalytical detection of mercapto-compounds [15].

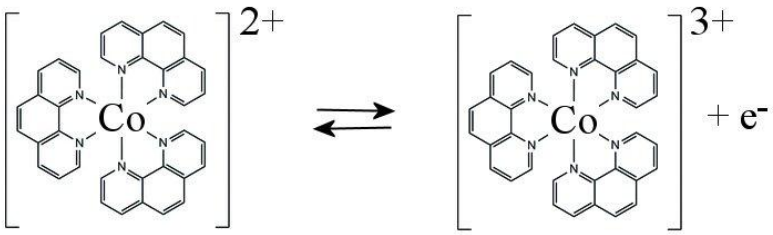

(1)

The oxidation is reversible and observed at ca. 0.3 V vs. SCE. Figure 7.2.A shows a set of voltammetric responses with a weak oxidation – reduction response. The fact that a cation exchanger Dowex 50 Wx4 is employed may cause some immobilisation of the metal complex and limited mobility and therefore only weak current responses are seen at ca. 0.2 V vs. SCE. In Figure 7.2.B the experiment is repeated but with co-immobilisation of 4-(3-phenylpropyl)-pyridine. In this case the voltammetric signature for the Co(III/II)

process is a little clearer and the reversible potential is shifted positive to ca. 0.4 V vs. SCE.

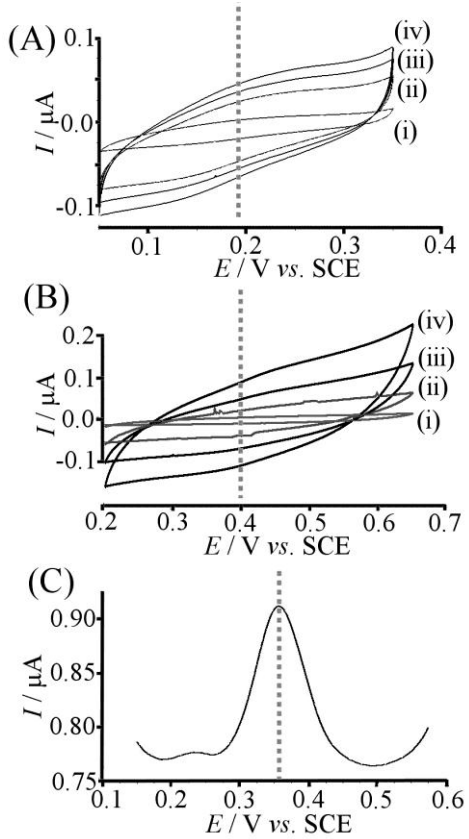

Figure 7.2. (A) Cyclic voltammograms (scan rates (i) 1, (ii) 5, (iii) 8, and (iv) 10 mVs^{-1}) for the oxidation and back-reduction of $Co(phen)_3^{2+}$ immobilised into Dowex 50 Wx4 and in contact to a 3 mm diameter glassy carbon electrode. (B) As above, but with addition of 4-(3-phenylpropyl)-pyridine. (C) Differential pulse voltammogram for the oxidation of $Co(phen)_3^{2+}$ on Dowex 50 Wx4 in the presence of 4-(3-phenyl-propyl)-pyridine.

In order to remove the capacitive background, differential pulse voltammetry methods can be employed. Here, the Co(III/II) system in the presence of 4-(3-phenylpropyl)-pyridine is investigated using a 25 mV amplitude and 50 ms pulse time. A clear peak is detected at 0.36 V vs. SCE. These measurements demonstrate that electrocatalysts such as $Co(phen)_3^{2+}$ can be immobilised and studied at Dowex 50W 1 x 4 ionomer particles.

Here, only humidified argon is employed as the background gas, but in future gas flow with components such as thiols or H_2S could be employed for gas sensing applications.

7.3.2. Voltammetric Characterisation of Prussian Blue Absorbed into Basic Dowex 50 1×2: Cyclic Volatmmetry

Prussian blue [16] and Prussian blue analogs have attracted attention in many area of electrochemical device application. One particular area of work is in the detection of H_2O_2 down to extremely low levels in bio-sensors [17].

Prussian blue is formed usually by precipitation from $Fe(CN)_6^{4-}$ and Fe^{3+} in aqueous media. The initial product has Fe^{3+} adsorbed in excess in interstitial sites and is called "insoluble" Prussian blue. After the initial potential cycles this is transformed into "soluble" Prussian blue with redox activity associated with K^+ exchange (see equation 2-4 [18]).

$$Fe_4[Fe(CN)_6]_3 \rightarrow 3\,Fe[Fe(CN)_6] + Fe^{3+} + 3\,e^- \quad (2)$$

"insoluble" Prussian blue Prussian yellow

$$Fe[Fe(CN)_6] + K^+ + e^- \rightarrow FeK[Fe(CN)_6] \quad (3)$$

Prussian yellow "soluble" Prussian blue

$$FeK[Fe(CN)_6] + K^+ + e^- \rightarrow FeK_2[Fe(CN)_6] \quad (4)$$

"soluble" Prussian blue Everitt's salt

Here, this process is investigated within an ionomer matrix. Dowex 50 1x2 anion exchanger is employed initially to bind $Fe(CN)_6^{4-}$ (see experimental). The modified Dowex anion exchanger is then placed into aqueous Fe^{3+} where precipitation of Prussian blue is induced at the Dowex particle surface. The process is sensitive to the Fe^{3+} concentration and results in a green product (due to a combination of yellow and blue). In a post-treatment the Prussian blue modified particles are placed in appropriate phosphate buffer solution to adjust the particle pH. The Dowex 50 1x2 anion exchanger is able to adopt a pH due to the uptake of phosphate anions into the anion exchanger.

When placed into the electrochemical cell between a 3 mm diameter glassy carbon electrode and a KCl-saturated calomel reference-counter electrode under humid argon flow, distinct electrochemical responses are detected. Figure 7.3.A shows cyclic voltammetry data for sequential cycles at pH 7.1. Clearly the oxidation of Prussian blue to Everitt's salt (equation 4) is observed at ca. 0.8 V vs. SCE and the reduction of Prussian blue to Prussian yellow (equation 3) at ca. 0.1 V vs. SCE. In continuous potential cycles the oxidation is completely lost after a short period, probably due to degradation of the Prussian blue under these conditions.

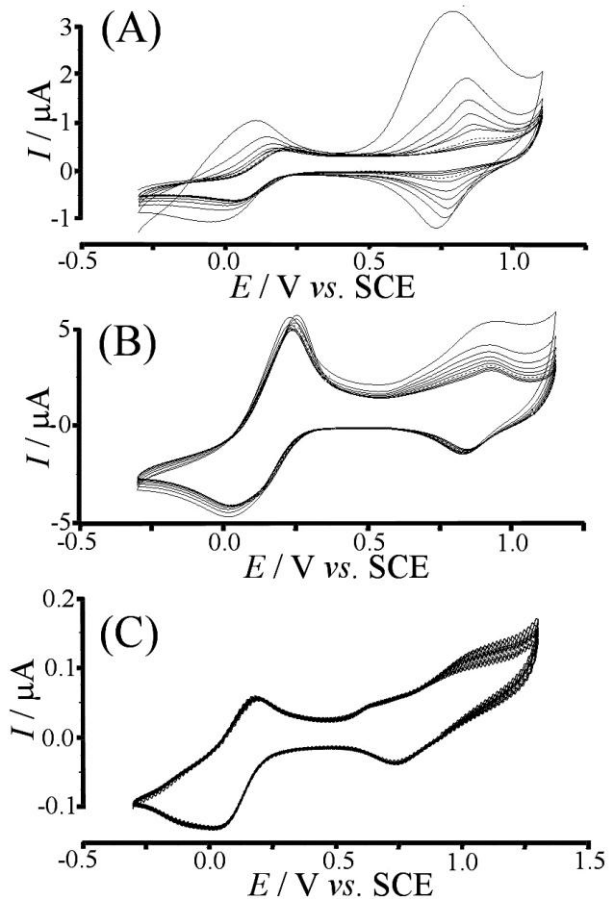

Figure 7.3. (A) Cyclic voltammograms (10 cycles, scan rate 0.05 Vs^{-1}) for the oxidation and reduction of Prussian blue immobilised onto Dowex 50 1x2 at pH 7.1 in contact to a 3 mm glassy carbon electrode. (B) As above, but at pH 4.7. (C) As above, but at pH 2.2.

By changing the pH in the Dowex particles, the redox behaviour of the Prussian blue deposit can be modified. Figure 7.3.B shows data obtained at pH 4.7 and both redox systems appear to remain stable during continuous potential cycling. Finally, at pH 2.2 again a more stable voltammetric response is obtained.

7.3.3. Voltammetric Characterisation of Prussian Blue Absorbed into Basic Dowex 50 1×2: Differential Pulse Voltammetry

In order to explore the redox processes of Prussian blue on Dowex 50 1x2 anion exchanger in more detailed differential pulse voltammetry experiments have been carried out. Figure 7.4.A shows the peak responses associated with the oxidation of Prussian yellow to Prussian blue (ca. 0.0 V vs. SCE) and the oxidation of Prussian blue to Everitt's salt (ca. 0.7 V vs. SCE). When investigating the Prussian blue redox system over a period of time the second oxidation appears unstable and it decays rapidly at pH 7. Figure 7.4.B shows data before and after decay of the signal. The first oxidation is shifted positive to ca. 0.1 V vs. SCE probably due to structural changes with a high level of $Fe(CN)_6^{3-/2-}$ dominating the voltammetric signal.

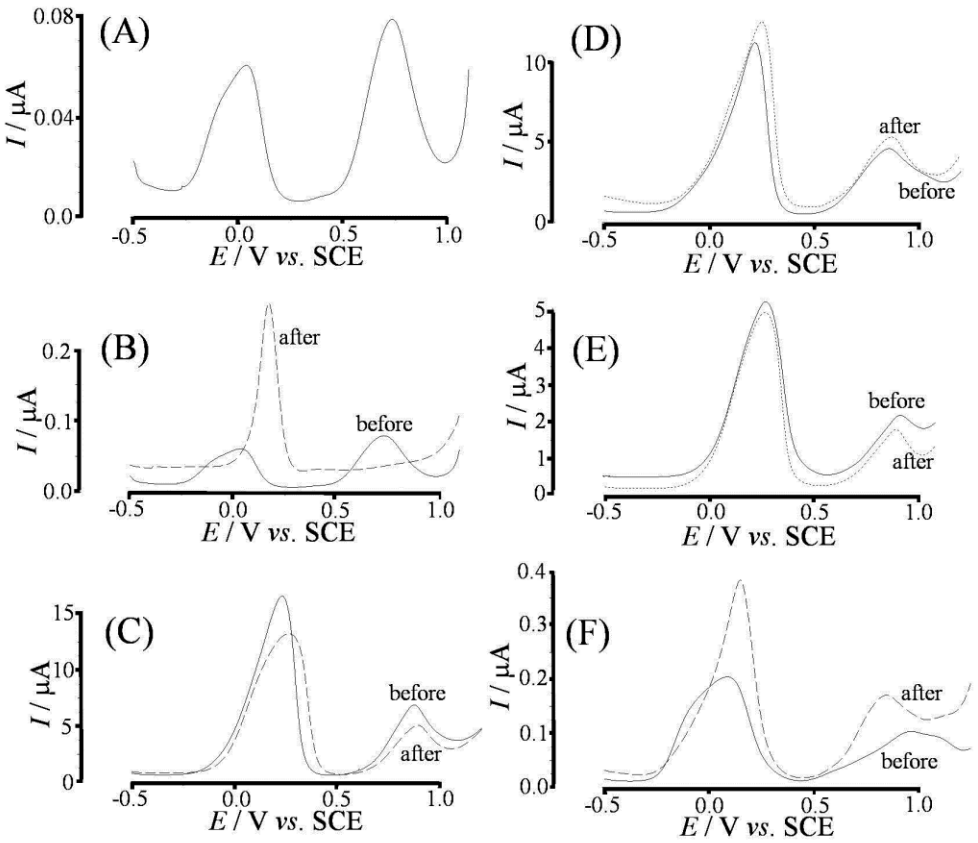

Figure 7.4. (A) Differential pulse voltammogram (first scan) for Prussian blue immobilised onto Dowex 50 1x2 at pH 7.1 in contact to a 3 mm diameter glassy carbon electrode. (B) As above, at pH 7 comparing the 1st scan and the 10th scan. (C) As above, pH 5.2. (D) As above, pH 4.7. (E) as above, pH 3.1. (F) As above pH 2.2.

By changing the pH of the Dowex particles, the stability of the differential pulse voltammetric response can be improved. Figure 7.4.B, C, D, E, F have been recorded at pH 7.1, 5.2, 4.7, 3.1, and 2.2, respectively. Mild acidic conditions appear most beneficial with signals at pH 4.7 and 3.1 appearing most reproducible and stable. Both the oxidation of Prussian yellow and the oxidation of Prussian blue are maintained and are available for future electrocatalysis studies.

7.4. Conclusions

In summary, two methods of redox system immobilisation have been demonstrated for sensor related electrochemical systems. First a metal complex with Co(III/II) redox activity has been immobilised onto Dowex 50 Wx4 and differential pulse voltammetry has been shown to provide better sensitivity. Second, Prussian blue has been precipitated onto the surface of Dowex 50 1x2 and shown to be redox active in contact to a glassy carbon electrode. Perhaps surprisingly, the pH of the Dowex particles (stabilised by immersion of the anion exchanger particles into aqueous phosphate buffer) completely changes the stability with more acidic conditions maintaining the Prussian blue redox system. It is known from the literature that alkaline conditions (e.g. during reduction of H_2O_2) attack Prussian blue and lead to loss of sensor responses. The simple immobilisation of the phosphate buffer provides a tool for stabilising the sensor response.

In future, this kind of experiment could be employed for a wide range of applications. The detection of H_2O_2 gas is important in hospitals (monitoring cleaning gas levels) and in medicine where peroxide is a marker for inflammation e.g. in lungs. Other chemical systems may be introduced to provide an almost unlimited range of chemical selectivity and opportunities for fast gas sensing in very thin responsive films.

7.5. References

[1] F. Ricci, G. Palleschi, Biosensors & Bioelectronics 21 (2005) 389-407.

[2] W. Chen, S. Cai, Q.Q. Ren, W. Wen, Y.D. Zhao, Analyst 137 (2012) 49-58.

[3] W. Zhao, J.J. Xu, H.Y. Chen, Electroanalysis 18 (2006) 1737-1748.

[4] A.A. Karyakin Electroanalysis 13 (2001) 813-819.

[5] R. Koncki, Crit. Rev. Anal. Chem. 32 (2002) 79-96.

[6] N.R. de Tacconi, K. Rajeshwar, R.O. Lezna, Chem. Mater. 15 (2003) 3046-3062.

[7] R.C. Millward, C.E. Madden, I. Sutherland, R.J. Mortimer, S. Fletcher, F. Marken, Chem. Commun. 19 (2001) 1994-1995.

[8] N. Leventis, Y.C. Chung, J. Electrochem. Soc. 138 (1991) L21-L23.

[9] B. Haghighi, H. Hamidi, L. Gorton, Sens. Actuators B-Chem. 147 (2010) 270-276.

[10] H. Karadeniz, B. Gulmez, A. Erdem, F. Jelen, M. Ozsoz, E. Palecek, Front. Biosci. 11 (2006) 1870-1877.

[11] S.E.C. Dale, C.Y. Cummings, F. Marken, Electrochem. Commun. 13 (2011) 154-157.

[12] M.T. Carter, M. Rodriguez, A.J. Bard, J. Amer. Chem. Soc. 111 (1989) 8901-8911.

[13] A. Kulczynska, R. Johnson, T. Frost, L.D. Margerum, J. Chem. Education 88 (2011) 801-805.

[14] M. Isaacs, J.C. Canales, A. Riquelme, M. Lucero, M.J. Aguirre, J. Costamagna, J. Coord. Chem. 56 (2003) 1193-1201.

[15] P.N. Zhou, L.Q. He, G.L. Gan, S.Y. Ni, H. Li, W.S. Li, J. Electroanal. Chem. 665 (2012) 63-69.

[16] K. Itaya, I. Uchida, V.D. Neff, Acc. Chem. Res. 19 (1986) 162-168.

[17] N.A. Sitnikova, A.V. Borisova, M.A. Komkova, A.A. Karyakin, Anal. Chem. 83 (2011) 2359-2363.

[18] A. Dostal, B. Meyer, F. Scholz, U. Schröder, A.M. Bond, F. Marken, S.J. Shaw, J. Phys. Chem. 99 (1995) 2096-2103.